NTNU

Norwegian University of
Science and Technology

A Novel Tool for Cement Evaluation

Sondre Jakobsen Fagerås

Petroleum Geoscience and Engineering
Submission date: June 2017
Supervisor: Sigbjørn Sangesland, IGP
Co-supervisor: Jesus De Andrade, IGP

Norwegian University of Science and Technology
Department of Geoscience and Petroleum

Summary

The annular casing cement is an important part of the well barrier throughout the life cycle of a well. With the increasing number of plug and abandonment (P&A) operations, increased attention is now given to annular cement evaluation and the ability to prove adequate zonal isolation. If an existing annular barrier can be verified, heavy and time-consuming operations to restore the annular seal can be avoided. One of the concerns when it comes to cement integrity is the frequently occurring microannulus at the casing-cement interface. How such a microannulus forms and how it affects the integrity of the well, has been presented in this thesis. The acoustic logging tools used for cement evaluation today have also been presented. Their individual strengths and deficiencies have been discussed, and their response to a microannulus has been highlighted.

A novel logging tool for cement evaluation – the Annulus Verification Tool (AVT) – has been developed at the Department of Geoscience and Petroleum at the Norwegian University of Science and Technology (NTNU). The tool is meant to complement the acoustic tools used today, to improve evaluation of the cement sheath's sealing capability – especially in cases where a microannulus is detected or suspected. The AVT applies a radial force on the inner casing wall while recording the displacement of the casing. This gives a measurement of the stiffness of the casing and any surrounding material, explaining how the tool can detect the presence of an annular cement. By measuring the casing displacement with high resolution, a microannulus can be both detected and its size can be quantified. This enables an evaluation of the microannulus's effect on the integrity of the annular cement.

A prototype of the AVT has been constructed and an experimental set-up has been designed to allow for initial testing of the tool. This includes construction of full-scale diameter samples representing a typical production casing cement job, with the possibility to generate a uniform microannulus of a known size at the casing-cement interface. The experimental testing performed, has shown that the AVT is able to differentiate a casing supported by an annular cement sheath from a free pipe, due to the stiffness contrast. This makes the tool able to detect the presence of an annular cement – even in cases where a microannulus exists. Results also showed that a microannulus gives a characteristic logging response, and that the microannulus size can be quantified with good accuracy. Inferring the quality of the cement sheath itself proved to be challenging, as the logging response seemed to depend on other factors than solely the mechanical properties of the casing, cement, and formation. Experimental tests performed with tool eccentricity and tilting has shown that the AVT is prone to improper centralization within the casing.

Numerical simulations (finite element analysis) have been performed to further increase the understanding of the AVT's logging response in specific cases. This was done using the geometry of the experimental set-up, to be able to directly compare with the experimental results and aid for an increased understanding of these. The simulated free pipe stiffness was found to match decently with the experimental results, while the simulated well-cemented stiffness was found to be significantly higher than for the experimental results. Further, the simulation results showed that a casing without annular cement support is deformed almost exclusively by ovalization, rather than compression of the steel. This confirmed the underlying principles behind determining the microannulus size from the AVT logging response.

Experimental testing of the AVT should be continued, to further evaluate the uncertainty related to the microannulus size calculations. Testing on more complex casing-cement-formation samples should also be performed. The work on the numerical simulations should be continued, to resolve the discrepancy in the well-cemented stiffness. Simulations should also be used further to evaluate potential damage to the casing and cement, imposed by logging. In a longer perspective, the AVT should be made ready for downhole application. Suggested modifications (compared to the prototype) have been presented, as well as the AVT's possible role in future cement evaluation.

Sammendrag

Sementen i ringrommet bak foringsrøret er en viktig del av brønnbarrieren gjennom en brønns livssyklus. Med det økende antallet av brønner som permanent plugges og forlates, blir det nå viet økt oppmerksomhet til evaluering av ringromssementen og evnen til å påvise tilstrekkelig soneisolering. Dersom en eksisterende ringromsbarriere kan påvises, kan tunge og tidkrevende operasjoner for å gjenopprette tetning i ringrommet unngås. Én av bekymringene når det kommer til sementintegritet er det ofte forekommende mikroringrommet mellom foringsrøret og sementen. Hvordan et slik mikroringrom dannes, og hvordan det påvirker integriteten i brønnen, har blitt presentert i denne oppgaven. De akustiske loggeverktøyene som i dag brukes for sementevaluering har også blitt presentert. Deres individuelle styrker og svakheter er blitt diskutert, og deres respons til et mikroringrom har blitt belyst.

Et nytt loggeverktøy for sementevaluering – Annulus Verification Tool (AVT) – har blitt utviklet på Institutt for geovitenskap og petroleum ved NTNU. Verktøyet er ment å supplere de akustiske metodene som brukes i dag, spesielt i situasjoner hvor et mikroringrom er påvist eller antas å eksistere. Verktøyet påfører en radiell kraft på den indre veggen av foringsrøret, mens forskyvningen av foringsrøret måles. Dette gir en måling av stivheten av foringsrøret og eventuelt omliggende materiale, og forklarer hvordan verktøyet kan påvise tilstedeværelsen av sement i ringrommet. Ved å måle forskyvningen av foringsrøret med høy oppløsning, kan et mikroringrom både påvises og dets størrelse kan bli kvantifisert. Dette muliggjør en evaluering av mikroringrommets innvirkning på sementens integritet.

En prototype av det nye sementevalueringsverktøyet har blitt konstruert, og et eksperimentelt oppsett har blitt utformet for å muliggjøre eksperimentell testing av verktøyet. Dette inkluderer konstruksjon av prøver i fullskaladiameter som representerer en typisk sementjobb for et indre foringsrør, med mulighet for generering av et uniformt mikroringrom av en kjent størrelse mellom foringsrøret og sementen. Den eksperimentelle testingen som er blitt gjennomført, har vist at verktøyet er i stand til å differensiere et foringsrør omgitt av sement fra et usementert foringsrør, på grunn av en kontrast i stivhet. Dette gjør at verktøyet kan detektere tilstedeværelsen av sement i ringrommet – også i tilfeller hvor et mikroringrom eksisterer. Resultater har også vist at et mikroringrom gir en karakteristisk loggerespons, og at størrelsen på mikroringrommet kan måles med god nøyaktighet. Det viste seg å være utfordrende å evaluere kvaliteten på sementen i seg selv, ettersom loggeresponsen synes å avhenge av andre faktorer enn kun de mekaniske egenskapene til foringsrøret, sementen og formasjonen. Eksperimentell testing gjort med verktøyet eksentrisk plassert, samt rotert, har vist at verktøyet er sensitivt til utilstrekkelig sentrering inni foringsrøret.

Numeriske simuleringer har blitt utført for å øke forståelsen av det nye verktøyets loggerespons i ulike tilfeller. Dette ble gjort ved å bruke den samme geometrien som i den eksperimentelle testingen, for å muliggjøre en direkte sammenligning med de eksperimentelle resultatene, samt gi en økt forståelse av disse. Den simulerte loggeresponsen for et *usementert* foringsrør stemte rimelig bra med de eksperimentelle resultatene, mens den simulerte responsen for et *sementert* foringsrør viste en vesentlig større stivhet enn de eksperimentelle resultatene viste. Videre viste simuleringsresultatene at et foringsrør som ikke er omgitt av sement deformeres nesten utelukkende ved ovalisering, fremfor kompresjon av selve stålet. Dette bekreftet de underliggende prinsippene bak beregningen av mikroringromsstørrelsen fra verktøyets loggerespons.

Eksperimentell testing av verktøyet burde videreføres, for å nærmere evaluere usikkerheten knyttet til beregningen av mikroringromsstørrelsen fra loggen. Det burde også gjøres testing på mer komplekse prøver av foringsrør, sement og formasjon. Arbeidet med de numeriske simuleringene bør også fortsette, for å finne svaret bak det store avviket i loggeresponsen for et sementert foringsrør. Simuleringer burde også brukes videre for å vurdere potensiell skade på sementen og foringsrøret, påført av logging. I et lengre perspektiv burde verktøyet gjøres klart for nedihullsbruk. Foreslåtte endringer (sammenlignet med prototypen), samt det nye verktøyets mulige rolle i fremtidig sementevaluering, har blitt presentert.

Acknowledgements

This Master's thesis is written at the Department of Geoscience and Petroleum (IGP) at the Norwegian University of Science and Technology (NTNU) in Trondheim, Norway during the spring of 2017. It is the final product of the MSc program in Petroleum Geosciences and Engineering, with specialization in Drilling Engineering.

First of all, I would like to thank my supervisor, Professor Sigbjørn Sangesland, for providing me with this interesting topic. His support and advice along the way are highly appreciated.

A special thank you goes to my co-supervisor, Dr. Jesus De Andrade, for his valuable guidance and feedback throughout this work, as well as for assisting me with the numerical simulations. His mechanical knowledge and innovative mindset have been helpful.

I would like to thank the technical staff at NTNU, which has assisted me with the preparation and set up for the experimental testing performed during this thesis: Håkon Myhren and Terje Bjerkan for machining and preparation of the parts, Steffen W. Moen and Noralf Vedvik for assisting me with the electronics and other supporting equipment, and Roger Overå for guidance and training in the laboratory.

I would also like to thank Assistant Professor Erik Skogen for our always interesting discussions about cement logging. His ability to share his operational experience within the field has been valuable.

Sondre Fagerås

Trondheim, June 2017

Contents

List of Figures

List of Tables

Nomenclature

Acronyms

AC	Alternating current
AE	Acoustic emission
AI	Acoustic impedance
API	American Petroleum Institute
AVT	Annulus Verification Tool
BHA	Bottomhole assembly
BI	Bond index
BOP	Blowout preventer
CBL	Cement bond log
CCL	Casing collar locator
CT	Computed tomography
DC	Direct current
FEA	Finite element analysis
FIT	Formation integrity test
HPU	Hydraulic power unit
ID	Inner diameter
IGP	Department of Geoscience and Petroleum
LOT	Leak-off test
LVDT	Linear variable differential transformer

NCS	Norwegian Continental Shelf
NTNU	Norwegian University of Science and Technology
OBM	Oil-based mud
OD	Outer diameter
P&A	Plug and abandonment
PCA	Portland Cement Association
PRV	Pressure relief valve
PWC	Perforate, wash and cement
SCP	Sustained casing pressure
SLG	Solid-liquid-gas
TIE	Third interface echo
TOC	Top of cement
TVD	True vertical depth
VDL	Variable density log
WBE	Well barrier element
WBM	Water-based mud

Greek Symbols

α	Attenuation rate (of a sonic signal)
α	Coefficient of thermal expansion
β	Forchheimer coefficient
μ	(Dynamic) viscosity
ν	Poisson's ratio
ρ	Density
θ	Wellbore inclination

Roman Symbols

A	Amplitude
A	Area
d	Diameter
E	Young's modulus
E_1	Amplitude of the first detected sonic signal
F	Force
f	Frequency
g	Gravitational acceleration
h	Height
h	Thickness
I	Current
k	Permeability
k	Spring constant
L	Length
p	Pressure
Q	Volumetric flow rate
r	Radius
S	Standoff
T	Temperature
t	Time
V	Voltage
v	Velocity
w	Width
Z	Acoustic impedance

Subscripts

0	Equilibrium point
0	Resonant
ann	Annulus
cmt	Cement/cemented
csg	Casing
far	Far receiver
flex	Flexural
fm	Formation
fp	Free pipe
i	Inner
ma	Microannulus
max	Maximum
min	Minimum
near	Near receiver
o	Outer
p	Compressional (primary) wave

Chapter 1

Introduction

1.1 Cementing for Eternity

As several of the major offshore petroleum-producing regions are now maturing, an increase is seen in offshore plug and abandonment (P&A) operations, and a further increase is expected in the near future. It has been estimated that, on the Norwegian Continental Shelf (NCS) alone, 3,000 wells need to be plugged and abandoned [1]. This is a job which will take up to 40 years to complete, at a total cost of almost 900 billion Norwegian kroner. Due to tax regulations, the government indirectly pays a large share of the costs through tax deductions for the licensees. When also considering the environmental responsibility associated with plugging of oil and gas wells, it is clear why reducing the operational expenses as well as ensuring proper integrity of the plugged wells is – and should be – a high priority for the stakeholders involved.

Figure 1.1 illustrates the requirements for a well barrier for permanent abandonment, according to NORSOK D-010 [2]. The barrier shall be placed adjacent to an impermeable formation with sufficient formation integrity, and extend across the full cross section of the well – including all annuli. This means that, if an annular barrier (conventionally a cement sheath) can not be verified/proven, it has to be restored by performing operations *behind* the casing. This typically involves establishing access to the annulus for cementing by either casing *removal* by section milling or cutting and pulling, or by casing *perforation* using the perforate, wash and cement (PWC) system [3]. Such operations will contribute to an increased time and cost spent on the P&A, explaining why the cost of plugging an offshore well is often similar to the cost of the original drilling operation [4]. Contrary, if an annular barrier can be verified, significant time – and hence also cost – can be saved by only performing plugging operations *within* the casing. In this case, placing a cement plug inside of the casing is sufficient to establish a cross-sectional barrier. This can also be an enabler for performing more of the P&A without a drilling rig (often referred to as rigless P&A), further reducing the costs and the operational footprint.

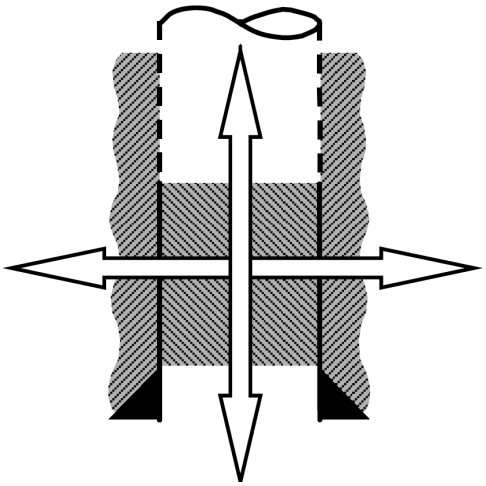

Figure 1.1: Requirements for a well barrier for permanent abandonment, according to NORSOK D-010 [2].

Following this, increased attention is now given to cement evaluation and the ability to prove adequate zonal isolation, motivated mainly by the potential P&A cost savings if an existing annular barrier can be verified. Considering the potential environmental consequences of using an inadequate cement as a permanent barrier, it is clear that this decision should be taken on the best possible foundation of data and with the best possible understanding of the cement's sealing capability. Also considering the cost paid by the licensees as well as the government for restoring an annular barrier, it is clear that the same goes for the decision of *not* using an existing annular cement. Therefore, the objective of this thesis is to contribute to an improved evaluation of the annular cement sheath's sealing capability, in particular in cases where a microannulus is suspected. This is done by introducing, testing and evaluating a novel tool for cement evaluation.

1.2 Structure of the Report

Chapter 2 is meant to give the reader the sufficient background knowledge on the topics of well cementing, the cement microannulus, as well as the different techniques presently used for cement evaluation. This chapter is written, based upon the work performed by the author in the Specialization Project at NTNU, the fall of 2016 [5]. In Chapter 3, a novel cement evaluation tool – designed for detecting and quantifying the size of a microannulus – is presented. Chapter 4 describes the experimental setup for testing of the tool, the experimental tests performed, as well as the obtained results. Chapter 5 presents numerical simulations conducted to further evaluate the logging response of the tool, and also to increase the understanding of the experimental results. The implications of the results obtained throughout this work, as well as the new tool's possible role in future cement evaluation, is further discussed in Chapter 6. Concluding remarks are presented in Chapter 7, while recommendations for further work are given in Chapter 8.

Chapter 2

Background

2.1 Well Cementing Objectives

In oil, gas and water wells, cement is placed in the annulus between the casing and the exposed formation, by displacing a cement slurry down the casing and up the annular space. This process is referred to as *primary cementing* and was first used already in 1903 [6, 7]. The main objective of primary cementing is to provide zonal isolation by creating a hydraulic seal along the casing annulus. This will prevent fluids from flowing from subsurface formations to surface, and will also prevent crossflow between different subsurface zones. To achieve this, the cement sheath has to seal against both the casing and the formation, often referred to as casing-cement bond and cement-formation bond, respectively. In addition, there must be no possibility for fluids to migrate within the cement sheath itself. These requirements are illustrated in Figure 2.1. In addition to providing zonal isolation, the cement should also provide structural support of the casing.

This is also reflected in the well integrity standard NORSOK D-010, where it is stated that the function of the annular cement sheath is to *"provide a continuous, permanent and impermeable hydraulic seal along hole in the casing annulus or between casing strings, to prevent flow of formation fluids, resist pressures from above or below, and support casing or liner strings structurally."* [2].

Once the cement is fully set, most cement jobs provide sufficient structural support [8, 9]. Providing zonal isolation, on the other hand, has proven to be the hardest objective to achieve, yet the most important [6, 10]. The objectives and requirements for primary cementing arguably make it one of the most important operations performed on a well. The cement sheath serves as a well barrier element (WBE) through the entire lifetime of the well, and a successful cement job is crucial for well integrity. Contrary, a poor primary cement job could cause severe problems over the well's lifetime, e.g. sustained casing pressure (SCP), crossflow between zones, hydrocarbon-filled annuli and other well

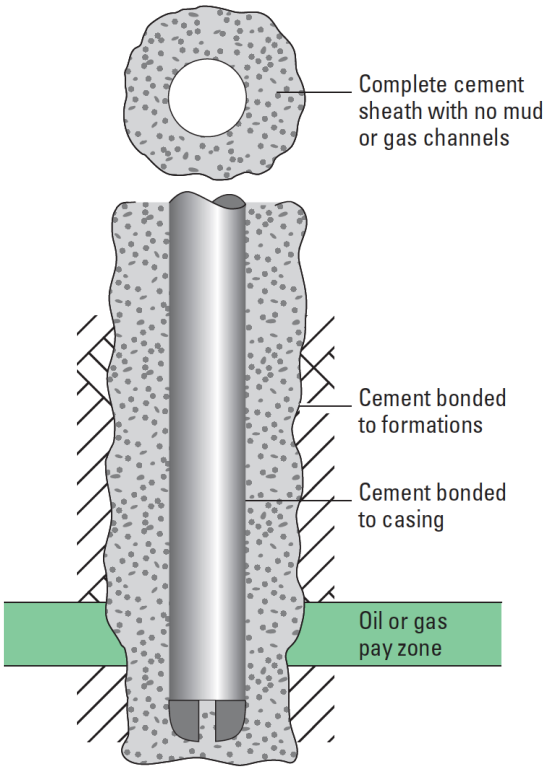

Figure 2.1: The requirements to fulfill the main objective of primary cementing; zonal isolation [6].

integrity issues. Also, it may put limitations on the production/injection capacity of the well, meaning the well may never reach its full potential. If the objectives of the primary cementing are not met, *remedial cementing* is often performed to remedy the problems associated with the unsuccessful primary cement job. This will increase well cost and the result may not be as good as for a successful primary cement job. In cases where remedial cementing is not possible or fails to fulfill the objectives, the well may be lost and abandonment, sidetracking or a re-spud is necessary.

Often, in P&A operations, the annular cement sheath is even evaluated for serving as a barrier in an eternal perspective. In these cases, it is especially important to assess the quality of the cement sheath and also evaluate potential cement degradation over time. The integrity of an initially good cement sheath can be compromised in several different ways. A schematic of the possible failure types is given in Figure 2.2 and is summarized below:

(a) Microannulus at the casing-cement interface.

(b) Microcracks or fissures within the cement, giving internal cement permeability.

(c) Fractures across cement sheath.

(d) Microannulus at the cement-formation interface.

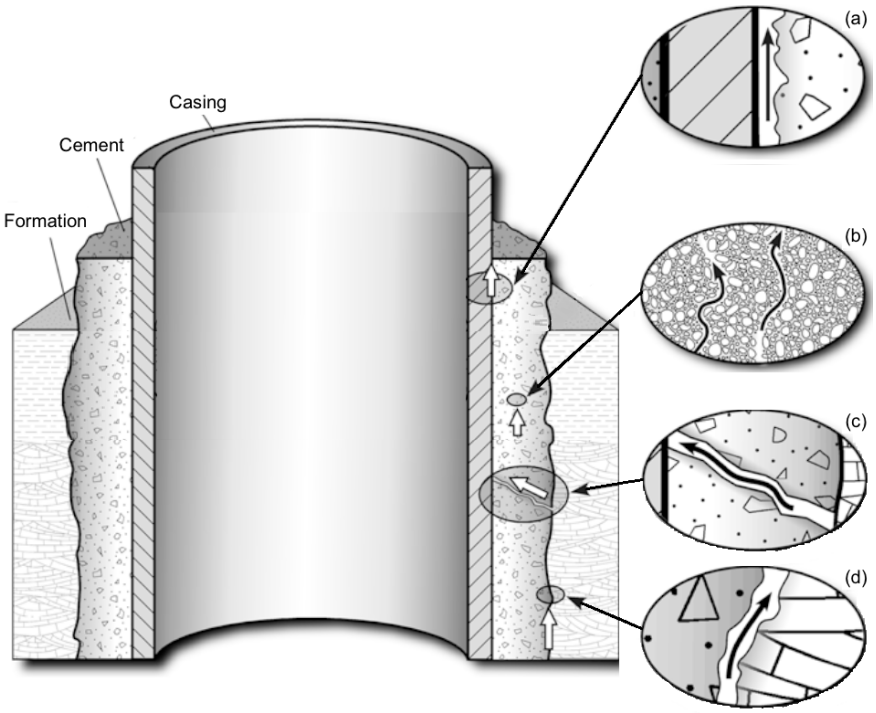

Figure 2.2: Possible types of cement sheath failure. Modified from [11].

2.2 Microannulus

A microannulus is a small gap, less than a few hundred micrometers thick, either between the casing and the cement or between the cement and the formation [6]. Gaps larger than a few hundred micrometers are usually referred to as mud layers, as they are typically caused by poor mud displacement during cementing. The focus of this report is the frequently encountered microannulus at the casing-cement interface, which is shown as failure (a) in Figure 2.2. Depending on its size and extent, a microannulus can result in loss of zonal isolation, as fluids can migrate along the interface of the cement sheath – even though the cement sheath itself is impermeable.

2.2.1 Formation of a Microannulus

Cement Shrinkage During Hydration

Neat cement shrinks chemically during hydration as the volume of the hydrated product is less than the volume of the hydrating components [12]. Early, it was therefore believed that a microannulus is formed due to cement shrinkage during hydration [13]. However, it is only the external volume change of the cement, often referred to as the *bulk shrinkage*, that contributes to the generation of a microannulus. The bulk shrinkage ceases after some time of hydration, at the point where a rigid structure is formed. After this point, the total chemical shrinkage continues by an increase in internal cement porosity, while

the external volume of the cement remains constant. Expansive cement systems have been designed to avoid microannulus generation due to shrinkage. However, it has been shown that the effect of shrinkage is negligible for microannulus generation for most well conditions [6]. This could be explained by the fact that bulk shrinkage occurs while the cement is still liquid. In this way, the top of cement (TOC) could be lowered to compensate for the shrinkage, rather than creating a microannulus. In addition, when the cement has access to additional water during hydration (which typically is the case downhole), the bulk shrinkage is significantly reduced. A slight *bulk expansion* has even been reported in such cases [6].

Pressure Variations in the Wellbore

An increase or decrease in pressure within the wellbore will cause the casing to expand or retract accordingly. Following this, a decrease in pressure can break the adhesion between the casing and cement and create a microannulus. This occurs for example when displacing the well to a lighter mud for drilling of the next section, or when displacing to a lighter completion fluid. An increase in pressure will deform either the cement or the formation, depending on which has the lowest compressional strength [14]. If the deformation is permanent and followed by a decrease in pressure, the casing will pull away from the cement sheath and a microannulus will form. This could typically occur during pressure tests conducted after the cement has set. To avoid this, the casing should be pressure tested immediately after the cement is in place, while the cement is still liquid (typically referred to as a *green cement pressure test*). When pressure testing the blowout preventer (BOP), the casing should be isolated by installing a plug just below the BOP.

By approximating the casing as a thin-walled pipe and assuming the casing is not bonded to, nor assisted by, the cement sheath, the radius variation of a casing subjected to a pressure change can be calculated as [15]:

$$\Delta r_{csg} = \left(1 - \frac{\nu}{2}\right) \frac{r_{csg}^2 \Delta p}{h_{csg} E} \tag{2.1}$$

where

$$\begin{aligned}
\Delta r_{csg} &= \text{Change in casing radius} && [mm] \\
\nu &= \text{Poisson's ratio of steel } (\approx 0.3) && [-] \\
r_{csg} &= \text{Mean casing radius} && [mm] \\
\Delta p &= \text{Change in pressure} && [Pa] \\
h_{csg} &= \text{Casing wall thickness} && [mm] \\
E &= \text{Young's modulus of steel } (\approx 200 \times 10^9) && [Pa]
\end{aligned}$$

If a 9 5/8-in 53.5# casing is set above a depleted reservoir, and the cement is displaced with a 1.7 kg/L mud, the mud weight could typically be reduced to 1.2 kg/L before drilling

the reservoir section. For a reservoir depth of 3000 m TVD, this would give a pressure reduction of 147 bar at the casing shoe, resulting in a microannulus of 67 µm, according to Equation 2.1. This problem could be solved by displacing the cement with the lighter fluid (if permitted). A microannulus could also be created in case of leaking floats in the casing shoe, making it necessary to hold pressure on the casing after displacing the cement (to avoid U-tubing of cement back into the casing). When this pressure is released after the cement has set, the contraction of the casing can create a microannulus.

However, a typical casing is not thin-walled, and Equation 2.1 is not exact. Using the Lamé equations for a thick-walled cylinder can give more exact calculations of the radius change. On the other hand, the error using the thin-walled approximation is not tremendous for a typical casing, and Equation 2.1 is sufficient to illustrate how a wellbore pressure change can generate a microannulus.

Temperature Variations in the Wellbore

An increase or decrease in temperature will cause the casing steel to expand or retract accordingly. By assuming that the casing is not bonded to, nor supported by, the cement sheath, the radius variation of a casing subjected to a temperature change can be calculated as [15]:

$$\Delta r_{csg} = \alpha r_{csg} \Delta T \tag{2.2}$$

where

$$\begin{aligned} \alpha &= \text{Coefficient of thermal expansion of steel } (\approx 12.4 \times 10^{-6}) && [(^oC)^{-1}] \\ \Delta T &= \text{Change in temperature} && [^oC] \end{aligned}$$

The exothermic reaction of cement hydration generates a significant amount of heat and a temperature increase of 30°C compared to the normal geothermal temperature is not uncommon [16]. After hydration, this heat will dissipate and the casing will contract accordingly. If a 30°C temperature reduction is experienced after cement hydration for a 9 5/8-in 53.5# casing, this will create a microannulus of 43 µm, according to Equation 2.2. A temperature decrease could also occur when circulating cool fluids in the wellbore, e.g. during drilling of the next section. For production wells, the temperature would increase as hot reservoir fluids are produced, resulting in the same effects as for an increase in internal pressure. For injection wells, the temperature is reduced as cold water or gas is injected, resulting in the same effects as for a decrease in internal pressure.

Oil-Wet Surface

If the casing is run in oil-based mud (OBM), the casing surface tends to be oil-wet. When cement is displaced up the annulus, an oil film may still be present at the surface,

prohibiting bond/contact between the casing and the (water-based) cement. A sufficient volume of spacer should be pumped ahead of the cement to remove the oil-film and to make sure the casing is water-wet before the cement is displaced up along the casing.

2.2.2 Impact on Well Integrity

Traditionally a microannulus has not been considered as a large issue for the integrity of the well [7, 14, 16]. However, a continuous microannulus will allow fluids to migrate along the cement sheath's interface.

Equations for estimating the leak rate through a microannulus are presented in Appendix A. Figure 2.3 shows the resulting leak rate for both an oil-filled and a gas-filled microannulus, plotted versus the microannulus size (using Equations A.4 and A.6). A typical case of a vertical 9 5/8-in casing was used, with a pressure differential of 50 bar over a 250 meter cemented interval. For the oil, a density of 0.6 g/cm^3 and a viscosity of 2 cP was used. For the gas, a density of 0.1 g/cm^3 and a viscosity of 0.02 cP was used. Second-order pressure losses for the gas case were neglected (assuming $\beta = 0$).

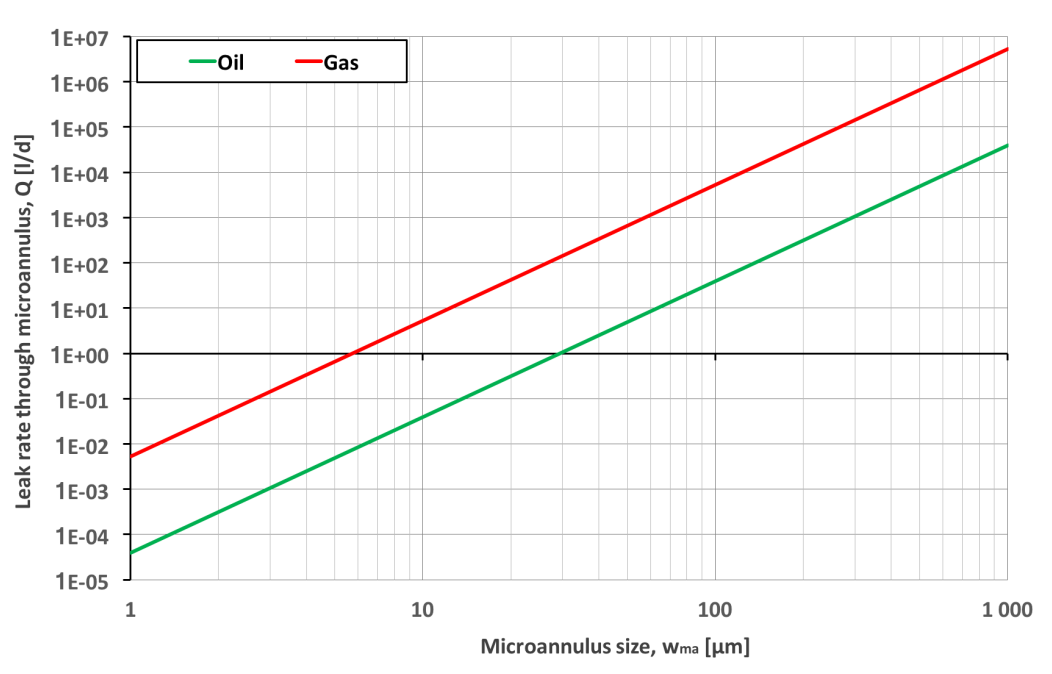

Figure 2.3: Leak rate through an oil-filled and a gas-filled microannulus as a function of the microannulus size.

A typical microannulus size of 50 µm, gives an oil leak rate of 4.9 liters per day. It is clear that the leak rate is heavily dependent on the size of the microannulus. If the microannulus size is doubled, the leak rate will increase by a factor of 8 (2^3), giving a liquid leak rate of 39.0 liters per day for a 100 µm microannulus.

The gas leak rate, on the other hand, will be 657 liters per day for a 50 µm microannulus and 5260 liters per day for a 100 µm microannulus. The significantly higher leak rate in the case of gas is mainly due to the lower viscosity (typically two orders of magnitude less than for a liquid). In addition, the gravitational pressure drop is lower due to the lower density of the gas, further increasing the leak rate. This is also reflected in published literature, where a liquid-filled microannulus is commonly considered unproblematic for the well integrity, while a gas-filled microannulus is considered as a potential integrity threat [15, 17].

Such leak rates will cause pressure build-up in the annulus, which is usually handled by regularly bleeding off the pressure, if possible (for subsea wells this would typically not be possible). After bleeding off the pressure, the differential pressure over the microannulus is again increased and the pressure will build again. This is what is referred to as sustained casing pressure (SCP), where a microannulus is one of the possible root causes. For wells permanently plugged and abandoned, there is no possibility to monitor nor contain the annular pressure, meaning that a leakage through a microannulus will be released to the ground, sea and/or atmosphere.

2.3 Cement Evaluation

This section gives an introduction to the different technologies presently used for cement evaluation. For a more in-depth review of both presently and previously used technologies for evaluation of cement, the reader is advised to read the report submitted by the author for the Specialization Project at NTNU, the fall of 2016 [5].

2.3.1 Background

Cement evaluation is the process of determining whether the casing cement meets the objectives described in Section 2.1. If so, the operations can proceed as planned. If not, remedial cementing can be planned, based on the results of the cement evaluation. One of the best indications of a good cement job are the parameters recorded during the job, e.g. the displacement rate, the volumetric returns and the pump pressure during displacement. If all the parameters behave as expected, the cement job is typically considered successful and volumetric calculations are used to estimate the top of cement (TOC). If the casing shoe is drilled out, a good pressure test – either a formation integrity test (FIT) or a leak-off test (LOT) – confirms this. However, if the parameters recorded during the job are not as expected, e.g. returns are lost during displacement, the quality of the cement job should be questioned.

This is also reflected in NORSOK D-010 [2], where it is stated that, for a cement job not defined as critical cement, 100% displacement efficiency based on records from the cement

operation (volumes pumped, returns during displacement, etc.) is sufficient verification of the cement length. In the event of losses, FIT/LOT can be used as verification method only if the cement serves as a well barrier element (WBE) for drilling of the next section. It shall not be used as verification for cement serving as a WBE during production/injection or abandonment. If so, the cement shall be verified by logging. A cement job defined as critical cement shall always be logged. Critical cement is defined by NORSOK D-010 as one of the following:

1. The production casing or production liner when set into/through a source of inflow with hydrocarbons.
2. The production casing or production liner when the same casing cement is part of the primary and secondary well barriers.
3. Wells with injection pressure which exceeds the formation integrity at the cap rock.

An example of a critical cement job is shown in Figure 2.4, where the same annular casing cement is part of both the primary and the secondary permanent barrier for a plugged well. As reflected by the figure, the annular cement shall be verified by logging.

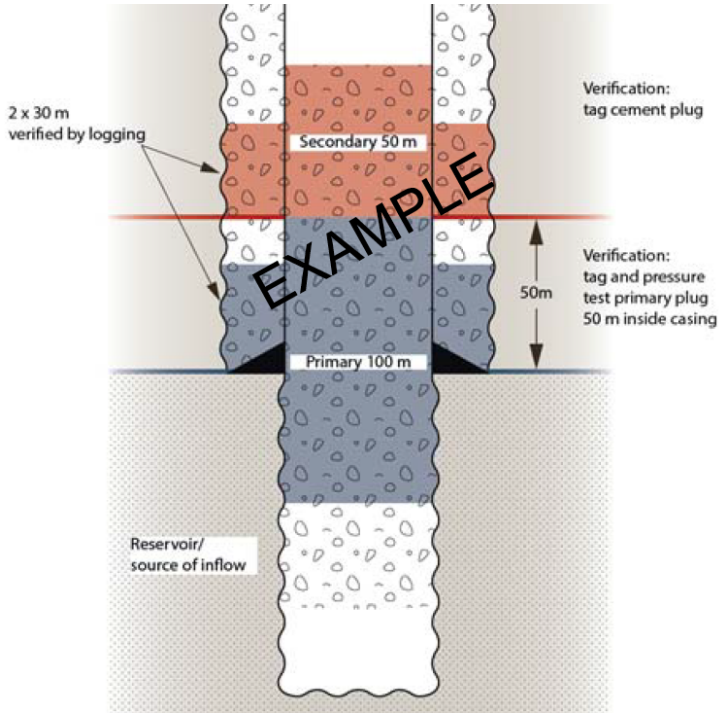

Figure 2.4: An example of a critical cement, where the production casing annular cement is part of both the primary and secondary permanent barrier envelope [2].

Today, cement evaluation by logging is performed almost exclusively using acoustic logging tools conveyed by wireline. The acoustic tools are acknowledged for both locating the TOC, as well as for evaluating the hydraulic seal of the annular cement. The remainder of this chapter is therefore devoted to these tools, and their measurement principles

are presented. The challenges and deficiencies related to the individual tools are also discussed, and special emphasis is made on their response in the case of a microannulus at the casing-cement interface.

2.3.2 Sonic Logging

The first acoustic logging tool for cement evaluation, the cement bond log (CBL), was introduced in the early 1960's [18, 19]. This sonic tool is still frequently used today.

2.3.2.1 Measurement Principle

A standard CBL tool consisting of one transmitter and two receivers, is shown in Figure 2.5. The transmitter emits short bursts of sonic energy, typically at a frequency of 20 kHz [6, 18]. The possible wave paths for the sonic signal traveling from the transmitter to the receivers are also shown.

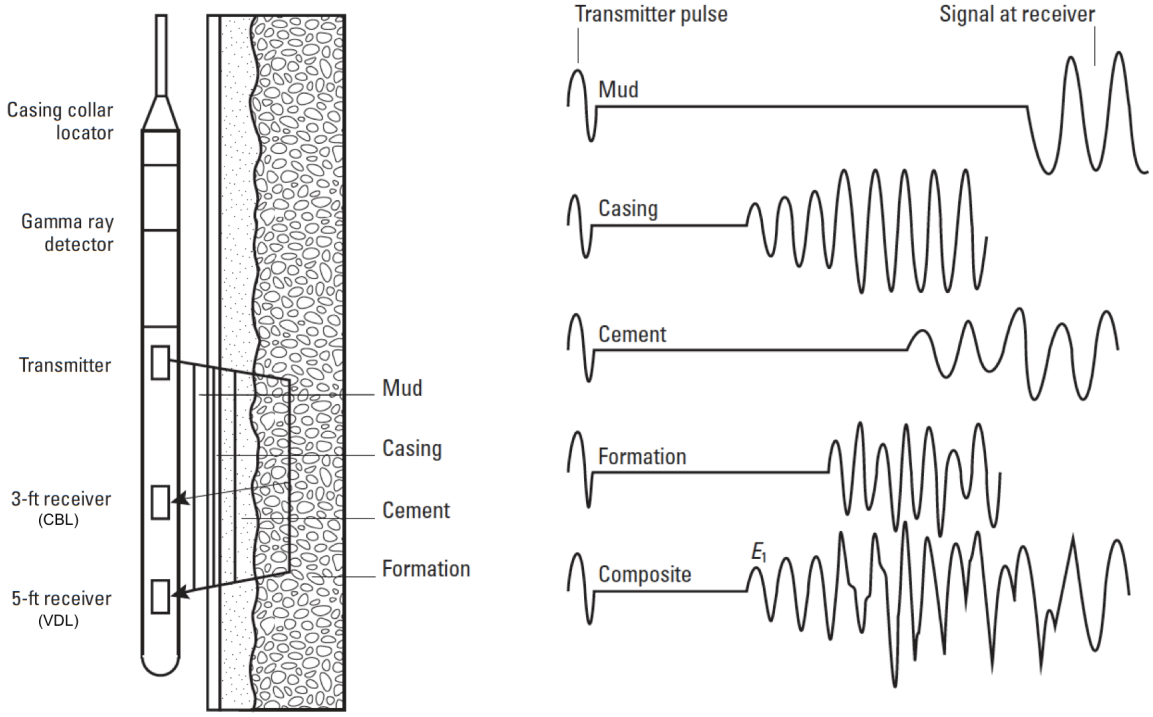

Figure 2.5: A typical CBL/VDL tool, with the possible wave paths for the sonic signal and the resulting waveforms picked up at the receivers. Modified from [6].

The sonic wave traveling along the casing is what forms the basis of the CBL measurement. It is a symmetric Lamb wave, a type of plate wave arising because the casing thickness is less than a few wavelengths [20], and its velocity is slightly lower than the compressional wave velocity [21]. The underlying principle of cement bond logging is that the strength of the casing signal recorded at the receiver is a function of the material surrounding the

casing. This signal strength is quantified by measuring the amplitude of the first wave arriving at the receiver. This amplitude is denoted by E_1 on the composite signal which is shown in Figure 2.5, and is typically measured at the 3 ft CBL receiver. Since the first wave is measured, the CBL measurement relies on the casing wave arriving before all of the other – which is the case in Figure 2.5. This is typically so, as the casing wave travels a relatively short distance and the acoustic velocity of steel is high.

As the wave propagates along the casing, it results in a motion of the casing. If the casing is surrounded by a fluid, the casing is relatively free to move and little energy is lost to the surroundings. Hence, an uncemented casing results in a high CBL amplitude reading – sometimes referred to as free pipe ringing. If the casing is surrounded by a solid material (e.g. cement), the motion of the casing wall is significantly damped. This results in a larger energy loss to the surroundings and a low CBL amplitude, explaining why the CBL is sensitive to the cement quality. As the particle motion created by the symmetric Lamb wave is mainly parallel to the casing surface, the amount of dampening of the signal depends on the shear coupling between the casing and the adjacent material: The greater the shear coupling, the greater the energy loss and lower the amplitude [22]. As there is no shear coupling to any fluid, all fluids are expected to look the same, with a high amplitude. With a sufficient shear coupling, the amount of dampening depends on the acoustic impedance (AI) of the cement, where a high AI results in more dampening and a lower CBL amplitude [23].

To improve the understanding of the cement quality and the interpretation of the CBL, the sonic tools also include a variable density log (VDL) [24]. All common CBL-tools today (including the one shown in Figure 2.5) use a 5 ft receiver for the VDL-measurement. As shown in Figure 2.5, it is not only the casing signal that arrives at the receiver, and the VDL receiver records the full waveform of the composite signal. The VDL is a micro-seismogram and is usually presented as a variable intensity display, where the amplitudes of the waveforms are converted to a gray scale or a color scale.

The use of the VDL in cement evaluation is qualitative and it is primarily used to evaluate the cement-formation bond, which the CBL amplitude is insensitive to as it only considers the wave traveling along the casing. This is done by evaluating the strength of the formation signal – the signal which travels the longest path, but usually arrives rather early due to the high acoustic velocity of most formations. If the casing-cement and cement-formation bonds are good, acoustic waves will travel across the cement sheath and along the formation and back across the cement sheath to the receiver. These formation arrivals typically appear as wavy bands on the VDL, after the casing arrivals. Hence, if the CBL amplitude is low and formation signals are evident on the VDL, it is an indication of both a good casing-cement bond and a good cement-formation bond. If the CBL amplitude is low, but the VDL formation arrivals are weak, it indicates a good casing-cement bond, but a poor cement-formation bond. The VDL can also be used to increase the confidence of the interpretation of the CBL. If the casing-cement bond is good (represented by a low CBL amplitude), the casing arrivals on the VDL should be

weak due to heavy attenuation of the casing signal.

Some CBL tools also measure the *attenuation rate*, a measure of the amplitude reduction of the sonic signal as it travels along the casing. Hence, also the attenuation rate is a function of the acoustic impedance of the annular cement, and high attenuation rates reflect a good cement bond [25]. The log display then typically show both the CBL amplitude and the CBL attenuation rate. These type of tools – sometimes referred to as *attenuation rate tools* – measure the amplitude at several transmitter-receiver spacings to compute a compensated attenuation rate. By comparing the amplitude at multiple receivers, this compensated attenuation rate is insensitive to the attenuation in the borehole fluid as it only considers the effect of traveling some extra distance along the casing.

2.3.2.2 Challenges in Sonic Logging

Azimuthal resolution: Due to the omnidirectional nature of the CBL's transmitter(s) and receiver(s), it can not detect azimuthal variations in cement quality but measures an average cement quality around the circumference of the casing [18]. This means that channeled cement, contaminated cement, and a cement not fully set all will give similar CBL-readings: The amplitude and the attenuation rate will be somewhere between the response for a free pipe and a well-cemented casing. Experimental testing has shown that the CBL attenuation rate is linearly dependent on the fraction of the circumference bonded [22]. Several schemes have been developed to exploit this to estimate the percentage of casing bonded to cement. The most used is the *bond index* (BI), which is often displayed on the log presentation [17]:

$$BI = \frac{\alpha(x) - \alpha_{fp}}{\alpha_{cmt} - \alpha_{fp}} \tag{2.3}$$

where

$$\begin{aligned} BI &= \text{Bond index} && [-] \\ \alpha(x) &= \text{CBL attenuation rate at a point x} && [dB/ft] \\ \alpha_{fp} &= \text{CBL attenuation rate in a free pipe section} && [dB/ft] \\ \alpha_{cmt} &= \text{CBL attenuation rate in a well-cemented section} && [dB/ft] \end{aligned}$$

Note that for the BI to represent the percentage of the casing bonded it requires a good cement with vertical channels of no cement. A BI less than 100% could also be caused by a contaminated or insufficiently set cement all around the casing. Segmented sonic tools have been developed to provide azimuthal resolution. Typically, six pads (all with one transmitter and one receiver) are used to segment the wellbore into 60° sectors [26].

Tool centralization: Proper centralization of the CBL is crucial to obtain a valid measurement. Hence, the tool should be fitted with a sufficient number of centralizers – especially in deviated wells. An eccentric CBL will give a long path and a short path available for the sonic signal, as shown in Figure 2.6. This results in the sonic energy

"smearing out" in time, giving a lower peak value for the CBL amplitude measurement. In addition, the CBL transit time (the time from firing the transmitter, to a signal above the detection level is detected at the receiver) decreases as the signal traveling the short path will reach the receiver earlier than for a centralized tool. Hence, the transit time should be used evaluate the centralization of the tool, and a travel time less than expected is an indication of tool eccentricity. The reduction in CBL amplitude with eccentricity have been shown to be quite dramatic: A 3 ft spacing CBL eccentered by 1/4 inch can result in an amplitude reduction of up to 50% [7]. If not recognized by the reduction in travel time, a partial cement fill could be interpreted as full cement coverage.

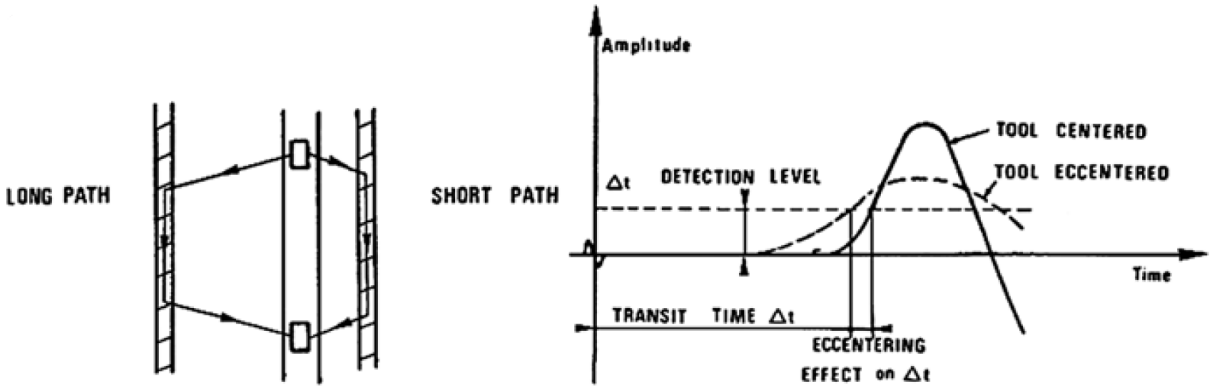

Figure 2.6: Tool eccentricity causing a reduction of the CBL amplitude and travel time [27].

Fast formations: As described, the measurement of the CBL amplitude relies on the casing signal arriving first. However, if the formation is significantly faster than the casing, the formation signal can overtake the casing signal and appear first at the receiver. A long transmitter-receiver spacing and a thin cement sheath increase the problem. This is one of the reasons why the relatively short 3 ft spacing is typically used for the CBL amplitude measurement. Some tools have in addition an even shorter spacing (typically less than 1 ft) that can be used for amplitude measurements in case of fast formations [17, 28]. Fast formations are easily detectable on the VDL, as the wavy formation arrivals will appear first on the VDL log display. The CBL amplitude measurement is invalid if the formation signal arrives prior to the casing signal, as the recorded amplitude will be that of the formation signal and not the casing. However, a fast formation response is actually an indication of a well-cemented casing, as both a good casing-cement bond and a good cement-formation are necessary to enable acoustic transmission to the formation.

Low-density cement: Low-density cement systems typically give a higher CBL amplitude and a lower attenuation rate compared to standard cement due to a lower acoustic impedance (AI). Experimental work has shown little correlation between the cement's AI and hydraulic isolation, so to ensure proper CBL interpretation, the cement system's effect on the CBL response has to be known. [29]. If the low cement AI is not taken into account, intermediate/poor bond may be indicated, even though the casing is well-cemented. The use of such cement, results in the fully cemented value being closer to that of free pipe, hence compromising the resolution of the log. When the amplitude and

attenuation of a fully cemented casing approach that of free pipe, it is no longer possible to infer the cement presence and quality from the CBL. However, distinct formation arrivals on the VDL could still be used as an indication of an annular cement fill.

Concentric casings: High CBL amplitudes are often experienced in sections of concentric casing strings, even when the cement quality is proven to be good just below the previous casing shoe. In the same section, the VDL shows clear parallel bands similar to a strong casing signal, indicating a poor cement job. Physically, there is no reason why the cement job should be worse in a concentric section unless the TOC accidentally is located at the depth of the previous casing shoe. It has been shown that the high CBL amplitude is caused by the arrivals from the third interface (between the cement and the outer casing) interfering with the signal from the inner casing [30]. A strong signal from the outer casing appears due to the high contrast in acoustic impedance between the cement and the casing. In addition, the signal from the outer cement boundary appears earlier than usual due to the high acoustic velocity of the outer casing. This is causing the CBL to measure a signal that is not only caused by the first casing but also the second casing, explaining the elevated amplitude. Paradoxically, the presence of this effect is actually a sign of a well-cemented annulus. For signals from the outer casing to appear, there has to be acoustic transmission between the two casing strings, i.e. a good cement sheath with good bonding to both surfaces.

2.3.2.3 Microannulus Response

The cement bond log is indeed just that – a *bond* log. For significant signal attenuation to occur, there has to be a shear coupling between the casing and the cement sheath. However, to fully understand the response of the CBL in the case of a microannulus, the effects that contribute to the attenuation of the sonic signal have to be understood. The amplitude reduction of the sonic signal between the transmitter and the receiver has been shown to be caused by two effects: (1) Attenuation from axial propagation along the casing (propagation attenuation) and (2) attenuation caused by the acoustic coupling between the transducers and the casing wave (coupling attenuation) [31]. The two mechanisms are both dependent on the annular material, but in different ways. In order to differentiate between the two effects, two or more CBL amplitude measurements at different transmitter-receiver spacings are necessary. The amplitude can be plotted versus spacing on a semi-log plot as shown in Figure 2.7. The slope of the straight line is directly proportional to the propagation attenuation rate, which represents the attenuating effect on the acoustic signal as it travels along the casing. This is the same attenuation rate that is measured by the attenuation rate tools presented earlier. It is clear that the propagation attenuation increases with the transmitter-receiver spacing, especially for the case of a well-bonded cement. The propagation attenuation *rate* (i.e. the slope) on the other hand, is constant as long as the cement quality does not change along the travel path of the wave. The coupling attenuation represents the E_1 amplitude reduction at an effective spacing of zero. In other words, this is the attenuation caused

by other effects than the travel along the casing. This includes the attenuation in the wellbore fluid and in the intersect/coupling with the casing. Following this, the coupling attenuation is independent of the transmitter-receiver spacing.

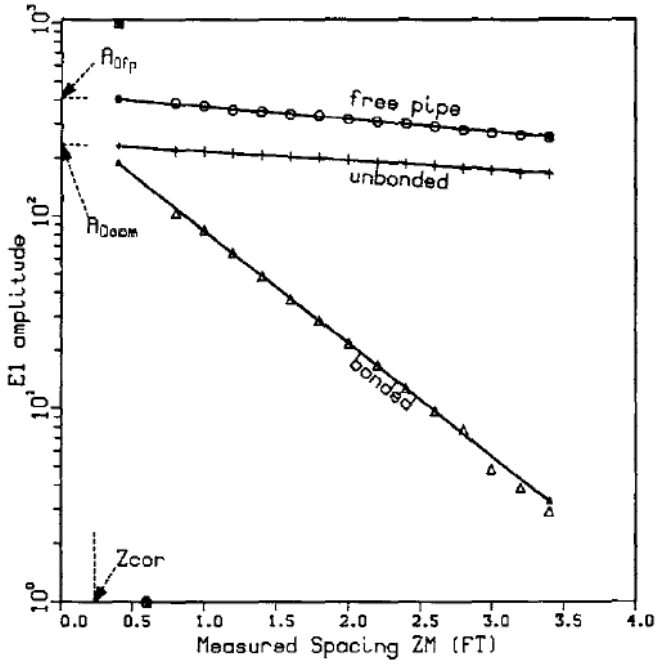

Figure 2.7: Effect of coupling and propagation attenuation on the CBL. E_1 amplitude is plotted versus transmitter-receiver spacing for free pipe and cemented casing with and without a microannulus [31].

Liquid-filled microannulus: Figure 2.7 also shows the results from experimental testing of a CBL with varying transmitter-receiver spacing for the case of a liquid-filled microannulus (denoted by "unbonded") [31]. It is clear that the propagation attenuation rate is significantly reduced (compared to a well-cemented casing), when a liquid-filled microannulus exists, as seen from the more gentle slope. Actually, a propagation attenuation similar to that of a free pipe is seen. This is explained by the fact that a shear coupling between the casing and cement is required to attenuate the plate wave traveling along the casing. Hence, it is extremely sensitive to a microannulus as the shear coupling is lost even for very small microannulus sizes. Experiments have shown that for a liquid-filled microannulus, the propagation attenuation is similar to that of free pipe for all common sizes of microannuli [15]. On the other hand, the coupling attenuation in the case of a liquid-filled microannulus is similar to the case of a well-cemented casing (and different from a free pipe). The coupling attenuation has been shown to be fairly insensitive to all common sizes of water-filled microannuli [31]. The coupling attenuation is mainly sensitive to the acoustic impedance (AI) of the annular material (regardless of a shear coupling) and has strong similarities with the ultrasonic pulse-echo measurements presented in Section 2.3.3. As the microannulus only affects the propagation attenuation, this means that a long spacing CBL-amplitude measurement is more affected by a microannulus than a short spacing amplitude measurement. This also means that the

attenuation rate tools are heavily affected by a liquid-filled microannulus, as they measure the propagation attenuation rate.

Conventional sonic tools, on the other hand, measure the CBL *amplitude* and are therefore affected by both coupling- and propagation attenuation. This is shown in Figure 2.8 where the E_1 CBL amplitude is plotted for different microannulus sizes. The amplitude is normalized such that 0% corresponds to the well-cemented reading, while 100% corresponds to the free pipe reading in water. It can be seen that the CBL amplitude does not change much with the change in microannulus size due to a fairly constant coupling attenuation. However, it is significantly higher than the well-cemented value due to the lost propagation attenuation. This shows that the CBL is affected by liquid-filled microannuli of all sizes [15].

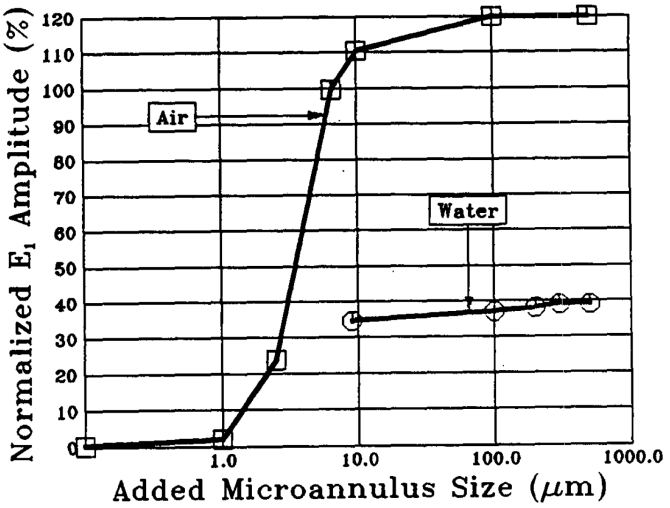

Figure 2.8: Effect of water- and air-filled microannulus on the CBL amplitude (3 ft spacing) [15].

Gas-filled microannulus: As shown in Figure 2.8, the microannulus effect is even more dramatic for a gas-filled microannulus. Experimental testing has shown that, in the case of a gas-filled microannulus, both the coupling attenuation and the propagation attenuation rapidly approach that of free pipe as the size of the microannulus increases [15]. The casing still appears well cemented at a size of 1 µm, but all sizes greater than approximately 6 µm resemble the amplitude of free pipe.

Field experience: Traditionally, a microannulus has not been considered problematic for the integrity of the annular cement. Rather, it has been considered a problem because it is hindering evaluation of the cement sheath behind the microannulus. A high-quality cement sheath of high acoustic impedance can be present, but with a slight separation of a few micron between the casing and cement, the CBL reports the cement job as poor, or even as free pipe. This is reflected in several efforts on how to reduce the "microannulus-effect" on the CBL [7, 14–16, 29, 31, 32]. On the other hand, little research addresses the effect of a microannulus on zonal isolation.

The solution to this problem has been to run the CBL under pressure to expand the casing and regain contact with the cement. This will regain the full attenuation, equal to that of a good casing-cement bond. If the microannulus effect vanishes when applying a moderate surface pressure, the cement job is typically considered successful. If the effect is still present, it is caused by channeling, poor mud removal or an even larger microannulus. A typical pressure applied is 1000 psi. For a typical production casing (9 5/8-in 53.5#), this will give a radius expansion of 31 µm using Equation 2.1. In other words; if the microannulus effect vanishes with 1000 psi added pressure, the size of the microannulus is less than about 31 µm. CBLs have been run with up to 6000 psi surface pressure [16]. It is always recommended to first run a CBL without pressure and to minimize the added pressure in any subsequent pressure runs, as exposing the casing for unnecessary high pressures could make the situation even worse by creating an even larger microannulus.

2.3.3 Ultrasonic Pulse-Echo Logging

In the early 1980's a new generation of cement evaluation tools was introduced [33]. These tools operate on a higher frequency than the conventional sonic logging tools, and are therefore referred to as ultrasonic logging tools. Ultrasonic cement logging was developed to overcome some of the deficiencies of the sonic tools, mainly the lack of azimuthal resolution and the high microannulus-sensitivity. The early ultrasonic tool design used 8 ultrasonic transducers arranged in a helical spiral around the tool to obtain circumferential coverage [33]. Today's tools use a single transducer mounted on a rotating sub to obtain circumferential coverage [34]. Measurements are performed between 36 and 100 times per rotation, giving full azimuthal coverage and a high azimuthal resolution [6].

2.3.3.1 Measurement Principle

The measurement principles of ultrasonic pulse-echo logging are summarized in Figure 2.9. The ultrasonic transducer emits a pulse containing acoustic energy in the range 200 to 650 kHz [8]. After emitting the burst, the ultrasonic transducer functions as a receiver and listens to the echo of the signal by recording the signal amplitude versus time. The tools are therefore often referred to as *pulse-echo* tools. The frequencies used, cover the resonant frequency of all common casings, which is given by:

$$f_0 = \frac{1}{\Delta t} = \frac{v_{p,csg}}{2h_{csg}} \tag{2.4}$$

where

$$\begin{aligned} f_0 &= \text{Resonant frequency of the casing} && [Hz] \\ \Delta t &= \text{Two-way travel time in the casing} && [s] \\ v_{p,csg} &= \text{Compressional wave velocity of the casing steel} && [m/s] \\ h_{csg} &= \text{Casing wall thickness} && [m] \end{aligned}$$

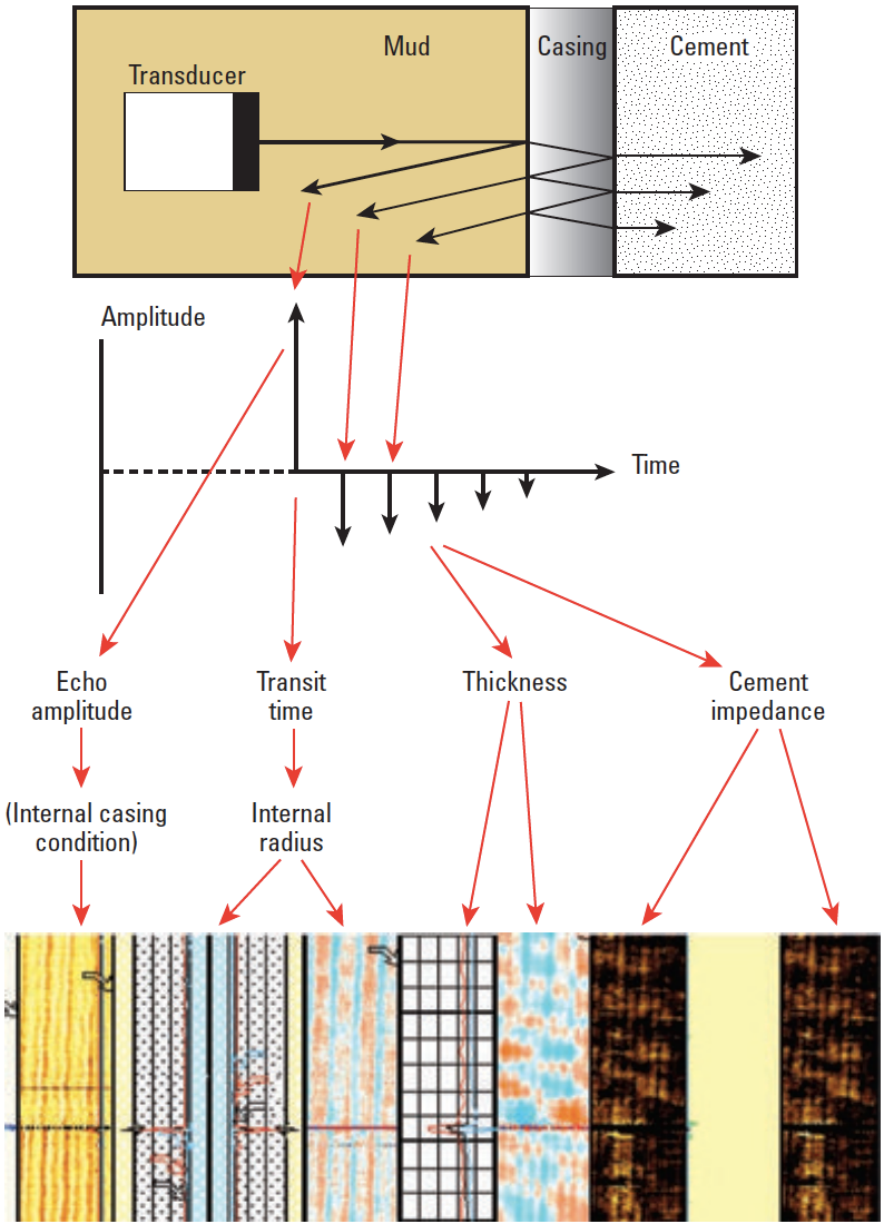

Figure 2.9: Measurement principles of ultrasonic pulse-echo cement evaluation [6].

The wave front is cylindrically focused, resulting in the wave front intersecting the casing parallel to the surface [8]. When the wave hits the casing wall, most of the signal will be reflected due to the high contrast in acoustic impedance (AI) at the mud-casing interface. This results in a large amplitude of the first echo, which is the reflected signal. The amplitude of the first echo can be used to obtain a qualitative indication of the inner casing wall condition. If the pipe wall is in a good condition, a high amplitude is expected as most of the signal will be reflected back to the transducer. A low amplitude corresponds to a high casing rugosity, as the signal will be scattered in several different directions when intersecting the casing wall.

The ultrasonic tool also functions as an ultrasonic caliper, giving the inner radius of the casing. This is done using the transit time between firing the transducer and measuring the first echo amplitude to calculate the distance from the transmitter to the casing (standoff):

$$S = \frac{t_1 v_{p,mud}}{2} \tag{2.5}$$

where

$$\begin{aligned} S &= \text{Transducer to casing distance (standoff)} && [m] \\ t_1 &= \text{Time from firing transducer to recording first echo amplitude} && [s] \\ v_{p,mud} &= \text{Compressional velocity of the wellbore fluid} && [m/s] \end{aligned}$$

By correcting for eccentricity (effectively moving the tool to center), the internal radius of the casing can be calculated by using the known tool dimensions. This can be used to indicate casing wear, corrosion, erosion, restrictions, etc. The tools use a built-in reflector to measure the properties of the wellbore fluid [6]. A transducer, either the rotating one or an additional one, is faced against the reflector to measure the acoustic compressional velocity and the acoustic impedance of the wellbore fluid.

The energy which is not reflected at the mud-casing interface will be transmitted into the casing where it will propagate back and forth between the two casing surfaces – each time losing some energy to the annulus and some energy to the wellbore. The energy lost to the wellbore will be picked up by the receiver as the resonance signal. By rewriting Equation 2.4, the wall thickness of the casing can be calculated using the measured frequency of the resonance signal:

$$h_{csg} = \frac{v_{p,csg}}{2 f_0} \tag{2.6}$$

Cement evaluation from ultrasonic pulse-echo logging is performed on the basis of the form of the resonance signal – a series of exponentially decaying amplitudes. The energy loss to the wellbore fluid is constant and can be estimated from the measured fluid properties. The energy loss to the annulus is dependent on the annular material – represented by the acoustic impedance of the annular material, which is the primary result of ultrasonic pulse-echo logging. This is illustrated in Figure 2.10, where it is shown that for a cemented casing, the resonance decays faster than for a free pipe (surrounded by a fluid). This is caused by the cement having a higher AI than the fluid, giving an increased dampening. Note that the resonance frequency, which is used for casing thickness calculations, is not affected by the presence or absence of cement.

The processing scheme for acquiring the AI of the annular material varies between the different tools. However, the basic principle is the same; the form of the resonance signal is used to infer the AI of the annular material. A map of the annular material's acoustic impedance is typically presented on the log (as shown in Figure 2.9). The AI of neat

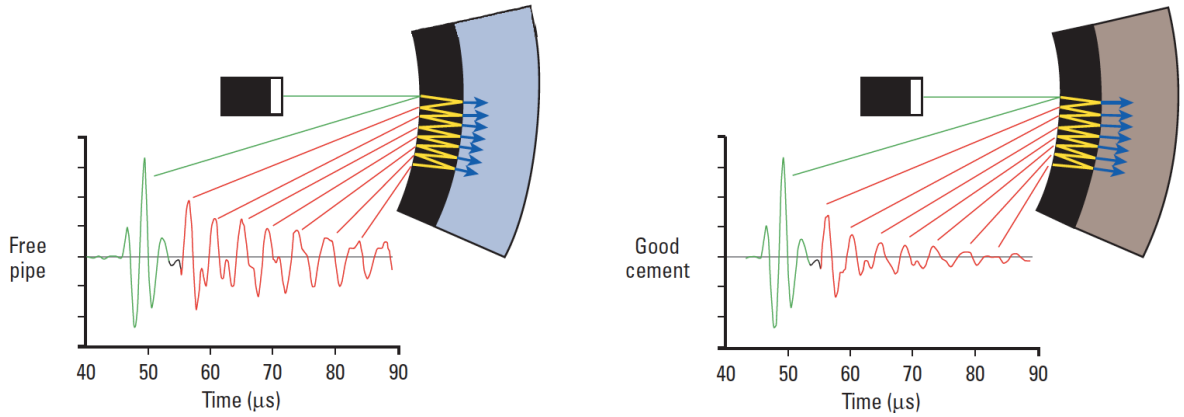

Figure 2.10: Decay of the ultrasonic resonance signal for a free pipe (left) and a cemented casing (right). Note that that the amplitude of the resonance signal (red) is magnified, compared to the initial echo amplitude (green) [6].

cement is about 6 MRayl [6]. For all common liquids (both water- or oil-based), the AI is in the range between 1 and 3 MRayl. This gives a good contrast between common liquids and common cement. Gas has an AI below 0.1 MRayl, providing an excellent contrast. However, this also causes gas acting as a barrier, totally reflecting ultrasound. This makes the ultrasonic logging tools prone to a gas-filled microannulus (further discussed later).

2.3.3.2 Challenges in Ultrasonic Pulse-Echo Logging

Casing rugosity: Rugosity on the first interface (inner casing wall) can heavily degrade the log results as it results in signal dispersion. The rugosity can be caused by e.g. corrosion, deposits or casing wear, and can give false indications of channeling [6]. The problem is fairly trivial to detect from a low first echo amplitude reading or from the casing radius or thickness measurement. This illustrates how all the available log data, not only the final cement AI map, should be included in the interpretation for log quality control and increased understanding of the downhole situation.

Heavy muds: Heavy muds pose serious issues to the ultrasonic measurement, because of high signal attenuation. This will reduce the signal strength, hence lower the signal-to-noise ratio. The signal attenuation in oil-based muds (OBMs) is approximately twice as high as in water-based muds (WBMs) of the same density [34]. The newer tools can tolerate heavier muds than the early tools and are typically limited by approximately 1.6 g/cm^3 in OBM and approximately 1.9 g/cm^3 in WBM [6].

Third interface echoes: The third interface, the cement-formation interface, is not included in the model used for processing of the resonance signal to give the AI. This means that, if echoes from the third interface appear within the measurement window, the model is no longer valid and the results are degraded. The phase of the third interface echoes (TIEs) compared to the casing resonance, will determine whether they will increase

or decrease the AI measurement. To minimize the problem, the measurement window is placed quite early. However, in certain situations, TIEs will affect the measurement. Factors increasing the problem are a thin cement sheath, low attenuation within the annular material (i.e. a hard and good cement), a high AI contrast at the third interface and a smooth surface at the third interface [6]. This is typically the case for concentric casing strings. High AI formations (like e.g. dolomite) also increase the probability of TIEs affecting the measurement. These are the same formations that were referred to as fast formations when discussing the CBL, as the AI is heavily dependent on the acoustic velocity. A thin cement sheath can also occur if the casing is eccentric, typically in highly deviated wells were the casing tend to drop towards the low side of the wellbore. As the ultrasonic tools have a good azimuthal resolution, this will show up on the log as a characteristic "galaxy pattern" caused by the interference from the third interface, centered around the azimuth corresponding to the narrow side of the annulus (typically the low side) [34]. These patterns are easily spotted on the log, and the AI-readings should not be trusted if they are present. However, the AI-reading on the high side of the hole may still be valid.

Cement-formation bond: The third interface echoes could be used to indicate the quality of the cement-formation bond. However, they are usually too weak to be exploited to infer the cement-formation bond quality, due to the high attenuation in cement. This means that the ultrasonic tools do not give an indication of the cement-formation bond, but is rather a measurement of the cement coverage right next to the casing. This is one of the reasons why the ultrasonic tools are typically combined with a sonic tool including a VDL-measurement for cement-formation bond evaluation.

Low-density cement: Lightweight cement can have an acoustic impedance as low as 2.5 MRayl [35]. Hence, these cement systems are difficult to evaluate using ultrasonic measurements, as their acoustic impedance is close to that of common liquids. If a relatively heavy mud is present in the annulus, the contrast between fluid and cement is even further reduced and they may even overlap. The accuracy of the ultrasonic pulse-echo tools is approximately 0.5 MRayl, meaning that there has to be a contrast of about 1 MRayl in order to confidently separate cement and fluids [35]. It is important to know what acoustic impedance to expect from both the fluid- and the cement system, when interpreting the AI cement map. This should also be considered when selecting the tools used for cement evaluation – there is no use of running a tool that is not capable of differentiating the used cement from the annular fluid.

2.3.3.3 Microannulus Response

Liquid-filled microannulus: The ultrasonic tools do not rely on a shear coupling between the casing and the cement, as the wave motion is normal to the casing wall. Hence, they are far less affected by a liquid-filled microannulus. In theory, the measurement should be unaffected by a shear coupling, if the waves intersect parallel to the casing

wall. However, in practice, the waves will intersect at an angle slightly different from the normal, giving an additional dampening in the case of a shear coupling [6]. This effect will cause a slight increase in the AI-reading for a well-bonded cement sheath, compared to a cement sheath with a slight separation to the casing. Other than that, the ultrasonic measurements are quite insensitive to a liquid-filled microannulus up to a certain size.

Experimental tests with an industry-leading ultrasonic pulse-echo tool have been performed to investigate the effect of a microannulus on the AI log result for a casing cemented with a neat cement [15]. The results are shown in Figure 2.11. It was found that the ultrasonic tool is fairly insensitive to a water-filled microannulus, up to a microannulus size in the order of 100 µm. For microannulus sizes much greater than 100 µm however, it becomes difficult to distinguish the cement from liquids. This allows for evaluation of the cement sheath for common sizes of liquid-filled microannuli in the field, without the need for a second logging pass with applied surface pressure (as for the CBL). This is one of the major advantages of the ultrasonic tools, together with the azimuthal resolution for channel detection. However, the effect on the microannulus itself on the integrity of the annular cement should be evaluated.

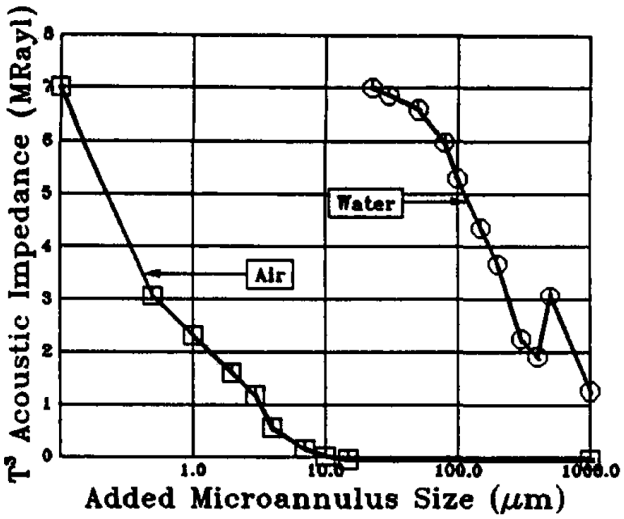

Figure 2.11: Effect of a water- and air-filled microannulus on the ultrasonic measurement [15].

Gas-filled microannulus: It is clear from Figure 2.11 that the ultrasonic tools are far more affected by a microannulus if it is gas-filled. The experiments conducted with air shows that a microannulus of 1 µm looks like a liquid, i.e. ultrasonic cement evaluation is impossible in this case [15]. For microannulus sizes approaching 10 µm, the AI reading reads as for a gas-filled annulus. This is one of the major weaknesses with the ultrasonic tools; even an extremely small gas-filled microannulus makes the measurement unable to detect an annular cement sheath due to the low AI of the gas. The gas acts as a barrier towards ultrasound and it is often said that, in the case of a gas-filled microannulus, an ultrasonic tool reads gas.

2.3.4 Flexural Ultrasonic Logging

In the later years, there has been a significant development in the design of low-density cement systems, mainly to avoid fracturing and losses in weak zones [36]. The acoustic impedance of such types of cement can be as low as 2.5 MRayl – overlapping with common drilling fluids [35]. As discussed, both sonic tools and ultrasonic pulse-echo tools struggle when evaluating lightweight cement due to the lack of impedance contrast between the cement and fluids. In addition, the ultrasonic pulse-echo tools are only sensitive to the cement immediately behind the casing and do not evaluate the cement-formation bond or defects within the cement sheath. To address these limitations, a new type of ultrasonic cement evaluation tools – flexural ultrasonic tools – was introduced in the mid-2000's.

2.3.4.1 Measurement Principle

A tool design consisting of four ultrasonic transducers is shown in Figure 2.12. One transmitter and two receivers (near and far) operating at 200 kHz are used for the flexural imaging [35]. In addition, there is a single transducer used for standard pulse-echo ultrasonic logging (as described in Section 2.3.3), mainly to give the AI of the cement (Z_{cem}). The pulse-echo transducer is oriented 180° from the three flexural transducers. All four transducers are mounted on the same rotating sub, to obtain an azimuthal resolution and coverage similar to the pulse-echo tools by sampling 36 times per rotation.

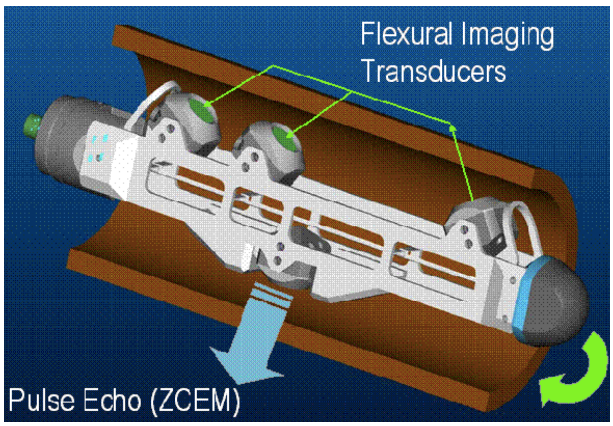

Figure 2.12: Rotating sub of a flexural ultrasonic logging tool, with one transmitter and two receivers for flexural imaging. A single transducer, spaced 180° apart, is used for the standard pulse-echo measurement [37].

When the ultrasonic wave emitted from the transmitter intersects the casing surface, *flexural* waves are generated in the casing [35]. The flexural wave is a type of plate wave occurring because the thickness of the casing is less than a few wavelengths [20]. It is also referred to as an asymmetric Lamb wave (not to be confused with the *symmetric* Lamb wave used for the CBL), and the particle motion is mainly perpendicular to the

plate. As the flexural wave propagates along the casing it is losing energy to both the wellbore fluid and the annular material. By comparing the signal amplitude at the two receivers, an attenuation rate which is insensitive to the attenuation within the borehole fluid can be calculated, as it only considers the effect of traveling the additional distance along the casing. The flexural attenuation rate is calculated by using the first amplitude measurement at the near and far receivers, as [37]:

$$\alpha_{flex} = \frac{20}{\Delta L} \log_{10} \frac{A_{near}}{A_{far}} \tag{2.7}$$

where

$$\begin{aligned} \alpha_{flex} &= \text{Flexural attenuation rate} && [dB/ft] \\ \Delta L &= \text{Spacing between the near and far transmitter} && [ft] \\ A_{near} &= \text{First amplitude reading at the near receiver} && [mV] \\ A_{far} &= \text{First amplitude reading at the far receiver} && [mV] \end{aligned}$$

The attenuation of the flexural wave as it travels along the casing is caused by the generation of compressional waves and shear waves in the adjacent material, as illustrated in Figure 2.13 [35]. In a fluid, only compressional waves can be generated, and the attenuation is approximately proportional to the AI of the fluid. If a solid material is present in the annulus (e.g. cement), the flexural wave can also be attenuated by the generation of shear waves – giving an increased attenuation. For a "slow" cement (with low AI), this results in an increased flexural attenuation rate, which is the basis of the measurement. However, in a "fast" cement (with high AI), no compressional waves are generated as the cement's compressional velocity is greater than the velocity of the flexural wave front in the casing. This results in the flexural attenuation first increasing with increasing AI,

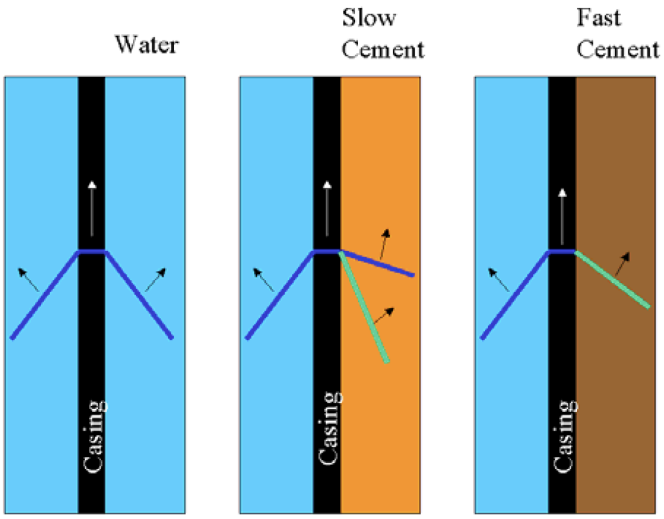

Figure 2.13: Flexural wave attenuation by compressional (blue) and shear (green) wave generation [35].

then when the compressional wave velocity in the cement exceeds that of the flexural wave in the casing, the flexural attenuation suddenly drops as the energy loss to compressional waves is lost. The point where this occurs is known as the evanescence point. The shear wave velocity in the cement is always less than the casing flexural wave velocity, such that shear waves are generated in all types of cement [35].

The flexural attenuation rate is used *together* with the AI from the ultrasonic pulse-echo measurement to infer the annular material adjacent to the casing. A solid-liquid-gas (SLG) map is generated, using the expected properties of the cement and mud in the annulus of the particular casing string. Gas is always defined as low AI and low flexural attenuation. An example of such an SLG map is shown in Figure 2.14, where the x-axis represents the AI-reading from the pulse-echo measurement and the y-axis represents the flexural attenuation rate. A typical low-density cement point is plotted. With only the AI-measurement of 2.5 MRayl, it would not be possible to discriminate this cement from a liquid. However, if a flexural attenuation rate of 0.6 dB/cm is also measured, it is possible to detect the cement by using the flexural attenuation rate in combination with the AI.

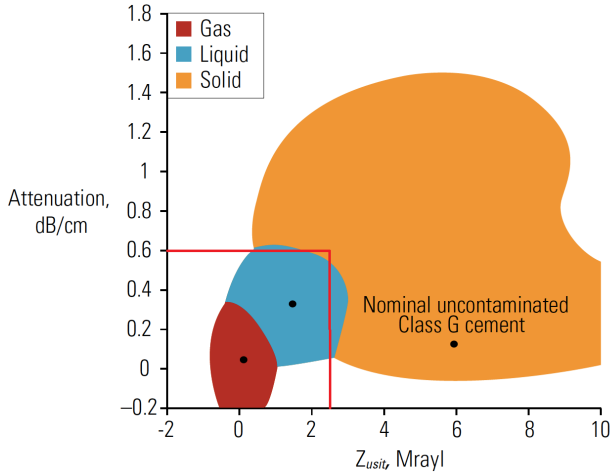

Figure 2.14: Example of an SLG map for combined pulse-echo and flexural cement evaluation with a typical low-density cement point [35].

Like the AI-reading from the pulse-echo ultrasonic logging, the flexural attenuation rate is only sensitive to the material immediately behind the casing. However, the waves radiated into the annular material as the flexural wave propagates along the casing may be reflected at the third interface (against the formation or an outer casing). These echoes can be detected at the receivers and are referred to as third interface echoes (TIEs). This is illustrated in Figure 2.15. Since the TIEs propagates through the annulus, they contain information about both the annular material and geometry. For the normal incidence pulse-echo logging, the TIE is too weak to be used for cement evaluation and is only considered disturbing for the estimation of the AI. For the flexural tools, on the other hand, the TIE can be used to evaluate the cement sheath, beyond the casing-cement interface [35]. Figure 2.15 also shows a simulated received waveform for a water-filled annulus and a hard formation. This gives a large acoustic contrast at the third interface,

resulting in a large amplitude of the TIE for the flexural measurement. By comparison, the TIE from the normal incidence pulse-echo measurement is barely visible.

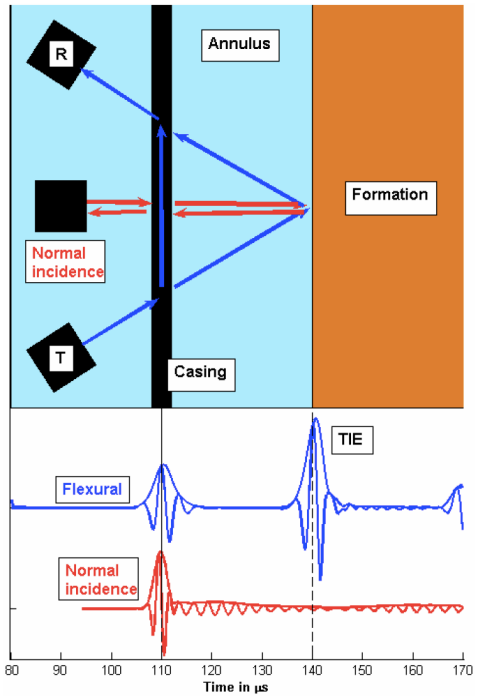

Figure 2.15: TIE from both pulse-echo logging (red) and flexural logging (blue) [35].

The difference in travel time between the casing flexural wave arrival and the TIE arrival is used for evaluating the annular cement and geometry. Note that, since the difference between the two travel times is used, the measurement is independent of the wellbore fluid, the tool standoff, and the transmitter-receiver spacing. It only depends on the annular thickness and the wave velocity in the annular material. As the measurements are sampled around the borehole as the tool rotates, it is possible to calculate the casings eccentricity as a dimensionless unit (assuming a uniform velocity of the annular material with respect to azimuth). If either the annulus thickness or the annular wave velocity is known, the other can be calculated from the difference in travel time. For example, if the size of the borehole or the outer casing is known, the wave velocity of the annular material can be calculated as:

$$v_{ann} = \frac{2h_{ann}}{\delta t} \tag{2.8}$$

where

$$\begin{aligned} v_{ann} &= \text{Wave velocity of annular material} && [m/s] \\ h_{ann} &= \text{Annulus thickness} && [m] \\ \delta t &= \text{Transit time difference between TIE and casing flexural wave} && [s] \end{aligned}$$

For a fluid, this would represent the compressional velocity, as only compressional waves are generated in the annulus. For a fast cement, it would represent the shear wave velocity. For a slow cement, both compressional TIEs and shear TIEs could be generated, and both velocities could be calculated (if both echoes are detected). Equation 2.8 is often used to produce a velocity map showing the velocity of the annular material as a function of depth and azimuth. Contrary, if the velocity of the annular material is known, the annulus thickness can be calculated by rearranging Equation 2.8 to give the annular thickness.

2.3.4.2 Challenges in Flexural Ultrasonic Logging

High-density cement: High-density cement typically has a compressional wave velocity greater than the flexural wave velocity in the casing. This results in low attenuation of the flexural wave as there is no radiation of compressional waves in the cement sheath. Therefore, such cement systems will have a flexural attenuation rate close to that of liquids and would not be possible to detect by the flexural attenuation alone. This is reflected by the point for neat class G cement shown in Figure 2.14. However, using the AI from the ultrasonic pulse-echo measurement to detect the cement is straightforward as there is a good AI contrast (compared to liquids) for these types of cement.

Undetectable TIE: Often, it is not possible to detect the third interface echoes, usually because their amplitude is too low, making it impossible to discriminate the TIE from background noise [35]. Factors reducing the amplitude of the TIE are highly attenuative annular material like contaminated or foamed cement, large annuli giving an increase in traveled length of the TIE, and a low acoustic contrast at the third interface. In addition, factors that are changing the direction of the signal reflected at the third interface will also reduce the measured amplitude, as less of the energy is reflected towards the receiver. This includes high surface roughness, as well as casing eccentricity in the wellbore. Following these factors, the expectation of detecting the TIEs is significantly greater in a concentric casing section, than for a casing cemented in an open hole.

Multiple unknowns: The difference in travel time between the TIE and the flexural wave is dependent on both the thickness and the wave velocity of the annular material. This means that one of the two has to be known (or assumed), in order to calculate the other through Equation 2.8. Often, a velocity map is presented based on the wellbore dimensions, as described earlier. This requires a good understanding of the annular geometry, in order to make valid assumptions and would probably work well in a concentric casing section. However, for a casing cemented in an open hole, the hole size could differ significantly from the bit size. This means that an apparent change in velocity on the velocity map could be caused by a change in wellbore dimensions and not a change in velocity. Caution should be taken before calculating such “pseudo-variables”, and the best log representation is often the primary measurements themselves: The flexural attenuation rate, the TIE amplitude and the difference in travel time between the TIE and the flexural wave. The full waveform of the measurement can also be presented in

a two-dimensional VDL-format as shown in Figure 2.16. This is a good visualization of the logged environment and as for the CBL, displaying the full waveform of the signal is beneficial for increased understanding and improved quality control. On a log presentation, this VDL would typically be presented for two perpendicular planes; one oriented in the 0°-180° direction and one in the 90°-270° direction. Attempts have been made to transform this from the time-domain to the distance-domain [37]. However, this requires a good knowledge of the velocity of the annular material and should be done with caution.

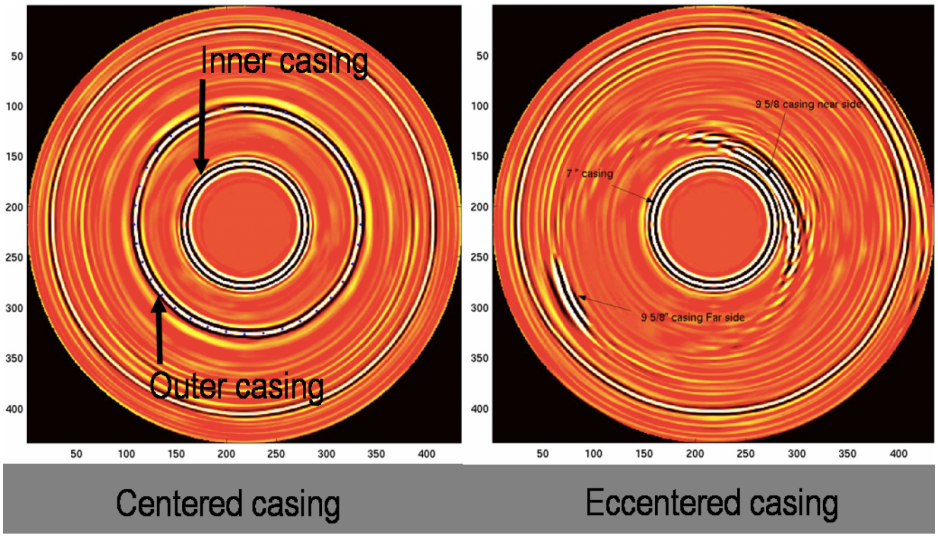

Figure 2.16: Two-dimensional VDL from flexural ultrasonic logging showing a 7-in casing centered and eccentered within a 9 5/8-in casing. Also notice how the casing eccentricity significantly reduces the amplitude of the TIE from the outer casing [37].

2.3.4.3 Microannulus Response

Liquid-filled microannulus: For a slow cement (compressional wave velocity less than the flexural wave velocity of the casing), the response of the flexural ultrasonic logging tools to a liquid-filled microannulus has been shown to be similar to that of the pulse-echo tools [35]. As soon as the casing-cement bond is lost, the flexural attenuation rate is reduced by approximately 15%, most likely owing to the loss of shear coupling. Apart from that, the flexural attenuation measurement is not significantly affected by a liquid-filled microannulus up to about 250 µm, which is in the same order as for the pulse-echo tools.

For a fast cement, a large increase in flexural attenuation is seen as soon as the cement is debonded [35]. This may be caused by the liquid-filed microannulus allowing for the radiation of compressional waves to the annulus, which effectively would increase the attenuation of the flexural wave compared to the case of only radiation of shear waves. Also here, the flexural attenuation measurement is further fairly insensitive to a liquid-

filled microannulus up to approximately 250 µm.

Gas-filled microannulus: The response of the flexural ultrasonic tools to a gas-filled microannulus is similar to that of the ultrasonic pulse-echo tools [38]. Gas has an AI close to zero and acts like a barrier towards ultrasound, making a gas-filled microannulus read gas.

2.3.5 Conclusion on Current Cement Evaluation Methods

Significant development has taken place within the field of acoustic cement evaluation since the CBL was introduced in 1961. What is interesting, is that even though new tools and technologies have been developed, the older ones have not become obsolete. A modern cement evaluation logging string includes a flexural tool, an ultrasonic pulse-echo tool, as well as a sonic CBL/VDL. This reflects the fact that every tool has its deficiencies, and that none are perfect as a stand-alone tool. However, with the combination of the different tools, most of these deficiencies are overcome and cement evaluation becomes superior to any of the tools run individually. This is reflected in Table 2.1, where the advantageous characteristics (green) and the disadvantageous characteristics (red) of the acoustic cement evaluation tools are summarized. The table is based upon the characteristics presented throughout this section, as well as the following sources [38,39]. A typical cement evaluation tool string used today, consisting of a combination of a CBL/VDL, an ultrasonic pulse-echo tool and a flexural ultrasonic tool is shown in the rightmost column.

Table 2.1: Summary of the characteristics of the acoustic cement evaluation methods. The combination of the three techniques is shown in the rightmost column.

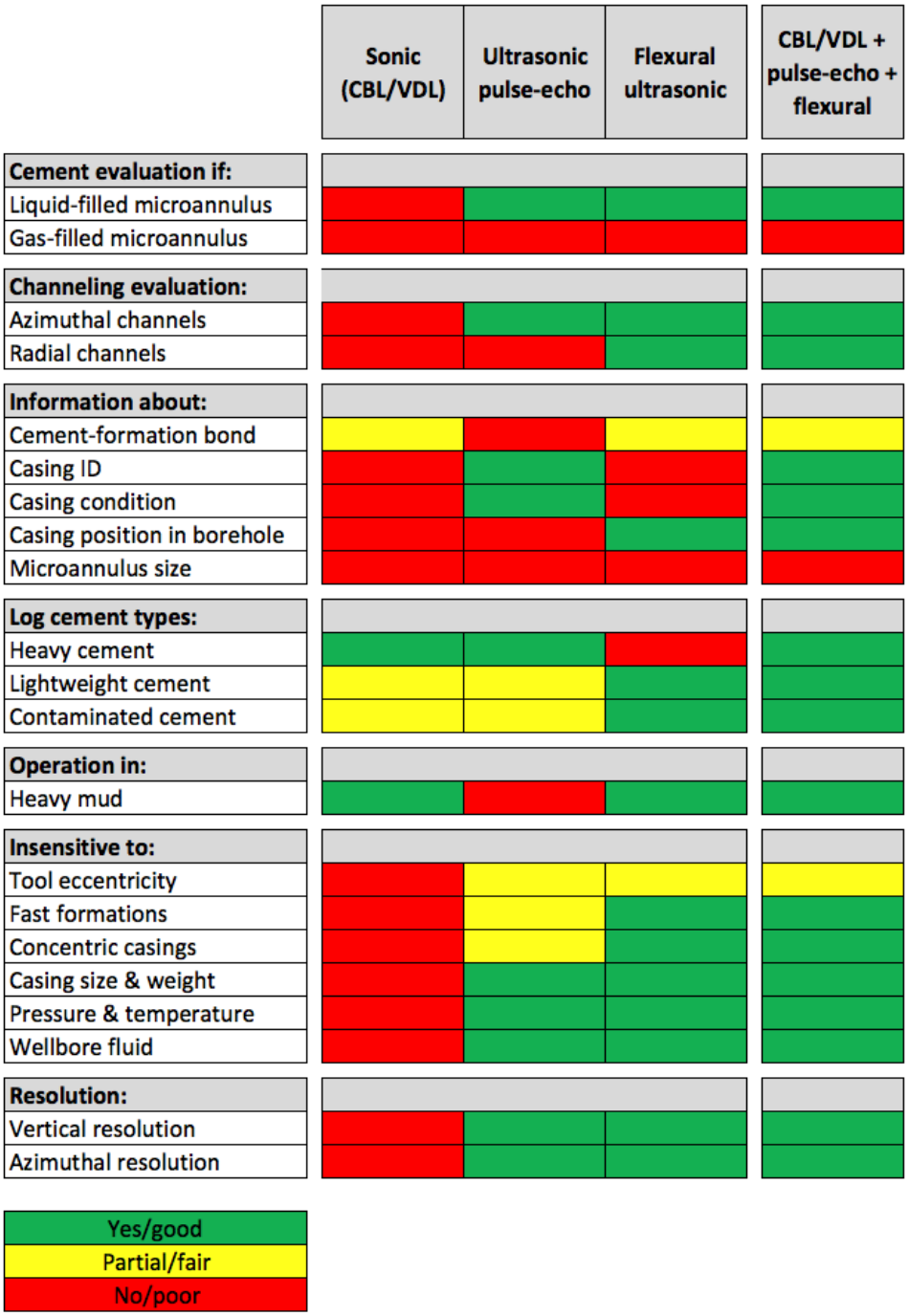

Chapter 3

A Novel Tool for Cement Evaluation – The Annulus Verification Tool

3.1 Background

The Annulus Verification Tool (AVT) is a novel logging tool developed at the Department of Geoscience and Petroleum (IGP) at the Norwegian University of Science and Technology (NTNU). The tool is designed with the objective to detect and quantify the size of a microannulus at the casing-cement interface. As presented in Section 2.2, a microannulus often occurs at the casing-cement interface and knowing its size is crucial for determining its effect on the integrity of the well. The industry-standard cement evaluation tools presented in Section 2.3, are all to a different degree affected by the microannulus. Hence, detecting a microannulus is typically not a big challenge with the existing technology. However, none of the tools are able to quantify the size of the microannulus, hence neither the effect it has on the integrity of the well. The AVT is therefore intended to complement the acoustic cement evaluation tools, in situations where a microannulus is either detected or suspected. Detecting and quantifying the size of a potential microannulus will increase the understanding of the situation, giving a foundation to take better decisions regarding the cement sheath's sealing capability.

3.2 Measurement Principle

The basic principle behind the AVT is illustrated in Figure 3.1. A mechanical force is applied radially to the inner casing wall, while the displacement of the casing wall is recorded. This gives a measurement of the stiffness of the casing and the surrounding material, and a linear response is expected as long as the deformations are within the linear elastic region. The underlying principle is that a casing supported by an annular cement has a greater stiffness than an uncemented casing. In the case of a well-cemented

casing, the combined stiffness of the casing, cement, and the surrounding formation will be experienced, as illustrated by the blue line. For an uncemented casing, the stiffness will be significantly lower as the casing is not backed by a cement, but a fluid. As the annular volume is large compared to the volume change caused by the displacement, there will be insignificant support from the annular fluid, such that only the stiffness of the casing itself will be experienced – as illustrated by the green line. In the case of a casing-cement microannulus, the casing will be unsupported as displacement starts, such that only the casing stiffness will be experienced for the initial displacement. However, as the force and displacement increase, the casing is pushed towards the cement and contact will be obtained as the microannulus is closed. At this point, the stiffness of the system will increase from only the casing stiffness to the combined stiffness of the casing, cement, and formation (as for a well-cemented casing). This is illustrated by the red line. The point where contact between casing and cement is obtained and an increase in stiffness is observed corresponds to the size of the microannulus.

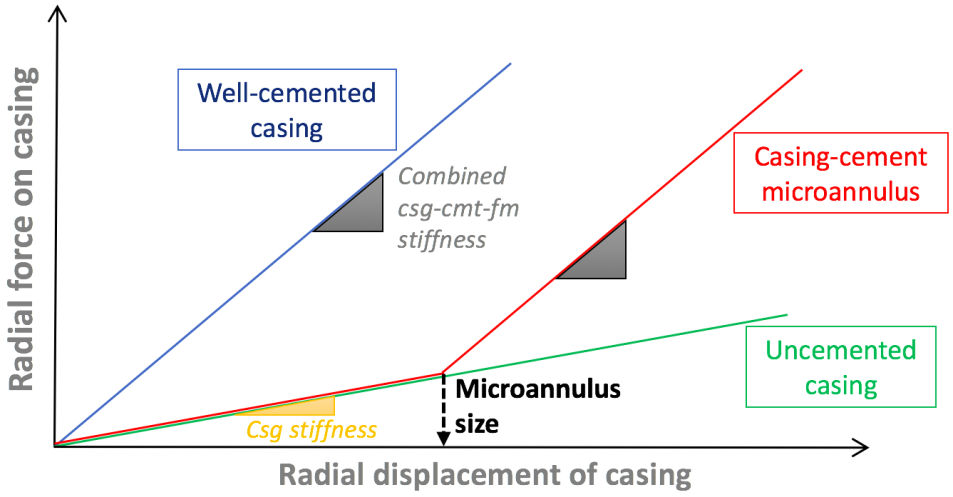

Figure 3.1: Measurement principle of the AVT.

A schematic of a prototype of the AVT is shown in Figure 3.2. The tool consists of two radial pads (5) with a curvature matching that of the inner casing wall. The two pads are spaced 180° apart and each pad is mounted on a piston (4 & 19). As the tool barrel (2) is pressurized with a hydraulic fluid, the pressure will act on the two pistons, making the pads move towards the casing. When the pads contact the casing wall, an increasing pad force is applied as the hydraulic pressure is further increased. Each piston is loaded by a spring (not shown in the figure), to make the pistons retract when the pressure is relieved.

Diametral Displacement

To be able to quantify the size of a microannulus, the casing displacement has to be measured with high resolution, as a microannulus is less than a few hundred micrometers

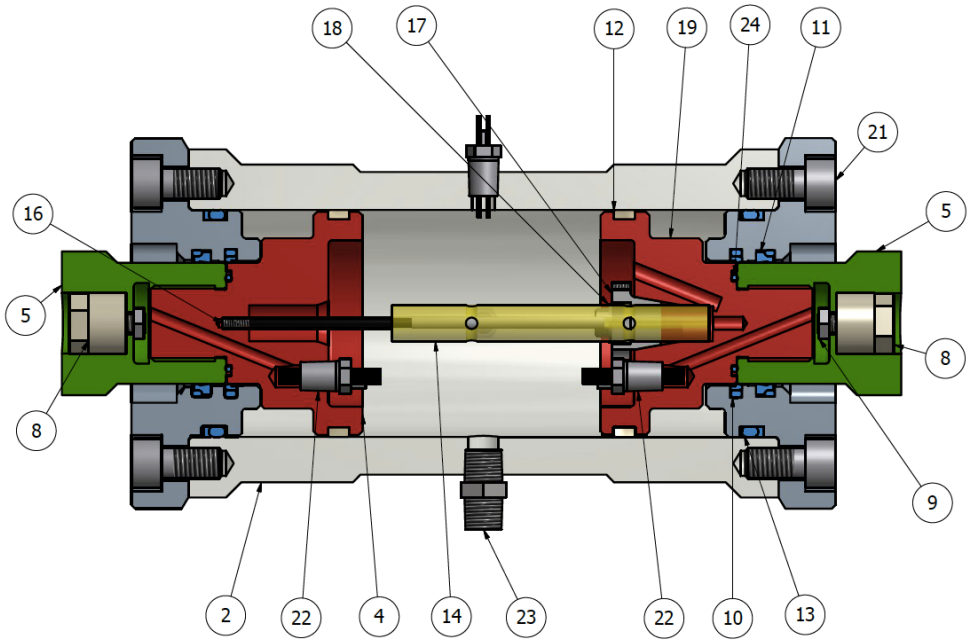

Figure 3.2: Schematic of a prototype of the Annulus Verification Tool. See text for explanation of the tool parts.

thick. For this purpose, a linear variable differential transformer (LVDT) is used. An LVDT is an electromagnetic transducer that converts the rectilinear motion of an object to an electric signal [40]. It is environmentally robust, friction-free and inherently has infinite resolution. However, the resolution is limited by noise, in addition to the signal conditioning equipment used.

The two moving pistons are coupled mechanically to the LVDT through a core (16) and a coil (14) assembly, as shown in Figure 3.2: One of the pistons is coupled to the LVDT core, while the other is coupled to the LVDT coil assembly. The coil assembly consists of three windings; one primary winding in the center which is excited by an input AC power, between two secondary windings. The secondary windings are identical and symmetrically positioned to the primary. The motion of the core relative to the coil assembly gives rise to a changing differential voltage, which is a linear function of the motion. Since the two pistons coupled to the LVDT are also coupled to the tool's pads, the LVDT can be calibrated to give the distance between the two pads, corresponding to the outer diameter of the tool. The diameter can then be recorded as the force is applied to the casing wall, enabling a measurement of the diametral displacement of the casing.

Radial Pad Force

When pressurizing the tool barrel, the force on the pistons will be dictated by the over-pressure (compared to the outside of the tool) exerted on the piston area:

$$F_{piston} = \Delta p A_{piston} \tag{3.1}$$

where

$$\begin{aligned} F_{piston} &= \text{Piston force exerted by hydraulic fluid} && [N] \\ \Delta p &= \text{Overpressure inside tool body} && [Pa] \\ A_{piston} &= \text{Area of piston} && [m^2] \end{aligned}$$

This piston force will be opposed by the spring that loads the piston. The springs are used in their linear-elastic region, meaning that Hooke's law can be used to express the spring force. As the LVDT measures the diameter and do not provide two independent radius measurements, the equation is rewritten in terms of diameter, giving:

$$F_{spring} = k(r - r_0) = k\frac{d - d_0}{2} \tag{3.2}$$

where

$$\begin{aligned} F_{spring} &= \text{Spring force} && [N] \\ k &= \text{Spring constant} && [N/m] \\ r &= \text{Radius of tool (distance from tool center to pad surface)} && [m] \\ r_0 &= \text{Radius of tool at spring equilibrium} && [m] \\ d &= \text{Diameter of tool (distance between the two pad surfaces)} && [m] \\ d_0 &= \text{Diameter of tool at spring equilibrium} && [m] \end{aligned}$$

The pad force applied on the casing wall will also oppose the piston force. From Newton's first law, it follows that the sum of the pad force and the spring force will equal the piston force if the pistons are stationary or moving at a constant speed. Applying Equations 3.1 and 3.2 gives the resulting pad force as

$$F_{pad} = F_{piston} - F_{spring} = pA_{piston} - k\frac{d - d_0}{2} \tag{3.3}$$

where

$$F_{pad} = \text{Pad force applied to casing} \qquad [N]$$

Here, the friction as the pistons move is not taken into account. In reality, there will be some friction (especially in the seal areas) and the friction force could be estimated and included in Equation 3.3. However, it is included in the spring characteristics (spring constant and equilibrium diameter) due to the procedure used for determining these, as explained in Section 4.2.3.

Casing ID

A more detailed description of the AVT's logging response in three different cases is shown in Figure 3.3. Prior to the pads obtaining contact with the casing wall, it is only the resistance within the tool (caused by the springs), that oppose the motion. In other words, the piston force will equal the spring force and the pad force is zero. As the pads obtain contact with the casing wall at diameter d_1, the pad force will start increasing. This gives a direct measurement of the inner diameter (ID) of the casing.

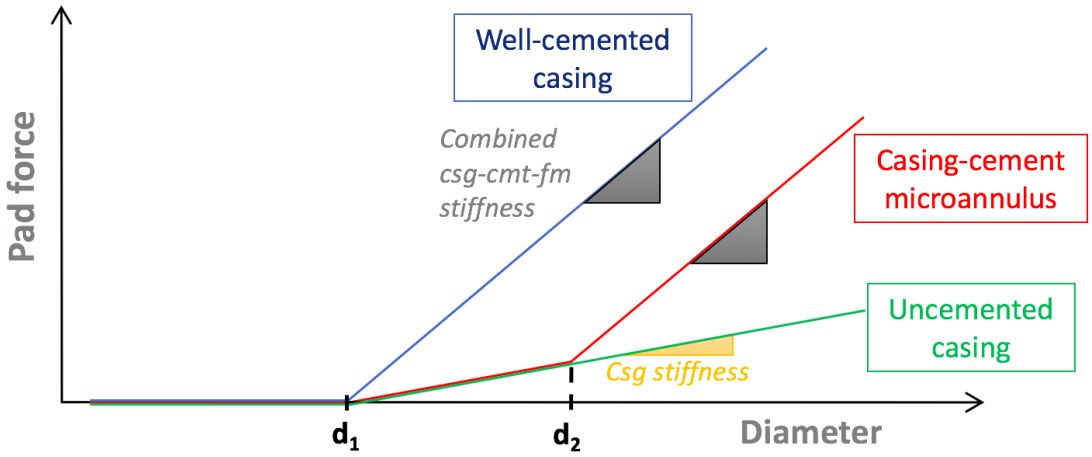

Figure 3.3: Logging response of the AVT in three different cases.

Cement Presence

If cement without a microannulus is present in the annular space, a large stiffness caused by the composite stiffness of the casing, cement, and formation is experienced immediately after obtaining pad-to-casing contact at diameter d_1, as shown in Figure 3.3. Hence, this can be used to prove the presence of an annular cement sheath. This could possibly also serve as a measurement of the cement quality, as the stiffness will depend upon the mechanical properties of the cement. If the casing is uncemented, only the stiffness of the casing itself should be observed. Note that an annular cement sheath can be proven, even in the case of a microannulus. As the pad force is increased, the microannulus will eventually be closed and the stiffness of a cemented casing should be experienced – proving the presence of cement. If the microannulus does not close at the maximum applied force, it could be caused by an even larger microannulus, a mud layer, a large channel in the cement sheath, or simply an uncemented casing.

Microannulus Size

In the case of a casing-cement microannulus, only the stiffness of the casing is experienced as the displacement continues after contact is obtained at diameter d_1. Then, when contact

between the casing and cement is obtained as the microannulus is closed at diameter d_2, further displacement will experience the combined casing, cement, and formation stiffness (as for a well-cemented casing). This is seen as an increase in the slope of the line at diameter d_2 in Figure 3.3. By assuming that the microannulus width is identical in the two pad directions, the difference between diameters d_2 and d_1 equals two times the width of the microannulus. Following this, the size of the microannulus can be calculated as:

$$\begin{aligned} d_2 - d_1 &= 2w_{ma} \\ \implies w_{ma} &= \frac{d_2 - d_1}{2} \end{aligned} \tag{3.4}$$

where

$$\begin{aligned} w_{ma} &= \text{Size of the microannulus} && [mm] \\ d_1 &= \text{Diameter at the first change in slope} && [mm] \\ d_2 &= \text{Diameter at the second change in slope} && [mm] \end{aligned}$$

Since the microannulus is situated at the outer casing wall, while the fixation points of the LVDT (which is measuring the displacement) is situated at the tool's pistons, this assumes that no deformation of the material between these points is taking place. In reality, there will be small deformations of the tool pads and the casing wall as the force is increased. Hence, the displacement measured with the LVDT will be somewhat greater than the displacement of the outer casing wall. However, these deformations are expected to be rather small as the casing is expected to deform by *ovalization*. In the case of a microannulus, the casing is not bonded to the cement and will have a relatively small resistance against ovalization. The resistance against *compressing* the steel of the casing wall or the tool pads, however, is believed to be significantly higher, such that Equation 3.4 can be used to quantify the microannulus size with reasonable accuracy.

Acoustic Measurements

As the pad force is applied to the casing, deformations will occur in the surrounding material; casing, cement, and formation. Sudden deformations of the material will release energy in the form of acoustic waves, referred to as acoustic emission (AE) [41]. To obtain additional information from the AVT, ultrasonic transducers (8) can be installed within the pads of the tool. The transducers are AE sensors recording any acoustic emission from the surrounding material during logging. Sudden changes/deformations like cracking of the cement or cement debonding should be possible to discriminate from the background noise. This will help increase the understanding of the downhole situation, as well as enable an evaluation of possible damage imposed to the cement sheath by logging.

3.3 Challenges with the AVT

Tool Centralization

To obtain a proper measurement of the stiffness of the casing and any adjacent material, the AVT has to be centralized and aligned within the casing to obtain the desired contact between the pads and the casing wall. If the tool is either eccentric or tilted with respect to the casing, the curvature of the pads will not match the curvature of the casing. First of all, this will result in the pads obtaining contact with the casing at a diameter which is less than the ID of the casing. Secondly, the improper alignment will give an apparent lower stiffness as only part of the pads is in contact with the casing, increasing the pressure exerted on local regions of the casing wall. If these areas or the tool's pads are deformed significantly, more and more of the pad area will contact the casing wall, giving a gradual increase in the recorded stiffness. If the eccentricity is modest, full pad contact could eventually be obtained and the stiffness should approach a value similar to as if the tool was properly centralized.

Improper centralization is especially challenging with respect to microannulus detection and for estimating the size of it, as the effects of eccentricity occur early in the displacement – coinciding with the microannulus response. This will render it difficult to pick the diameter where contact is obtained, as well as the diameter where a change in stiffness should be observed. Detecting the presence or absence of an annular cement sheath, however, should still be possible if full pad contact is eventually obtained.

The tool will be, to a certain degree, self-centralizing as the tool will tend to pull itself towards a centralized position when the pads start to push against the casing wall. This effect will be strongest along the axis of the pads, while eccentricity perpendicular to the pad movement is expected to be more challenging. The tool should be fitted with a sufficient number of centralizers to ensure proper tool centralization. This is not a new challenge, as the acoustic logging tools – especially the CBL/VDL – also require sufficient centralization. Nevertheless, the AVT is believed to be rather sensitive to eccentricity.

Changes in Casing Size or Weight

The pads are designed to match the curvature of a specific casing, meaning that if the casing size or weight changes along the interval that is to be logged, logging is not possible with the same tool. However, this is known on beforehand and could be solved by stacking two (or more) AVTs, to enable logging of several casing sizes or weights in a single run.

Irregular Casing Wall

Corrosion or erosion of the casing, as well as casing wear from drilling operations, can change the curvature of the casing wall or increase the roughness of the surface. This will result in insufficient pad contact area, hence giving similar effects as discussed for the case of eccentricity.

Solids

Solids in the wellbore may alter the measurement if they are pinched between the pads and the casing wall. This could be debris or precipitation on the casing wall, or simply weight material in the wellbore fluid. Conventional barite used as a weighting agent in drilling fluids (API barite) has particle sizes ranging from 2 to 100 micrometer [42]. One could imagine such particles disturbing the measurement as their size is in the range of common microannulus sizes. In deviated wells, solids will tend to gather at the low side of the wellbore, and the problem could be minimized by not logging with a pad oriented towards the low side.

Stationary Measurement

The nature of the AVT necessitate stationary measurements, while the acoustic tools used for cement evaluation today are logging continuously as they are pulled up the wellbore, typically at a speed of 500-1,000 meters per hour [43]. If running a combined string (with acoustic logs and AVT), the string has to be stopped when AVT-measurements are to be performed. However, the need for AVT-measurements and in what intervals to perform them should be evaluated by using the acoustic log results – either in real-time or from a previous run. AVT-measurements should then be performed in any intervals where a microannulus is suspected, based on the acoustic logs. By also recording the AVT-measurements in real-time, the number of AVT-measurements could be limited as the understanding of the downhole situation is increased during the logging run.

Cement Channeling

Cement defects with respect to azimuth, such as channeling, will complicate the measurement. The logging response will depend on what direction the pads are oriented with respect to the azimuthal cement defects. However, channeling should be detectable from the ultrasonic measurements. AVT-measurements have a limited value in the case of channeled cement, and should not be taken in such intervals.

Partial Microannulus

The response illustrated by Figure 3.3 and the microannulus size calculated through Equation 3.4 assumes a uniform microannulus of constant width around the circumference of the casing. If the microannulus size differs in the directions of the two pads, the microannulus size calculated through Equation 3.4 will be an average of the two sizes, since the diameter is measured. For example, if a 100 µm microannulus is present at one of the pads while the cement is perfectly bonded in the opposite direction, a microannulus size of 50 µm will be calculated. As discussed in Section 2.2.2, the permeability of the microannulus – and hence the leak rate through it – is strongly dependent on the size of the microannulus. Following this, it is clear that a microannulus of 100 µm at half the casing circumference will give a higher leak rate than a 50 µm microannulus at the entire circumference of the casing. Measurements could be performed in different azimuthal directions to evaluate this.

Cement Sheath Damage

In the case of good cement without a microannulus, the AVT may damage the cement sheath in the direction of the pad force, by inducing cracks. If a large stiffness is identified, further pressurizing should be stopped when cement has been confidently verified, to minimize the damage to the cement sheath. This also applies to cases with a microannulus: When the gap between the casing and cement is closed and the cement sheath is confidently identified, further pressurizing should be avoided. However, the damage will be local, and the affected region is rather small. The AE measurement will assist in detecting any damage induced to the cement sheath.

Casing-Cement Debonding

When the pads are expanding the casing in the direction of the pad movement, the casing will retract in the direction perpendicular to the pad movement. This ovalization could break an initially existing bond and separate the casing and the cement – essentially creating a partial microannulus. This is another reason why logging should be discontinued as soon as the cement is confidently proven. On the other hand, the ovalization of a well-cemented casing is rather small, as the casing will not deflect much due to the large stiffness. For an uncemented casing or in the case of a microannulus, the ovalization will be greater. However, this is not an issue as there is no bond initially existing.

Cement-Formation Microannulus

If a microannulus exists at the cement-formation interface, the log response will be somewhat different. In theory, the combined stiffness of the casing and the cement sheath

should be experienced for the early displacement. When the cement obtains contact with the formation, the combined stiffness of casing, cement, and formation should be experienced. This will give a lower contrast in stiffness compared to the case of a casing-cement microannulus, making a cement-formation microannulus more difficult to identify. Also, it moves the point of interest (the microannulus) further away from the displacement measurement (the LVDT), hence reducing the accuracy of the measurement.

Insufficiently Set Cement

If the annular cement is not fully set, it will result in an incomplete stiffness. This means that the cemented stiffness is closer to the free pipe stiffness, making the cement more difficult to detect with the AVT. In the case of a microannulus, the change in slope will be less evident, complicating the microannulus evaluation. As it can take several days for the cement properties to stabilize [44], this would be problematic if logging a casing just cemented (prior to drilling ahead). In the context of evaluating an existing annular cement in P&A, however, this would pose no problems.

Chapter 4

Experimental Testing

This chapter describes the experimental work performed, to test a prototype of the Annulus Verification Tool (AVT). Further specifications on the parts and equipment used in the experimental work described throughout this chapter, can be found in Appendix E where the data sheets are included.

4.1 Sample Construction

To facilitate for experimental testing of the AVT, a laboratory set-up for construction of full-scale diameter samples representing a casing/cement/formation system has been designed. The set-up consisted of two concentric pipes representing the formation and the casing, and the annular volume between the two was cemented with a standard well cement. During the course of this work, the laboratory set-up has been modified based on the experience gained throughout the process. This section describes the laboratory set-up used, the procedures used for sample construction, evaluation of the resulting samples, and the actions implemented to improve sample construction. A summary of all the samples constructed in the laboratory is included in Appendix B.

4.1.1 Cementing Procedure

For cementing of the annulus, Portland API Class G cement was mixed with a water-cement weight ratio of 0.44, according to ISO 10426-1 (equivalent to API Spec 10A) [45]. To represent a realistic well cementing procedure as best as possible and minimize the air entrapped in the slurry, the annulus was cemented from the bottom and up using the equipment shown in Figure 4.1. The cement slurry was poured into the funnel and distributed in the annulus through several 1/2-in hoses placed at the bottom of the annulus – three or four hoses were used to ensure proper azimuthal distribution of the cement. A ball valve (operated by the red handle) was closed when the top of cement approached

the height of the sample and the hoses were slowly pulled out. To compensate for the displacement of the hoses, the ball valve was slightly opened as the hoses were pulled upwards (not unlike setting a balanced cement plug). It was ensured that the funnel stayed filled with cement during the entire process, to avoid air entering the hoses and ending up in the annular cement.

Figure 4.1: Equipment rigged up for cementing of the annulus.

4.1.2 Initial Set-Up Using Aluminum Pipe

Figure 4.2 shows a schematic of the initial laboratory set-up that was designed to construct full-scale diameter samples. A 9 5/8-in (244.5 mm) outer diameter (OD) 53.5 lb/ft P-110 casing with an inner diameter (ID) of 8.535 inch (216.8 mm) was used. For representing the formation, a 320 mm OD aluminum pipe of 6082 T6 alloy was chosen. Its ID was 290 mm, hence representing a borehole diameter of 11.42 inches. This resulted in an annulus between the casing and aluminum pipe with a thickness of 22.8 mm. The aluminum pipe was chosen, as it provides a stiffness resembling that of a typical formation (Young's modulus of about 15 GPa). If actual formation was to be used, a large and inconvenient formation sample would be necessary in order to provide the sufficient stiffness. In addition, as aluminum allows radiant energy to pass through it with little attenuation, it provides the opportunity to use X-ray computed tomography (CT) scanning of the sample to investigate the quality and condition of the cement – both before and after experimental testing. The height of the test rig was chosen to 25 cm.

The casing and the aluminum pipe were placed on a rubber underlay and a silicone sealant

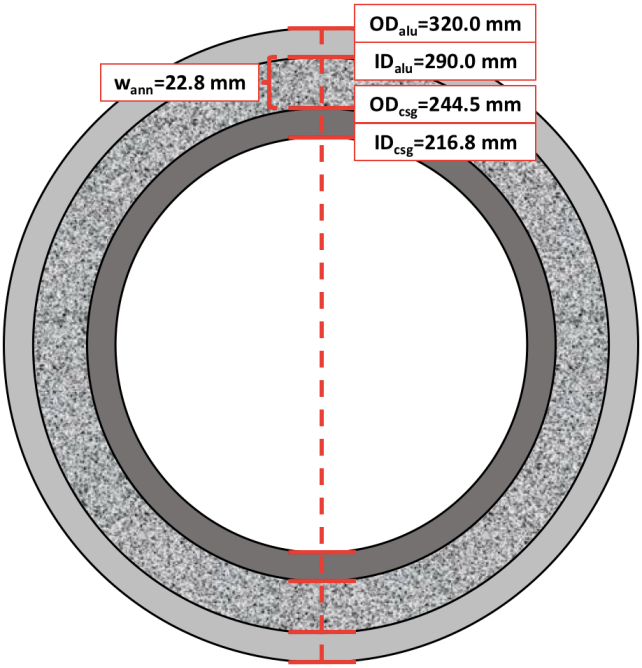

Figure 4.2: Schematic top view of the initial setup for construction of samples, showing the casing, cement and aluminum pipe with dimensions.

was applied to create a seal in the bottom of the annulus to avoid leakage of the cement slurry. A heating cable was wound onto the aluminum pipe and a thermistor was mounted at the top surface of the pipe to monitor and control the temperature. The aluminum was pre-heated to the chosen curing temperature, before cementing as described in Section 4.1.1. The temperature was kept constant during cement hydration.

To be able to also construct samples with a microannulus at the casing-cement interface, some modifications were implemented for selected samples. A schematic presentation of the modifications implemented for microannulus generation is shown in Figure 4.3. The outer casing wall was machined with a chosen taper, from the original OD at the top to a smaller OD at the bottom. A flange was welded onto the top of the casing, as shown. By tightening the bolts, the conical casing is lifted upwards (relative to the cement sheath and the aluminum pipe), creating a separation between the casing and the cement, i.e. a casing-cement microannulus. Each bolt fits in a pit on the top surface of the aluminum pipe to ensure casing centralization during cementing and to minimize rotation and tilting of the casing as it is lifted/lowered. Finely threaded bolts (1 mm thread spacing) were chosen to maximize the control of the microannulus size. By measuring the position of the casing compared to the initial "cemented-in" position, the size of the microannulus can be calculated from the machined taper, as:

$$w_{ma} = \left(\frac{\Delta r_o}{\Delta L}\right)_{csg} \Delta h \tag{4.1}$$

where

$$w_{ma} = \text{Microannulus size} \qquad [\mu m]$$
$$\left(\frac{\Delta r_o}{\Delta L}\right)_{csg} = \text{Radial casing taper} \qquad [\mu m/mm]$$
$$\Delta h = \text{Change in casing position} \qquad [mm]$$

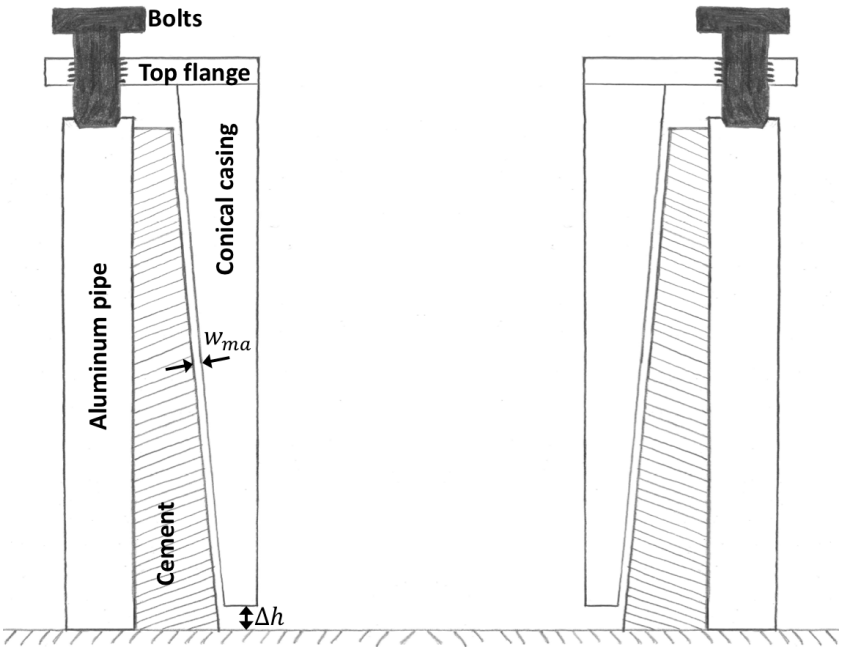

Figure 4.3: Set-up for generation of a casing-cement microannulus of a known size.

Figure 4.4 shows the conical casing positioned inside the aluminum pipe, ready for cementing. The flange's open slots give direct access to the annulus for cementing. After cement hydration, the initial casing-cement bond had to be broken in order to be able to hoist and lower the casing using the three bolts to vary the microannulus size. This was done using a hydraulic puller as shown in Figure 4.5. The hydraulic puller had three arms, explaining why three open slots were chosen for the casing top flange. The arms are pulling upwards on the aluminum pipe, while the rod is pushing down at the casing through a piece of steel matching the casing OD. It was also evaluated to use temperature or pressure variations to break the initial casing-cement bond, and also to vary the size of the microannulus. However, this would require a more complicated set-up and would also make the measurement of the microannulus size less accurate.

For the first few samples, a curing temperature of 66°C was used during cement hydration. During curing of these samples, water consumption was significant and the samples were drying up rather quickly. Water was therefore regularly added to the top of the cement during hydration, in an effort to reduce cement cracking. To avoid altering the properties

Figure 4.4: Conical casing with top flange positioned for cementing.

Figure 4.5: Using hydraulic puller to break casing-cement bond (note that the sample is upside down).

of the set cement, water was only added after the cement had developed into a fixed structure. In an effort to reduce the consumption of water, the curing temperature was lowered to 40°C for later samples. This was also done to ease the generation of a microannulus (as described later). In addition, the samples were covered using a plastic overlay surrounding the sample to limit evaporation and also to ensure a more uniform temperature throughout the sample by reducing the heat loss to the surroundings. This somewhat reduced the consumption of water, but still, water had to be added quite regularly to avoid the samples drying up too quickly.

Difficulties Extruding Conical Casing

When machining the taper on the outer casing wall for the microannulus samples, it was made sure that the surface had a smooth finish to minimize the degree of bonding between the casing and cement. It was therefore believed that the casing and cement would separate rather easily. However, for the first conical sample, it was not possible to extrude the casing – even when reaching the 75 metric ton limit of the hydraulic puller. From this, it can be concluded that there is most likely a significant adhesion between the casing and the cement – even with a smooth casing surface. In addition, the temperature reduction when removing the heating cable after cement hydration may have imposed stresses in the sample. As the coefficient of linear thermal expansion for aluminum is approximately twice of that of steel [46], the aluminum pipe would contract more than the casing when the temperature was lowered from the curing temperature (66°C for this sample) to ambient temperature. Effectively, this would cause the aluminum to squeeze around the cement sheath, hence increasing the friction between the casing and the cement, rendering it more difficult to pull the casing free.

For the subsequent samples, several measures were therefore undertaken to make it possible to break the initial bond. To reduce the adhesion between the casing and the cement, an oil-based form release agent was applied on the casing surface before cementing. This product is commonly used in the concrete industry to prevent adhesion of concrete to the formwork and to leave a smooth concrete surface. A cloth was used to apply the release agent in a thin film at the casing surface. The curing temperature was lowered from 66°C to 40°C to stay (comfortably) below the flash point of the form release agent (65°C). This would also reduce the stresses imposed on the sample due to the temperature contraction effects discussed earlier. To completely eliminate these stresses, the curing temperature could be chosen to ambient conditions. However, this would require cooling to keep the temperature stable, as heat is generated from the exothermic reaction of cement hydration. Also, it would be less representative of field conditions and prolong the cement hydration time. It was therefore decided to extrude the casing immediately after removing the heating cable (while the sample still holds curing temperature) to eliminate the effects of temperature contraction.

These measures made it possible to extrude the casing for the subsequent tapered casing samples. However, a significant force (tens of tons) still had to be applied with the hydraulic puller. After doing so, the heating cable was wound back on the sample and logging was performed at curing temperature. This was done to maximize the accuracy of the microannulus size – avoiding temperature contraction/expansion effects altering the size. The three bolts were used to hoist and lower the casing to vary the size and a caliper was used to measure the position of the casing relative to the initial position.

Cement-Aluminum Interaction

Within minutes after placing the cement in the annulus, bubbles were observed at the top of the cement as shown in Figure 4.6. At first, it was believed that it was caused by air that had mixed with the cement during placement in the annulus, that now was escaping to surface due to buoyancy. During cementing of the next samples, it was therefore emphasized on the previously described actions to minimize the air content of the cement. However, bubbles were still appearing at the cement surface shortly after cementing. It was also noticed that the cement level was rising, causing some cement to spill over the edge, even though a comfortable margin of about two centimeters was left uncemented. It was therefore decided to further investigate the quality of the set cement by pulling the conical casing out of the sample, as shown in Figure 4.7. Voids in the cement are clearly visible, especially in the top part. The bottom part of the sample appears to be in a better condition. In addition, some cement was sticking to the casing as it was pulled, indicating that the cement was not fully hydrated. Also notice the stain on top of the aluminum pipe, indicating that cement has spilled over the edge due to the rising level.

After further investigating this, it was found that Portland cement is incompatible with

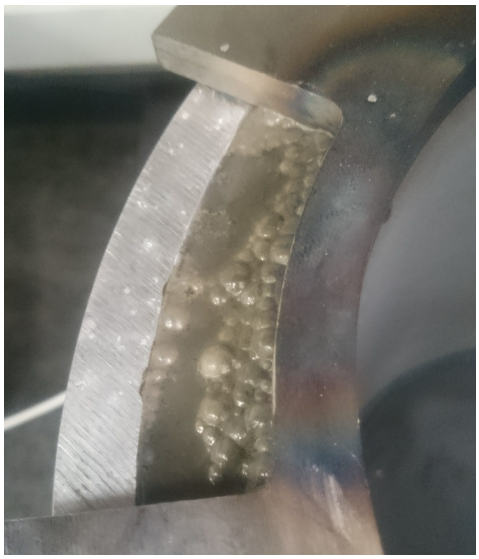

Figure 4.6: Bubbles appearing at the top of the cement during initial hydration.

Figure 4.7: Inspection of the cement sheath quality after pulling the tapered casing.

non-noble metals, like aluminum which was used to represent the formation in this set-up. In common environments – including atmospheric conditions and aqueous environments – aluminum has a high resistance to corrosion due to the formation of a protective oxide layer [47]. However, this oxide layer is not stable in alkaline environments with a pH above approximately 8.5, such as in wet cement [48]. The pH of the cement mixed for these experiments was later measured to 12.5, using a pH meter. In such environments, corrosion of aluminum occurs through the following reaction [49]:

$$Al + 3H_2O + OH^- \rightleftharpoons \tfrac{3}{2}H_2 + Al(OH)_4^- \tag{4.2}$$

As hydrogen gas is generated through the reaction and migrates upwards through the cement slurry due to buoyancy, it explains why bubbles were observed at the top of the cement during hydration. This migration of gas also explains why the bottom part of the cement sheath looks significantly better than the top part. The gas generation will also cause the slurry to expand, explaining why the cement level was rising and causing the slurry to spill over the rim of the pipe. As the cement sets, gas bubbles become entrapped within the set cement, increasing its porosity and degrading its strength and sealing capability [48].

As also described by Equation 4.2, water is consumed when aluminum corrodes in contact with wet cement. This most likely explains why such large amounts of water had to be added during cement hydration, to avoid early desiccation of the sample. This explanation is further strengthened by the fact that the consumption of water did not reduce much when the sample was covered with a plastic overlay – i.e. the water consumption was mainly due to aluminum corrosion and not solely due to evaporation as was first

believed. Once all the water is consumed, aluminum corrosion and gas generation will cease. However, at this point, cement hydration will also cease, as water is required for hydration of cement as well. Kinoshita et al. showed through experimental research on ordinary Portland cement with the addition of aluminum powder, that water is preferentially consumed by the corrosion of aluminum over the hydration of cement [48]. This results in an increased portion of unhydrated cement in the final structure, and also this is likely to contribute to an increase in porosity. This is in line with the experienced final cement sheath quality that was shown in Figure 4.7, where the cement does not appear like one solid and fully hydrated sheath.

The situation is further worsened with the presence of steel in addition to aluminum, as galvanic corrosion can occur if the two metals are coupled mechanically or through an electrolyte [50, 51]. This is therefore especially relevant for the set-up for microannulus generation, where the steel is mechanically coupled to the aluminum through the bolts used for centralization and hoisting of the casing. This will work similarly to cathodic protection, where aluminum is corroding as a sacrificial anode, while the steel is acting as the cathode and hence is protected from corrosion. Also for the basic setup without the bolts, both aluminum and steel are present. However, the two are not mechanically coupled, and as the ion content of the cement slurry is low (mixed with fresh water and no additives) the galvanic contribution to the corrosion process is believed to be rather moderate in this case.

Due to the corrosion of aluminum, the cement quality and properties would not be representative of a proper cement job. In terms of cement evaluation with the AVT, the biggest concern was an insufficient stiffness (Young's modulus) due to two reasons; the increased porosity due to the generation of gas, and the larger quantities of unhydrated cement due to the corrosion reaction's consumption of water.

Coating Test

The Portland Cement Association (PCA) recommends the use of a protective coating to isolate the aluminum from the cement, to avoid aluminum corrosion [52]. The coating has to create a perfect seal on the aluminum surface, as well as endure the highly alkaline environment of wet cement. In addition, it should be possible to apply the coating in a thin and uniform layer to minimize its effect on the AVT measurement.

A test of several different coatings was therefore performed, in search for a coating fulfilling these requirements. To resemble the experimental set-up as closely as possible, the test samples were created by placing one piece of steel and one piece of coated aluminum in a sample of freshly mixed cement. The two metals were not mechanically coupled, as this could be avoided also in the laboratory set-up, by slightly unscrewing the bolts connecting the casing and aluminum pipe. The samples were cured for five days covered with a plastic overlay. In total, six different coatings were used, in addition to one sample with bare

aluminum. Figure 4.8 shows three of the samples after curing. Figure 4.8a shows the sample with bare aluminum for reference, and it is clear that significant corrosion has occurred. There is a separation between the aluminum and cement, indicating that gas has migrated up along the interface. In addition, a layer of white residue is visible on the sample, which most likely is aluminate ions; a product of the corrosion reaction described by Equation 4.2. Four of the coatings did not fulfill the requirements described, and such an example is shown in Figure 4.8b. Corrosion appears to be less severe than for the uncoated sample, as both less separation at the aluminum-cement interface and less corrosion product is visible. However, corrosion is still evident and it can also be seen that the coating has partly loosened from the aluminum. Only two out of the six coatings provided a satisfactory seal on the aluminum and endured the highly alkaline environment. The one that was easiest to apply in a thin and uniform layer, and hence would affect the AVT measurement less, is shown in Figure 4.8c. Here, aluminum corrosion is not very evident and it is also clear that the quality of the set cement is significantly improved.

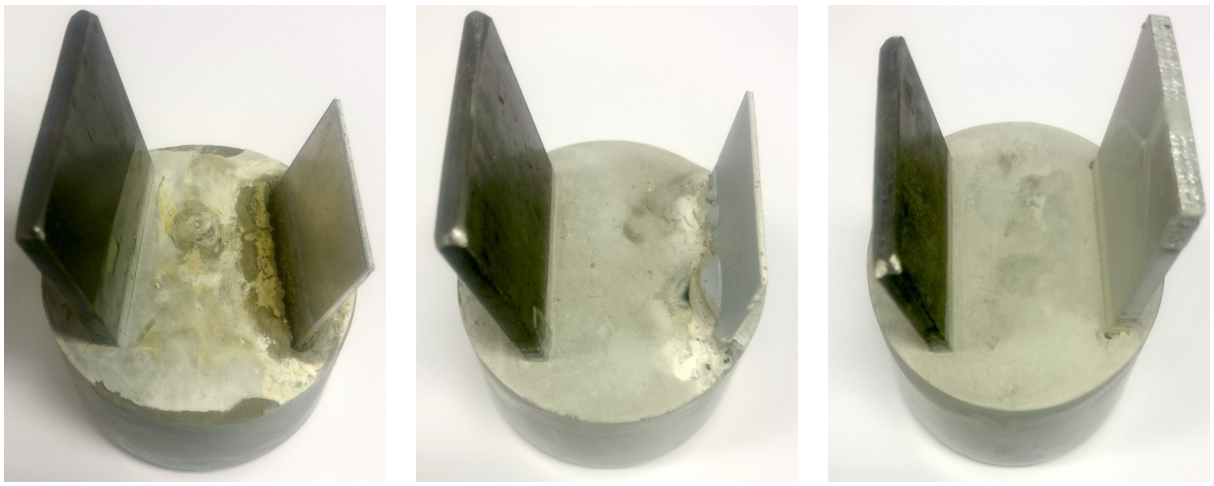

(a) Uncoated aluminum **(b)** Ineffective coating **(c)** Effective coating

Figure 4.8: Test of aluminum coatings by placing a piece of steel (left) and a piece of aluminum (right) in fresh cement.

Coated Aluminum Samples

The coating used for the sample shown in Figure 4.8c – an acetone-based spray coating – was applied to the inner wall of the aluminum pipe before cementing the subsequent samples. For the samples for microannulus generation, the bolts were slightly unscrewed to eliminate the mechanical contact between the aluminum and the steel. Otherwise, the samples were constructed as described earlier. Figure 4.9 shows a sample during initial hydration, and it is clear that the generation of hydrogen gas is significantly reduced or even eliminated (compared to Figure 4.6). No bubbles could be observed at the top of the cement during hydration. In addition, no rise in the cement level due to gas expansion was experienced. The consumption of water was also significantly reduced and the cement

stayed humid for several days of hydration. Together with the covering of the sample, this made it unnecessary to add water during hydration, which is in accordance with ISO 10426-1 [45]. These observations prove that the coating was able to effectively isolate the aluminum from the cement, ultimately resulting in a significant improvement in the quality of the cement sheath.

After hydration, the hydraulic puller was used in order to break the casing-cement bond, to allow for the generation of a microannulus. However, when the force was applied, the bond broke at the cement-aluminum interface, and not at the casing-cement interface as was expected since the release agent was applied to the casing. This was attributed to the coating prohibiting a proper cement bond, hence resulting in a weak cement-"formation" bond. This resulted in that no microannulus was created as there was no relative movement between the casing and the cement. As there was no taper on the cement-aluminum interface, the cement and casing did not come free as it was pulled upwards. In an effort to get the casing free, a hammer was used to impose shock loads on the casing-cement bond by knocking on the inner casing wall while still pulling with the hydraulic puller. In the end, the casing did separate from the cement and it was possible to lift the casing. However, at this point, the cement-aluminum bond was also broken and the cement sheath had moved relative to the outer aluminum pipe. In addition, the cement sheath may have been damaged due to the rough handling. It was therefore concluded that the uncertainties were too large in order to be able to generate a casing-cement microannulus of a known size, adjacent to a good cement sheath.

Figure 4.9: Sample with coated aluminum during initial hydration. No generation of gas was observed.

Figure 4.10: Inspection of the cement sheath quality after pulling the casing from a sample using coated aluminum.

To inspect the effect of the coating on the quality of the set cement sheath, the casing was pulled out of the sample as shown in Figure 4.10. Notice how the cement sheath is elevated from the floor, caused by the relative movement between the aluminum pipe and the cement when attempting to pull the casing. It is clear that the cement quality

is significantly improved, compared to the uncoated sample that was shown in Figure 4.7. No large voids within the cement are visible and the cement appears to be more like one solid sheath. In addition, no cement was sticking to the casing, indicating that the amount of unhydrated cement is reduced. Also notice that the top of cement is lower for this sample, compared to the sample of uncoated aluminum, even though the cement level was similar when the cement was placed in the annulus. This agrees well with the previously described cement expansion due to the generation of gas. Altogether, these observations confirm a significant reduction – or even an elimination – of aluminum corrosion and gas generation. For microannulus generation, however, it was clear that the set-up had to be modified.

Coated Casing?

It has been argued that severe corrosion of aluminum in cement does not occur unless steel is present to provoke galvanic corrosion [50]. It was therefore evaluated to coat the casing, rather than the aluminum pipe. This would isolate the steel from the cement, as well as ensure a strong bond at the cement-aluminum interface and a weak bond at the casing-cement interface. Hence, it would also render the form release agent superfluous. Effectively, this is the same as removing the steel from the cement, so to simulate this, a simple test was performed by placing a piece of aluminum in fresh cement (with no steel present). The result after hydration is shown in Figure 4.11 and it is clear that even though steel is not present, severe aluminum corrosion has occurred. The result is actually comparable to the sample of uncoated aluminum *with* steel present, as was shown in Figure 4.8a. This proves that, for this experimental set-up, the corrosion is not driven by galvanic effects (at least when the two metals are not mechanically coupled). It certainly also proves that coating the casing and not the aluminum pipe would not be a good solution.

Figure 4.11: Test of aluminum corrosion in cement without steel present – for evaluating the possibility of coating steel casing.

4.1.3 Improved Set-Up Using Steel Pipe

As it proved unattainable to obtain a satisfactory experimental set-up for microannulus generation using an aluminum pipe, even after several attempts with mitigating actions, it was decided to replace it with a steel pipe. A 323.9 mm OD pipe of S355J2H steel was then chosen to represent the formation. The pipe's ID was 307.9 mm, hence representing a borehole diameter of 12.12 inches. Apart from the replacement of the outer pipe, the set-up was identical to the initial set-up described in Section 4.1.2 and is cemented according to the same procedures described in Section 4.1.1. A schematic of the improved set-up is shown in Figure 4.12. Also for this set-up, the same modifications to allow for the generation of a microannulus – i.e. machining of a casing taper, a top flange with bolts and form release agent applied to the casing before cementing – were implemented on selected samples.

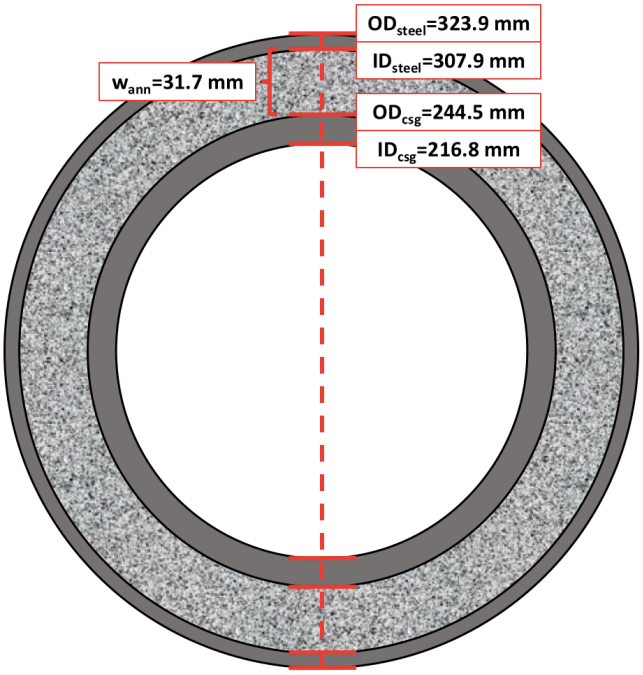

Figure 4.12: Schematic top view of the improved setup for construction of samples, showing the casing, cement and steel pipe with dimensions.

By replacing the aluminum with steel, all the challenges related to aluminum corrosion as well as the use of coating were eliminated. As expected, no generation of gas was observed during cement hydration and water consumption was similar to as for the coated aluminum samples. Another advantage, was the reduced effect of expansion and contraction due to temperature, as both the inner and outer pipe are steel alloys with similar coefficients of thermal expansion. In addition, the larger ID of the outer pipe (12.12 in) is more representative of a typical hole size for a 9 5/8-in casing. The larger ID was also chosen to compensate for the greater stiffness of steel (compared to aluminum) by reducing the wall thickness. On the other hand, a steel pipe renders it difficult to evaluate the quality

of the cement sheath using X-ray CT as it is comparably more attenuative to radiant energy. However, the cement sheath could still be visually examined after pulling the conical casing, which was considered sufficient for this work.

For the microannulus samples, the hydraulic puller was used after cement hydration to break the initial casing-cement bond, as described earlier. This time, the bond broke at the desired surface, enabling the generation of a casing-cement microannulus of a known size by measuring the position of the casing. Figure 4.13 shows the sample after a microannulus had been created, and it is clear that the cement has released properly from the casing, as no cement residue is left on the casing surface. Logging could then be performed with the AVT for microannuli of varying sizes, as described in Section 4.3.2. To further inspect the quality of the cement, the casing was pulled out of the sample after logging was completed, as shown in Figure 4.14. The quality of the cement sheath appears to be good, comparable to the case of coated aluminum (as shown in Figure 4.10).

Figure 4.13: Microannulus generation by hoisting the tapered casing.

Figure 4.14: Visual inspection of the cement sheath quality by pulling the casing after logging.

4.2 Experimental Set-Up of the AVT

4.2.1 Tool Assembly

A full-size prototype of the AVT has been constructed and assembled according to the design. The prototype was designed for logging of 9 5/8-in 53.5 lb/ft casing, as the tool pads match the curvature of an 8.535-in casing ID. A schematic of the tool prototype, together with the parts list, is shown in Figure 4.15. For the early phase testing performed during the course of this work, it was decided to not install the ultrasonic transducers (8) in the pads of the tool, but to focus on the tool's primary measurements.

The tool body is hydraulically sealed by the use of different sealing elements and is rated to a pressure of 3500 psi (241 bar) pressure (limited by the electrical feedthrough connectors). Static seals (13 and 24) are used where there is no relative movement between the parts, while dynamic rod seals (10) are installed to provide a seal between the piston housings and the moving pistons (5). The rod seals use an O-ring as energizing element and are designed to provide low friction and to minimize stick-slip effects between the seal and the rod. The rod seals are combined with a set of O-ring energized scrapers (11), to prevent ingress of solids or other contaminants into the system.

When pressurizing the tool, hydraulic fluid was leaking from around the tool pads, and it proved challenging to obtain a seal in the dynamic rod seals. The rod seals were changed several times, as it was suspected that the seals may have been damaged during insertion of the pistons. To minimize damage to the seals during insertion of the piston rods, a plastic guide of the same diameter as the rod was made. The guide had a tapered nose to allow it to enter the seals without creating damage. This significantly reduced the force needed to insert the rods as the seals were fully pushed into the grooves, and therefore also reduced the seal damage. However, the leaks were not cured and it was decided to polish the surface of the piston rods to smoothen the seal area – neither this did help on the leakage issue. The tolerances on the dimensions of the parts around the rod seals are in the micrometer range, and it was therefore decided to investigate these. It was found that the bore diameter of the housing was too large compared to the seal specifications, giving too large radial clearance between the piston and the housing. This resulted in insufficient support for the seals and was most likely the reason for leakage. A new pair of housings was therefore machined, with special emphasize on the dimensions being within the tolerances specified for the seals. After replacing the housings, no further leakage was experienced.

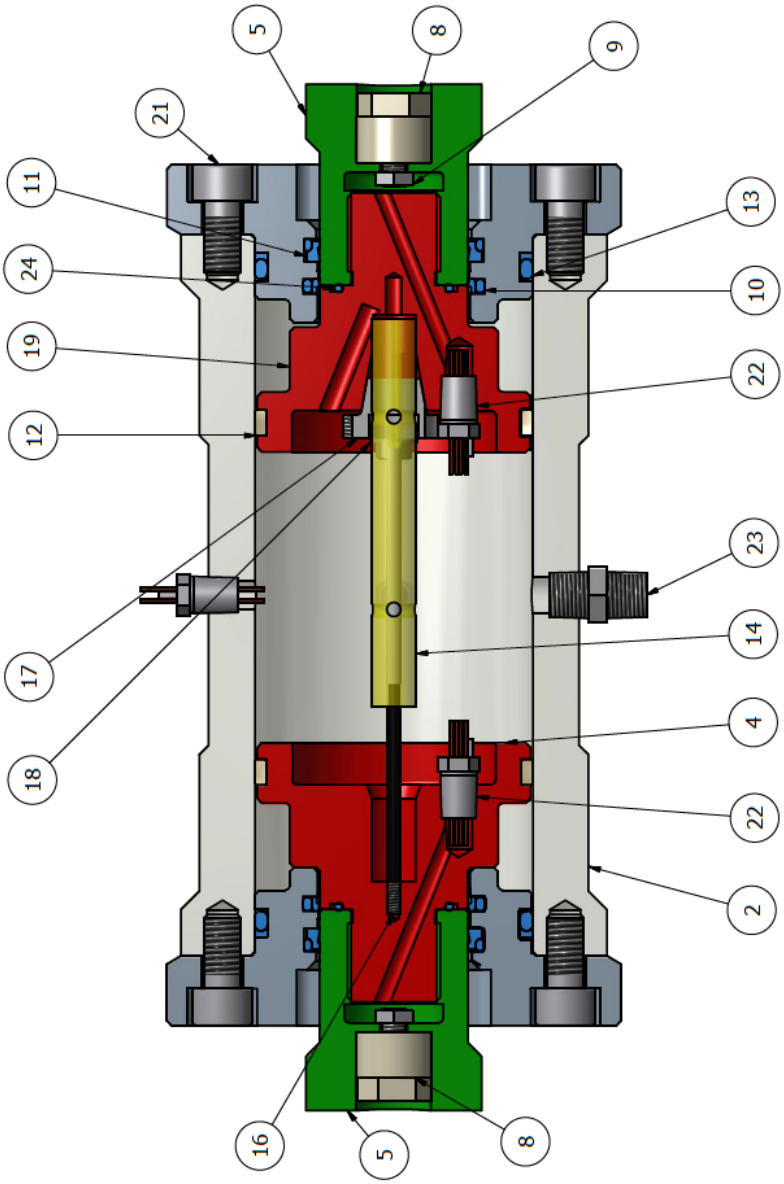

PARTS LIST			
ITEM	QTY	PART NUMBER	DESCRIPTION
2	1	Barrel	
4	1	Piston 1	
5	2	Radial pad	
6	1	Spring	
8	2	Ultrasonic sensor	
9	2	AS 1474 - M5	Hex Nut
10	2	RSK100320-M12V	Rod Seals
11	2	WE3100320-M12N	Scrapers
12	2	GP6500600-HM061	Wear Rings
13	2	BD2700600-PTKC	Static Seals
14	1	LVDT housing	
16	1	LVDT rod	
17	1	Bushing	
18	2	AS 1427 - M5 x 10	Screws
19	1	Piston 2	
21	8	AS 1420 - 1973 - M8 x 16	Hex. socket head cap screws
22	4	4-pin connector	
23	2	Hexagon Nipple 1/8	
24	2	O-ring	

Figure 4.15: Schematic of the Annulus Verification Tool prototype, including parts list.

4.2.2 Supporting Equipment

The AVT has been set up with the supporting equipment as shown schematically in Figure 4.16. Here, green color represents the hydraulic pressure equipment, while the LVDT signal equipment is colored red. A high-pressure positive displacement syringe pump was used to pressurize the tool with Exxsol D60 hydrocarbon oil. The pump had two cylinders, providing a pulse-free, controllable rate. To avoid friction in the hydraulic supply line affecting the pressure measurement, a 0-250 barg pressure transducer was installed at a separate "listening line" connected to the body of the AVT. The pressure transducer gave directly the differential pressure exerted on the pistons, as the tests were run at ambient surroundings and the gauge pressure is measured.

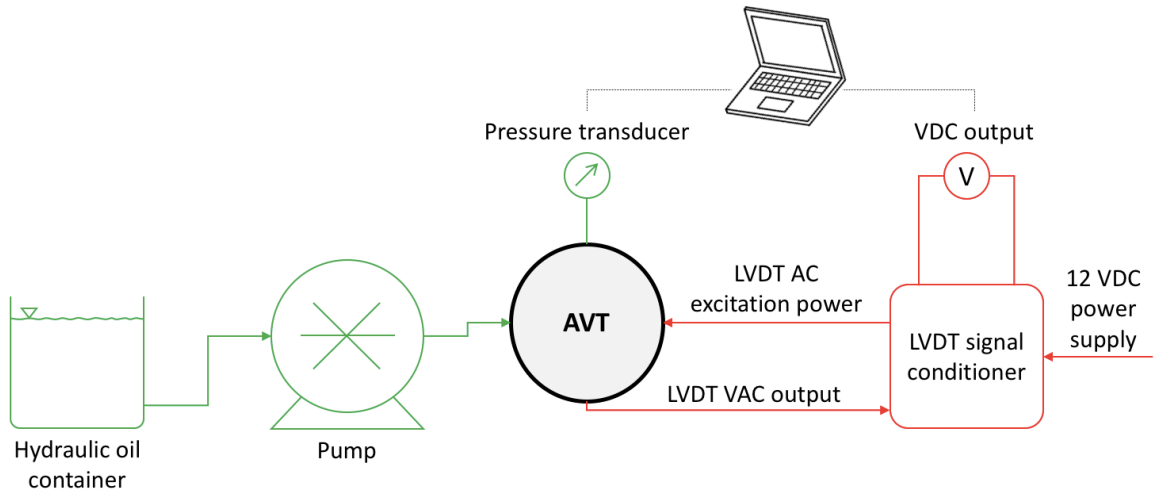

Figure 4.16: Schematic of the experimental set-up of the AVT with supporting equipment.

The tool's LVDT was connected to a signal conditioner, powered by a 12 volt DC supply. The signal conditioner supplied the AC excitation power for the LVDT primary winding. It also converted the low-level AC output voltage from the LVDT secondary windings to a more convenient to use DC output voltage. During operation, the pump rate was controlled through a computer software. A LabVIEW-program was constructed to both display and record the pressure and diametral displacement, using the output current from the pressure transducer and the output voltage from the LVDT signal conditioner, respectively.

4.2.3 Equipment Calibration

LVDT Calibration

Before logging, the LVDT was calibrated to give the outer diameter of the tool, i.e. the distance between the two pad surfaces. The signal conditioner provided a simple way of calibration by setting the endpoints. These points represent the expected minimum and

maximum travel of the LVDT, corresponding to the -10 V and 10 V DC voltage readings, respectively. As long as these end points are located within the LVDTs operational range, the voltage will be a linear function of the diameter, between the end points. The LVDT chosen had an operational range of 1 inch (25.4 mm): ±0.5 inches (12.7 mm) from the LVDT null point. The maximum position was chosen to be somewhat larger than the ID of the casing to allow for some displacement, while the minimum position was set to somewhat less than the ID of the casing. The distance between the tool pads at the minimum and the maximum position was measured using a caliper. By applying the linear relationship between output voltage and distance, the diameter was calculated as:

$$d = d_{min} + \frac{d_{max} - d_{min}}{V_{max} - V_{min}}(V - V_{min}) \tag{4.3}$$

where

$$\begin{aligned} d &= \text{Diameter (distance between the pads)} && [mm] \\ d_{min} &= \text{Diameter at LVDT minimum} && [mm] \\ d_{max} &= \text{Diameter at LVDT maximum} && [mm] \\ V &= \text{LVDT DC voltage output} && [V] \\ V_{min} &= \text{DC voltage output at LVDT minimum (-10)} && [V] \\ V_{max} &= \text{DC voltage output at LVDT maximum (10)} && [V] \end{aligned}$$

The resolution of the LVDT measurement depends on the signal conditioning equipment. The signal conditioner used, had an effective 15-bit output for the DC voltage. Following this, the LVDT range (between minimum and maximum) was divided into 2^{15} (32 768) intervals of constant voltage, giving a resolution of 0.78 µm if the full 1 inch (25.4 mm) range was used. By shortening the range, the theoretical resolution would improve. On the other hand, the gain would be increased, which would increase any noise and therefore reduce the resolution. Nevertheless, the LVDT resolution was sufficient to measure the diametral displacement with a resolution at the micrometer-scale, which is necessary in order to be able to quantify the size of a microannulus. To ensure a high accuracy of the diameter measurement, calibration was repeated every time the tool was modified and reassembled.

Pressure Transducer Calibration

The chosen transducer had a pressure range of 0-250 bar, hence covering the full operational range of the AVT. A six-point calibration procedure (0, 50, 100, 150, 200 and 250 barg) was used to calibrate the pressure transducer, using an air flask with a regulator as the pressure source. Two manometers were used for reference pressure measurements while the output current was recorded in the same LabVIEW program used for logging. The resulting points with the best-fit linear trend line is shown in Figure 4.17.

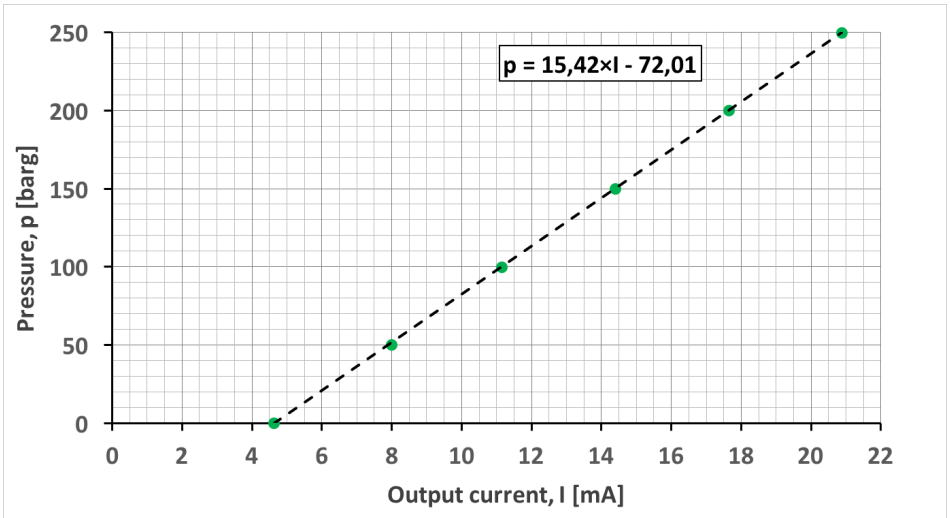

Figure 4.17: Result of pressure transducer calibration.

The results show that the transducer has drifted slightly from the 4-20 mA range specified by the manufacturer. However, a linear trend is clearly evident, proving that the equation for the linear trend line fitted to the data points could be used to give the pressure as a function of the output current during logging.

Spring Characterization

As earlier described through Equation 3.3, the pad force applied on the casing wall during logging, is calculated as the difference between the piston force and the spring force. To be able to quantify the spring force as a function of the recorded diameter, the spring characteristics were estimated. This was done by pressurizing the tool without any resistance on the pads, while recording the diameter and pressure as for ordinary logging (using the same set-up as described earlier). With no resistance on the pads, the pad force will be zero. Hence, according to Equation 3.3, the spring force will equal the piston force which again is given by Equation 3.1. Following this, the spring force can be expressed as:

$$F_{spring} = F_{piston} = \Delta p A_{piston} \tag{4.4}$$

The spring force calculated from the recorded pressure using Equation 4.4 was plotted versus the recorded diameter, as shown in Figure 4.18. The results clearly show a linear trend, as expected according to Hooke's law (see Equation 3.2). This also confirms that the springs were loaded in their linear-elastic region and that a permanent set was not imposed. Equation 3.2 can be rewritten to clearly show the expressions for the intercept and the slope of the straight line:

$$F_{spring} = k\frac{d - d_0}{2} = \frac{k}{2}d - \frac{kd_0}{2} \tag{4.5}$$

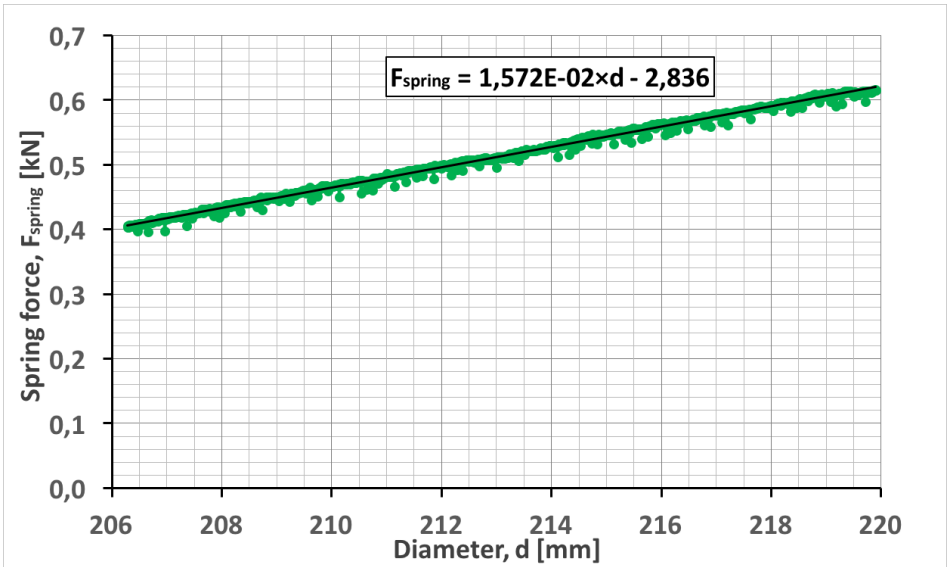

Figure 4.18: Linear regression to determine the spring characteristics.

A linear trend line was fitted to the data points using least squares regression and its equation is shown on the chart. The spring constant (k) was calculated from the slope of the trend line and the intercept was used to calculate the spring equilibrium diameter (d_0) using the found spring constant. The resulting values are summarized in Table 4.1.

Table 4.1: Resulting spring characteristics.

Parameter	Symbol	Value	Unit
Spring constant	k	0.03143	kN/mm
Equilibrium diameter	d_0	180.4	mm

As discussed earlier, friction effects are ignored when expressing the pad force through Equation 3.3. However, as the spring characteristics were found through a dynamic process (at a constant non-zero rate), the effect of dynamic friction is included in the spring characteristics. For the characteristics to be as representative of logging conditions as possible, the same procedures and parameters as used during logging, was used. This includes using the same set-up, the same computer program, and the same pump rate. On the other hand, the effect of friction is believed to be small compared to the spring force itself. During logging, the pad force should be zero until the pads obtain contact with the inner casing wall. Hence, if a pad force significantly different from zero is observed at small diameters, a recalibration should be performed. Note that it could be the LVDT calibration, the pressure transducer calibration and/or the spring characteristics that are erroneous in this case.

4.3 Experimental Testing of the AVT

This section describes the experimental testing of the AVT, conducted to evaluate the logging tool's response in several different cases and environments (represented by the samples constructed as described in Section 4.1). The tool was set up as described in Section 4.2 and placed in a cradle-shaped holder during testing, as shown in Figure 4.19. The holder was designed such that the tool center is positioned around the midpoint of the sample height, to minimize end effects.

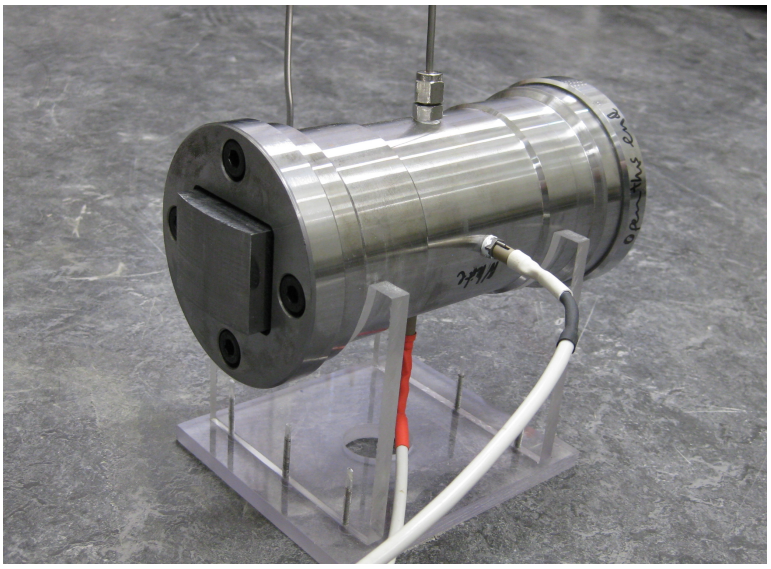

Figure 4.19: AVT set up and ready for logging.

4.3.1 Well-Cemented Casing Versus Free Pipe

A sample constructed according to the improved set-up using steel to represent the formation (as described in Section 4.1.3) was used to represent the case of a well-cemented casing. The sample did not have the modifications for microannulus generation, to be as representative as possible of a properly cemented casing – i.e. without the machined casing taper and with no form release agent applied to the casing. It was also considered to use a sample constructed using the initial set-up with coated aluminum. However, the improved set-up was considered more representative of a typical casing/cement/formation system – mainly due to the more representative wellbore diameter ("hole size") and the elimination of the use of the coating which could have a slight effect on the measurement. In addition, the improved samples were less affected by temperature contraction effects as both the inner and outer pipe were of steel.

Before cementing, the casing was logged to establish the response for the uncemented case (free pipe). After cement hydration, logging was performed in the same direction as before cementing. By using the same casing and log in the same directions to compare

the cemented an uncemented case, the effect of a slight difference in the dimensions is eliminated. This could, for instance, be a slight difference in casing ID resulting in the recorded diameters not matching completely between the cemented and uncemented case. For the recorded stiffness, on the other hand, it would not make a large difference. During logging, it was made sure that the tool was centralized and aligned as good as possible.

4.3.2 Casing-Cement Microannulus

To test the response of the AVT in the case of a casing-cement microannulus, a sample constructed using the improved setup, with the modifications for microannulus generation, was used. This was the only set-up where it was possible to controllably create a microannulus of a known size at the casing-cement interface, adjacent to a solid cement sheath.

Also here, the casing was logged before cementing to establish the response of free pipe. This was also done to determine the maximum possible displacement of the casing wall, to estimate the maximum microannulus size where the cement sheath could still be detected. If the size of the microannulus is greater than this value, the casing would not obtain contact with the cement sheath during logging and the response would be similar to that of a free pipe. Due to the machining of the taper reducing the casing wall thickness, this free pipe stiffness was expected to be slightly lower than for the original casing described in Section 4.3.1.

After cement hydration, logging was performed before breaking the casing-cement bond to establish the well-cemented stiffness. This was also done to identify a potential microannulus generated due to the form release agent that was applied to the casing before cementing. As discussed in Section 2.2.1, an oil-wet casing surface could cause a microannulus to form, as it may prohibit the cement to bond to the casing surface. If so, a microannulus would be present already before extruding the casing, and the actual microannulus size would be greater than the one calculated from the casing taper through Equation 4.1. Also here, the stiffness was expected to be slightly less than for the well-cemented casing described in Section 4.3.1, due to the machining of the taper removing some of the casing steel and replacing it by cement (which has a lower stiffness). To ensure minimum damage to the cement sheath and to avoid altering the size of the microannulus for later tests, this test was not run to full pressure but was stopped when a stiffness representing that of a good cement was clearly identified.

After breaking the casing-cement bond using the hydraulic puller, the size of the microannulus was controlled using the three bolts and a caliper was used to measure the casing position. Figure 4.13 shows the sample after a microannulus has been created. The microannulus size was increased in steps by alternately tightening the bolts by a quarter of a turn, to avoid tilting of the casing causing it to scratch and jam against the cement sheath. For each microannulus size, logging was performed with the AVT. It was made

sure that the tool was kept centralized and aligned as good as possible during logging, and the tool was kept in the same position as the size of the microannulus was varied. However, the casing was lifted as the microannulus size was increased, causing the pads not to contact the casing at the same point for each size. Logging was performed at curing temperature to maximize the accuracy of the microannulus size calculated from the casing taper, by avoiding contraction/expansion effects due to temperature changes.

4.3.3 Poorly Cemented Casing

Samples constructed using the initial setup (as described in Section 4.1.2) were used to represent the case of a poor cement job. As discussed, the aluminum-cement interaction resulted in a cement sheath with increased porosity due to the generation of hydrogen gas, bearing a resemblance with a cement affected by gas migration. Together with the increased portion of unhydrated cement due to the corrosion reaction's consumption of water, this was expected to degrade the strength/stiffness of the set cement, as well as its sealing capability. To be able to compare with a well-cemented sample of the same geometry, a sample with a coated aluminum pipe was used. This means that a sample with a cement sheath similar to the one shown in Figure 4.7 was compared with a sample with a cement sheath similar to the one shown in Figure 4.10. It was made sure that the tool was kept centralized and aligned as good as possible during logging.

4.3.4 Tool Eccentricity and Tilting

Improper tool centralization was presented in Section 3.3 as one of the major challenges with the AVT, as it results in improper alignment between the tool's pads and the casing wall. Experimental testing was therefore performed to further investigate the effect of insufficient centralization on the AVT measurement. These tests were performed on a well-cemented casing sample, constructed according to the improved set-up described in Section 4.1.3. The size of the tool itself limits the amount of eccentricity possible, as the outer diameter of the tool is not very much less than the casing ID. The eccentricity experiments were run with the maximum possible eccentricity to clearly see the effect.

Testing was first performed with the tool centralized and aligned as good as possible, to establish a reference case for proper centralization. This is shown in Figure 4.20a, where it can be seen that both pads appear to be in full contact with the casing. Figure 4.20b shows the tool during testing of eccentricity in the direction of the pad movement – causing one pad to obtain casing contact before the other. Here, the pad in the lower part of the picture has already obtained contact with the casing, and the alignment appears to be good for this pad (similar to for the centralized case). The pad in the upper part of the picture, however, is still some distance away from obtaining casing contact. Figure 4.20c shows the tool during testing of eccentricity in the direction perpendicular to the pad movement. Here, both pads are in contact with the casing wall – however, only partial

contact is obtained. The effect of tilting of the tool was also investigated by placing the tool in the center and slightly rotate the tool body. This is shown in Figure 4.20d, where it can be seen that the pads do not align properly with the casing wall, resulting in only partial pad contact. This is similar to the case of eccentricity perpendicular to the pad movement, however less severe.

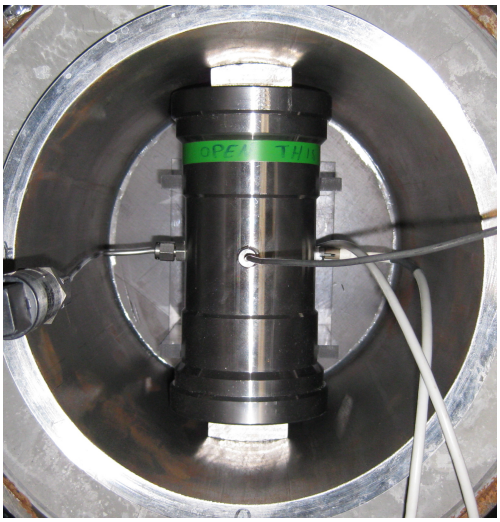

(a) Properly centralized.

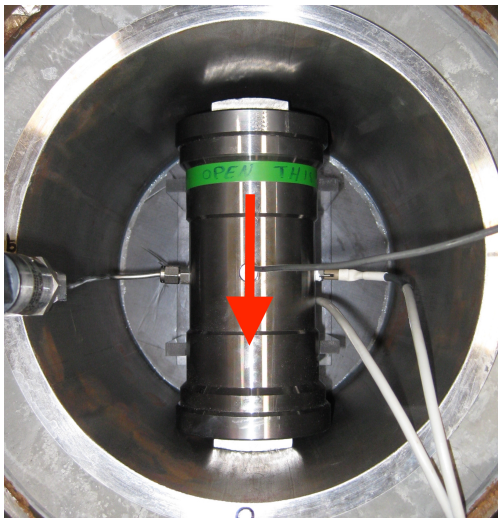

(b) Eccentricity in the direction of the pad movement.

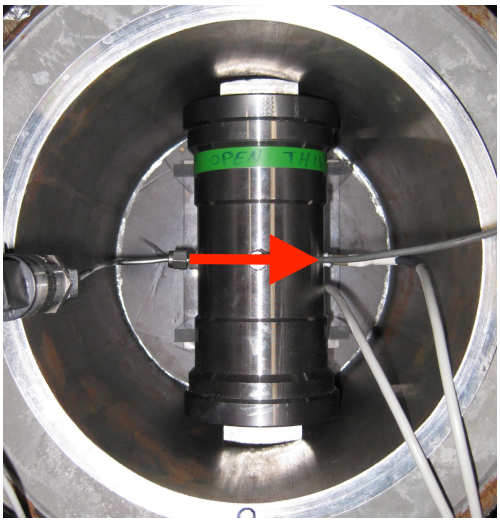

(c) Eccentricity perpendicular to the pad movement.

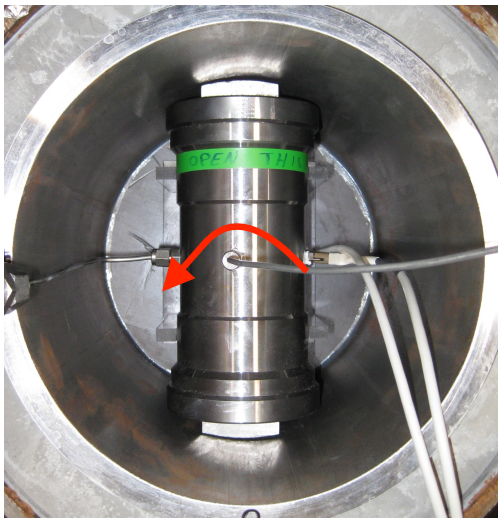

(d) Tilting of the tool.

Figure 4.20: Experimental testing procedure to evaluate the effect of tool eccentricity and tool tilting. The red arrows represent the direction in which the tool was eccentered/tilted.

4.4 Experimental Results

4.4.1 Well-Cemented Casing Versus Free Pipe

Figure 4.21 shows the results from logging the same casing, in the same direction, before and after it was cemented. The improved set-up using steel to represent the formation was used. Except for the initial displacement region, a clear linear trend is seen in both cases, as expected. This confirms that the deformation is mostly elastic. Linear least squares regression was used to determine the stiffness of the system, represented by the slope of the best fit straight line. Only the part of the data where a linear trend was seen, was included in the regression (i.e. the initial displacement was not included). The straight line, as well as the value of the slope, is shown on the plot. It is clear that the well-cemented case shows a significantly greater stiffness than the uncemented case; 59.3 kN/mm compared to 37.4 kN/mm. This proves the underlying principle of the AVT; a casing supported by a cement sheath has a greater stiffness than a free pipe. Note that this is a prerequisite for being able to detect the change in slope when casing-cement contact is obtained in the case of a microannulus (as illustrated in Figure 3.3).

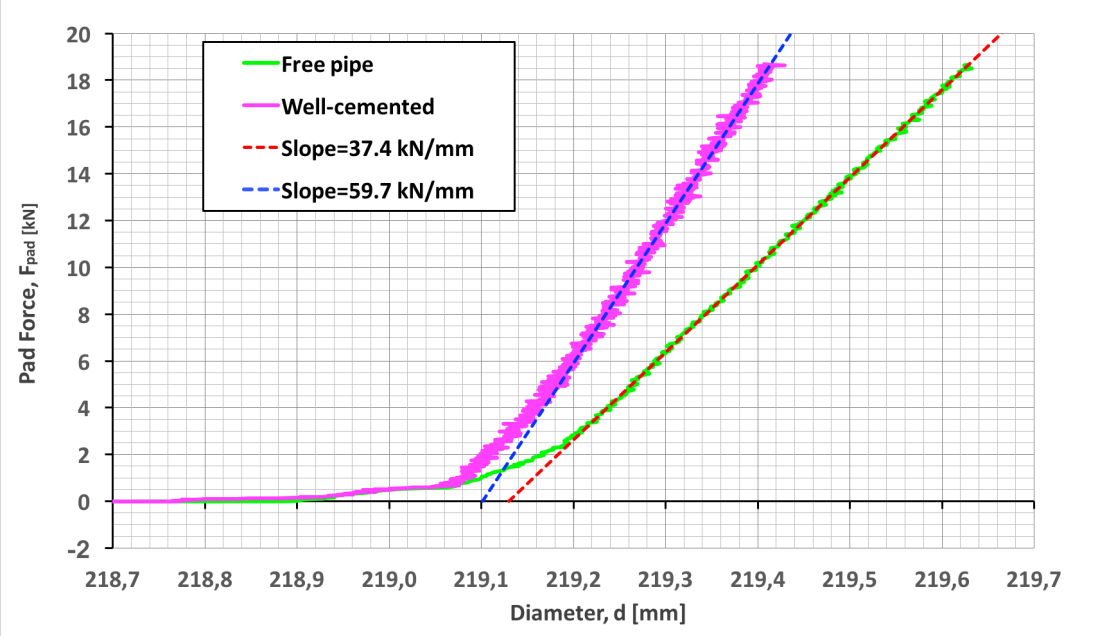

Figure 4.21: Results from logging the same casing before and after cementing. Sample constructed according to the improved set-up using steel to represent the formation.

However, the response is not as perfect as was depicted in Figure 3.3. For the initial displacement region, after pad contact is first obtained with the casing wall, a stiffness less than the one represented by the straight line is experienced. For both tests, significant pad contact appears to occur at a diameter of about 219.07 mm, while the full stiffness (straight line) is not seen before reaching a diameter of about 219.20 mm. This is believed to be caused by a slight mismatch in the alignment between the pads and the casing – either

caused by a difference in curvature or slight eccentricity/tilting of the tool. This would result in only partial contact between the pads and the casing for the initial displacement. However, as the pad force is increased, the pads and/or the casing would deform slightly in the areas where contact was first obtained – resulting in more and more of the pads to contact the casing. This would then give an apparent gradual increase in stiffness before the full stiffness (i.e. the straight line) is seen when full pad-to-casing contact is obtained.

For the well-cemented case, it could actually look somewhat like a microannulus, as a lower stiffness is seen initially before the full cemented stiffness is reached. However, as this effect is also present for the free pipe, it is believed to be caused by the same effects in the two cases (and hence not a microannulus). In addition, this initial displacement is very different from the free pipe response for the same diameter interval. In the case of a microannulus, it should (ideally) be similar. This means that is more likely caused by improper alignment (as described) than a microannulus. This topic is further discussed in Section 4.4.2 where the results from the microannulus tests are presented.

4.4.2 Casing-Cement Microannulus

Figure 4.22 shows the results from the experiments conducted to establish the free pipe and well-cemented (0 µm microannulus) response for the setup used for microannulus generation (with a steel pipe representing the formation). As expected due to the machining of the casing taper, the stiffness for both cases is somewhat lower than what was found in Section 4.4.1. Still, the two are distinguishable, which should make it possible to detect the change in slope as the microannulus is closed. It appears that the casing ID is somewhat different for the two cases – however, only by roughly 100 µm. This could be caused by logging in slightly different directions for the two cases and is not believed to have a significant impact on the measured stiffness. No microannulus is visible for the 0 µm test conducted before extruding the casing, and the response is quite similar to the response of the well-cemented casing presented in Section 4.4.1. Following this, Equation 4.1 can be used to calculate the "known" microannulus size from the casing taper, as the form release agent applied to the casing did not generate a (significant) microannulus. This is also in line with the relatively high force needed to break the casing-cement bond when pulling the casing.

Figure 4.23 shows the result from logging a 175 µm microannulus. Initially, a more or less constant slope representing an uncemented casing is seen. This stiffness is somewhat lower than the free pipe stiffness shown in Figure 4.22 due to the casing taper giving a reduction in wall thickness when the casing is hoisted to increase the microannulus size (while the tool is kept in the same position). After some displacement, an increase in slope is seen, indicating that contact between the casing and the cement is obtained. The stiffness is then increasing towards the stiffness of a well-cemented casing. In this test, a stiffness of about 42 kN/mm is reached before logging is aborted, which is representative of a well-cemented casing (also here, a slightly lower stiffness compared to Figure 4.22

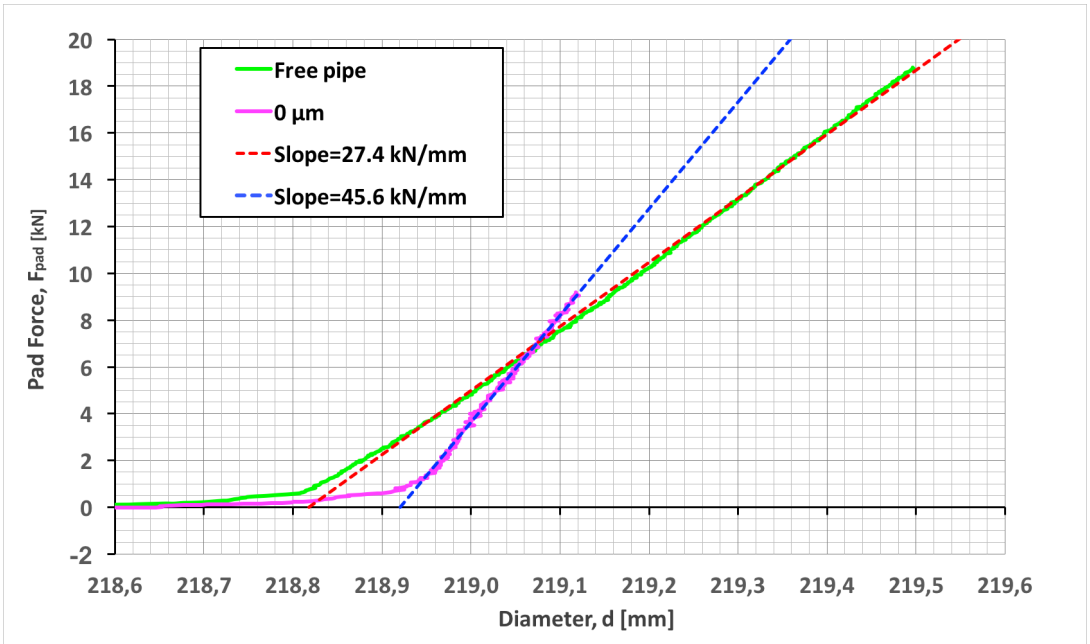

Figure 4.22: Results from experiments conducted to establish the free pipe and well-cemented (0 µm microannulus) response for the microannulus setup.

is expected due to the casing taper). This shows that the AVT is able to prove the presence of an annular cement, even in the case of a relatively large microannulus. It also shows that the AVT is able to detect the presence of a microannulus at the casing-cement interface as an increase in slope from the uncemented stiffness to the cemented stiffness.

However, the response is not as ideal as it was depicted schematically in Figure 3.3. The changes in stiffness – from zero stiffness to the free pipe stiffness and from the free pipe stiffness to the well-cemented stiffness – occur through a gradual increase and not as a sudden change in slope. Following this, picking the diameters d_1 and d_2 to calculate the microannulus size, becomes less straightforward. Linear least squares regression was once again used to fit the straight line representing the free pipe stiffness. The following assumptions were then made when selecting the two diameters:

d_1: The initial displacement occurring before the full free pipe stiffness is seen, is not contributing significantly to the displacement of the casing. In this region, the displacement is mostly caused by the tool positioning itself for displacement and obtaining proper pad alignment. Following this, d_1 is chosen as the point where the straight line is first reached (represented by the triangle in Figure 4.23).

d_2: Casing-to-cement contact is obtained when a stiffness in excess of the free pipe stiffness is seen. This represents the point where the microannulus is closed. Following this, d_2 is chosen as the point where the logged data starts to deviate (upwards) from the straight line (represented by the diamond in Figure 4.23).

To avoid random noise affecting the picking of the diameters, a threshold of 0.15 kN was used. In other words, the diameters were picked as the points where the logged data

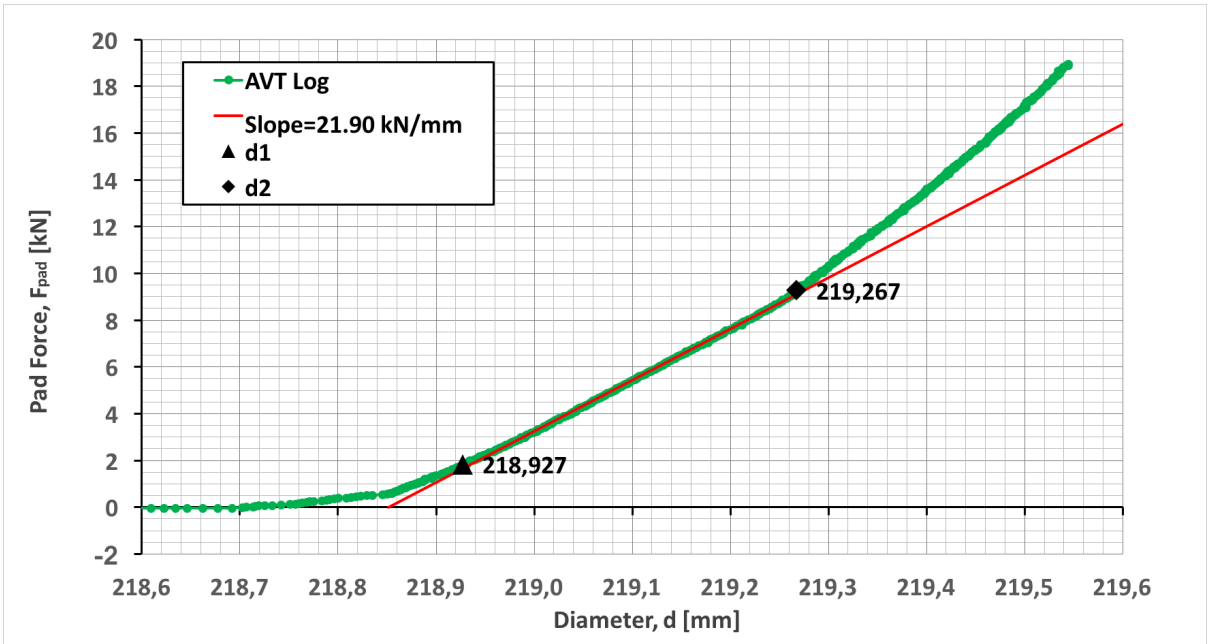

Figure 4.23: Result from logging a 175 µm microannulus.

differs from the straight line with more than 0.15 kN. This was found to be sufficient to filter out random noise and small enough to detect where the logged data departs from the straight line. For the 175 µm test shown in Figure 4.23, this results in the following microannulus size from the AVT measurement, according to Equation 3.4:

$$w_{ma} = \frac{d_2 - d_1}{2} = \frac{219.267\ mm - 218.927\ mm}{2} = 170\ \mu m$$

For consistency, the same procedure was used for all microannulus sizes logged. The logging results for all sizes with the resulting diameters are included in Appendix C.1. From these logging responses, it can be seen that, as the microannulus size increases, more is seen of the low free pipe stiffness and correspondingly less of the higher cemented stiffness. This is also reflected in the fact that the total diametral displacement (at the end of the test) is increasing. The resulting microannulus sizes for all the tests are given in Table 4.2 below.

Table 4.2: Resulting microannulus sizes from the AVT measurements for all the "known" microannulus sizes logged.

Known [µm]	26	35	45	55	65	75	85	95	105	115	125	135	145	155	165	175	185
AVT [µm]	38	43	53	54	64	77	87	101	105	115	118	135	136	153	169	170	183
Error [µm]	12	8	8	-1	-1	2	2	6	0	0	-7	0	-9	-2	4	-5	-2

Figure 4.24 shows a graphical presentation of the results in Table 4.2. The resulting microannulus sizes found from the AVT measurements are plotted against the "known" microannulus sizes calculated from the casing taper. It is clear that the AVT is able

to quantify the size of the microannulus generated, with an associated and rather small uncertainty. The points follow the trend of the straight line representing the ideal case of identical values, proving that the incremental increase in microannulus size is reflected in the AVT measurements.

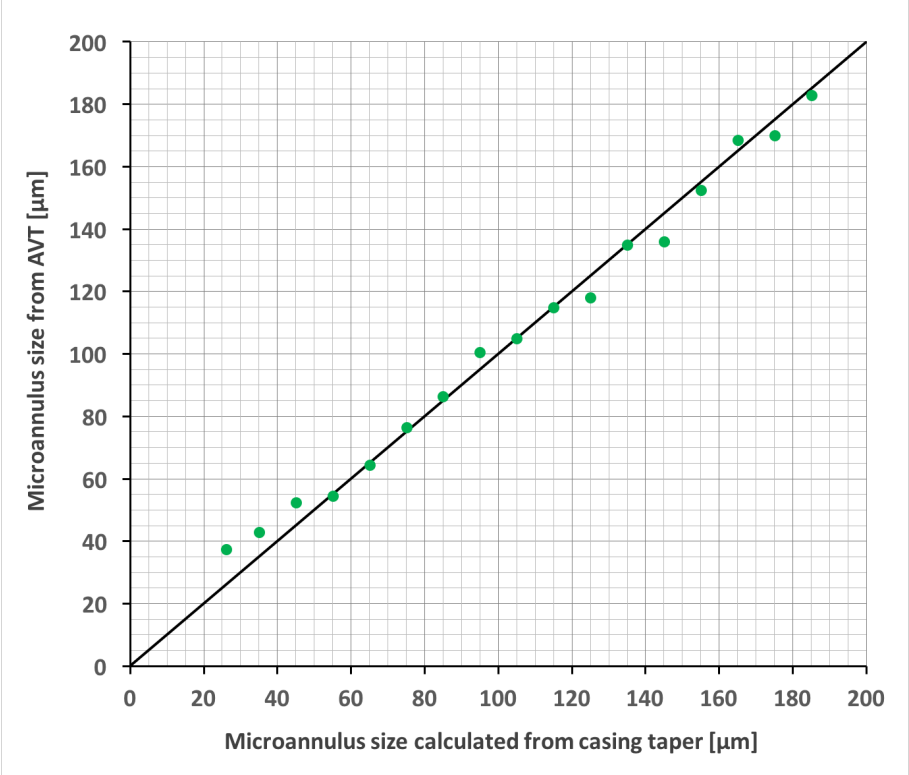

Figure 4.24: Resulting microannulus sizes from the AVT measurements plotted versus the "known" microannulus size calculated from the casing taper. The black straight line represents the ideal case of the two sizes being identical.

4.4.3 Poorly Cemented Casing

Figure 4.25 shows the results from logging of two samples of the same geometry – one sample with coated aluminum to represent the case of a good cement, and one sample with uncoated aluminum to represent the case of a poor cement. As two different casing samples were used, their diameter does not match completely, with the casing ID of the poorly cemented sample being slightly less than for the properly cemented sample.

Both tests show a clear linear trend and a stiffness in excess of that of free pipe, indicating that the casing in both cases is supported by an annular cement. Surprisingly, the sample representing a poor cement showed a greater stiffness than the sample representing a good cement (63.0 kN/mm versus 55.0 kN/mm). The opposite was expected, as the poorly cemented sample had a higher cement porosity and a higher content of unhydrated cement due to the aluminum-cement interaction described in Section 4.1.2.

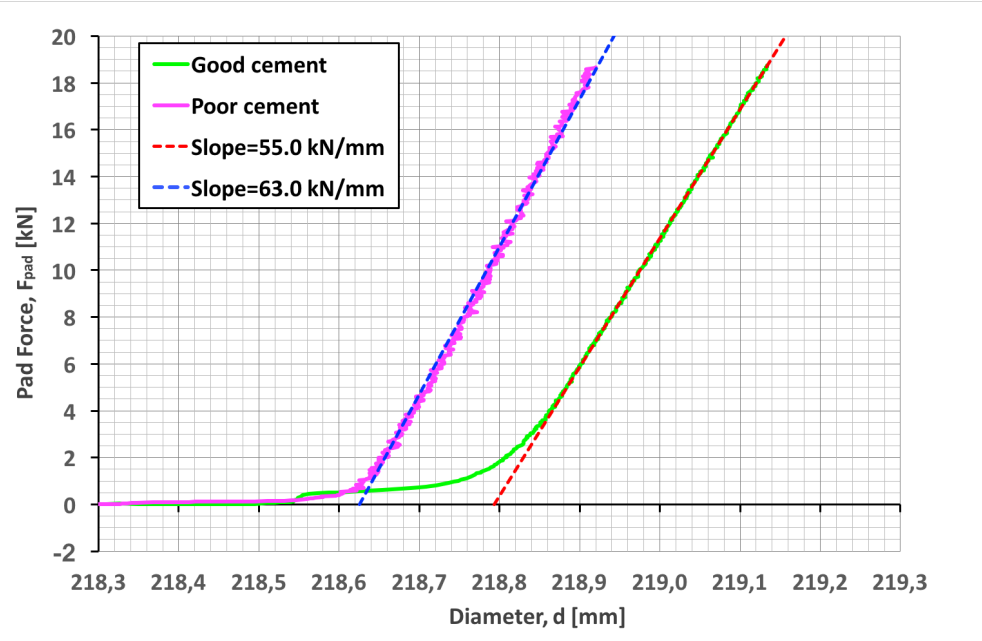

Figure 4.25: Results from logging two samples of the same geometry; one representing a good cement and one representing a poor cement.

This result is therefore not believed to be caused solely by the mechanical properties of the set cement. For the sample representing a poor cement job, a curing temperature of 66°C was used. For later samples (including the sample representing a good cement), the curing temperature was lowered to 40°C with the aim to reduce water evaporation as well as the stresses imposed on the sample due to temperature contraction when the heating cable was removed (as discussed in Section 4.1.2). Therefore, the temperature contraction were greater for the sample representing a poor cement job. This is believed to have improved the condition at the cement sheath's interfaces, as it effectively caused the aluminum pipe to squeeze the cement sheath towards the casing. This also changed the stress conditions of the sample. The reduction of this effect due to the lower curing temperature is therefore believed to be (part of) the explanation why a lower stiffness is seen for the sample with a good cement.

A simple test was performed to further test this hypothesis. The heating cable was wound back on the sample representing a good cement and the temperature was raised from ambient conditions (approximately 20°C) to 30°C before re-logging the sample. The result is shown in Figure 4.26. The result from the test at ambient conditions (same as was shown in Figure 4.25) is included for comparison.

It is clear that by increasing the temperature, the measured stiffness is reduced – in this case from 55.0 to 48.3 kN/mm. This result indicates that it is not only the mechanical properties of the cement sheath and the outer pipe ("formation") that is dictating the experienced stiffness when logging the sample with the AVT. Also other effects, like the condition at the cement sheath's interfaces and the stress conditions of the sample, have a significant impact on the logging response.

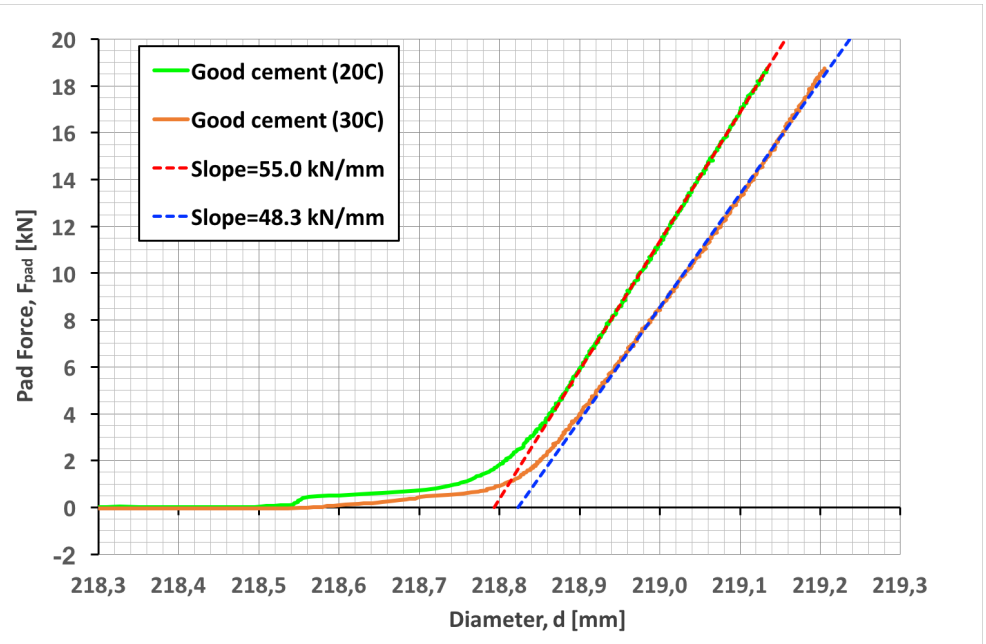

Figure 4.26: Results from logging a well-cemented sample at different temperatures to investigate the effect of aluminum contraction on the measured stiffness.

4.4.4 Tool Eccentricity and Tilting

Figure 4.27 shows the results from logging the same well-cemented sample with the tool properly centralized, eccentric in the direction of the pad movement, eccentric in the direction perpendicular to the pad movement and with the tool tilted. A more detailed view of the results for each of the individual tests is included in Appendix C.2.

It is clear that eccentricity in the direction of the pad movement does not significantly affect or disturb the AVT measurement. When comparing with the reference case of a properly centralized tool, the two responses are almost identical in both diameter and stiffness. This proves that the tool is self-centralizing in the direction of pad movement, as expected. This was also visually observed during the test, where it was seen that once the first pad obtained casing contact, it pushed the tool towards a centralized position. If looking closely at the region just before the increase in stiffness is occurring (around 218.7 mm diameter), it can be seen that the pad force for the eccentric case (red) is slightly higher than for the centralized case (green). This could be the pad force that is pushing the tool towards a centralized position. However, this force is small compared to the pad force which is later applied to the casing wall and is not disturbing the AVT measurement.

The case of eccentricity in the direction perpendicular to the pad movement, however, proved to have a significant impact on the measurement. In this case, both pads obtained casing contact simultaneously, but at a diameter far less than the casing ID. As was shown in Figure 4.20c, the eccentricity caused an incorrect contact angle between the pads and the casing. Actually, this also made the tool push itself towards a more centralized position after pad contact was first obtained, explaining the early peaks/bumps in logged pad

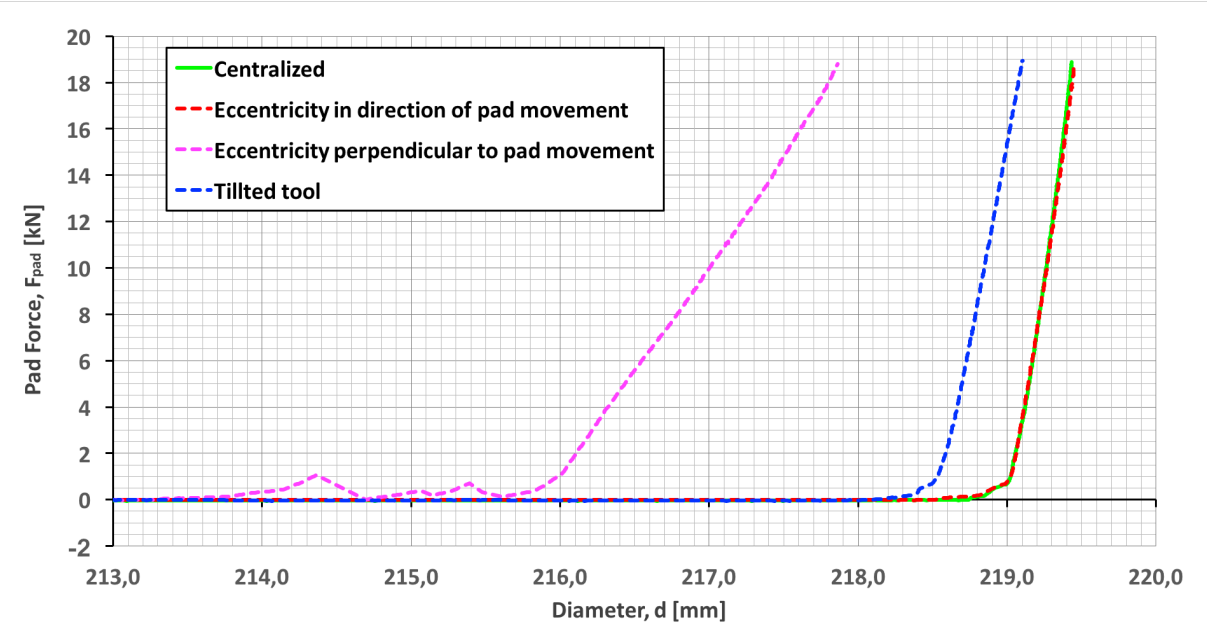

Figure 4.27: Results from experimental testing with tool eccentricity in two different directions and tool tilting. The properly centralized response is included for comparison.

force. This gradually improves the contact angle, and eventually, the tool did not move no more and an increasing pad force was applied. However, this happened at a diameter approximately 3 mm less than for the centralized case (216 mm versus 219 mm). It is also clear that the recorded stiffness is significantly lower than for the centralized case (9.4 kN/mm versus 45.4 kN/mm), explained by the fact that only part of the pads is in contact with the casing. This results in a smaller contact area, hence a greater pressure exerted on a local region of the casing and an increased displacement. As a more or less straight line is observed, it does not appear that the pads or the casing deform much to improve the contact (this should have been seen as a gradual increase in stiffness).

Similar effects can also be observed for the result from logging with a tilted tool – however, to a lesser extent. Also here, contact is obtained at a diameter which is less than the ID of the casing, due to the mismatch in alignment between the pads and the casing. The difference is about 0.5 mm. The recorded stiffness is also somewhat lower than for the centralized case (34.6 kN/mm versus 45.4 kN/mm), due to the insufficient contact area caused by the poor alignment. Also here, a clear linear trend is seen, indicating that no significant pad or casing deformation is occurring to improve the pad-casing contact.

Chapter 5

Numerical Simulations

This chapter describes the numerical simulations performed, to be able to further evaluate the logging response of the AVT for specific cases. This was done through finite element analysis (FEA), using the *ANSYS Structural Analysis* software.

5.1 Simulation Model

To be able to compare directly with the experimental testing described in Chapter 4, the geometry of the improved set-up using steel to represent the formation (as described in Section 4.1.3), was used also for the simulations. An illustration of the geometry is shown in Figure 5.1. The model included the 9 5/8-in 53.5# casing and the outer steel pipe

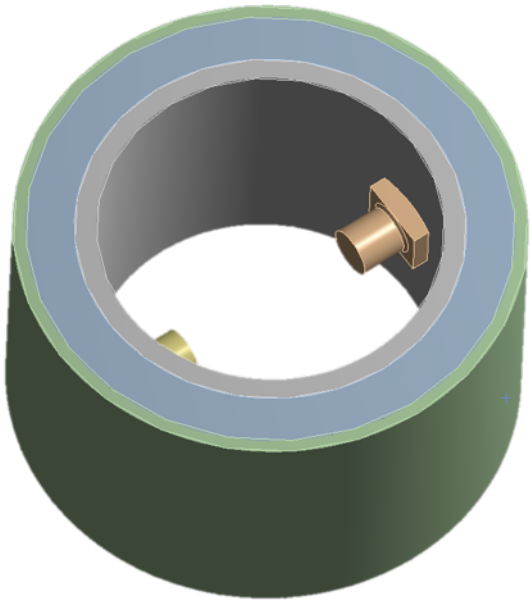

Figure 5.1: Geometry of the numerical simulation model, including the outer steel pipe, an annular cement sheath, the 9 5/8-in casing and the AVT pads.

with their dimensions, as well as an annular cement fill between the two. The height of all three parts was set to 25 cm, to resemble the experimental set-up. For the case of a free pipe, only the casing was included. To model the AVT, only the tool pads (with the associated piston rods) were included in the simulation model, as shown. This was done to improve the computational speed and reduce the complexity of the model, compared to including the full tool assembly. The two pads are placed at the midpoint of the casing height, spaced 180° apart.

The elastic material properties used, are summarized in Table 5.1. Young's modulus and Poisson's ratio are input, while other moduli are calculated from isotropic linear elasticity theory by the software.

Table 5.1: Material properties used for numerical simulations.

Object	Material	Parameter	Value	Unit
Outer pipe	Steel S355J2H	E	205	GPa
		ν	0.3	-
Cement	Neat G	E	5.5	GPa
		ν	0.2	-
Casing	Steel P-110	E	200	GPa
		ν	0.3	-
Tool pads	Steel AISI 4140	E	205	GPa
		ν	0.3	-

Bonding was included at the interfaces between the casing and cement and between the cement and the outer pipe. The contact between the pads and the casing was modeled as a frictionless contact. The bottom end of the casing, cement, and the outer pipe was modeled with a frictionless support, to resemble the experimental set-up where the samples were placed on the floor during logging. No temperature effects were considered.

The FEA mesh was refined in steps, each time running the simulation. When the results (displacement and stresses) showed no variation when increasing the number of elements, the mesh was considered sufficient.

5.2 Simulated Cases

AVT logging was simulated by applying a pressure on the back surface of the two pistons, corresponding to the piston area. As the springs were not included in the simulations, the pad force will equal the piston force, given as:

$$F_{pad} = F_{piston} = pA_{piston} \tag{5.1}$$

where

$$F_{pad} = \text{Force exerted by pad on the casing} \quad [N]$$
$$F_{piston} = \text{Force exerted on the piston} \quad [N]$$
$$p = \text{Pressure exerted on piston} \quad [Pa]$$
$$A_{piston} = \text{Area of piston} \quad [m^2]$$

The pressure was increased in steps from 0 to 250 bar, to give a force comparable to experimental testing. As a linear elastic response was expected, relatively large pressure increments could be chosen. At each step, the simulations give the resulting displacement and stresses imposed on the system, as the steady state solution of the simulation model.

5.2.1 Free Pipe

Logging of free pipe was simulated to investigate the stiffness of an uncemented casing. In addition, it can indicate whether the casing is deformed mainly by ovalization, as assumed and expected, or by compression of the steel in the pads and the casing wall. As this is the same system stiffness as is experienced during displacement to close a casing-cement microannulus, it can also assist in evaluating the procedures and assumptions used for microannulus size quantification from the experimental logging response.

5.2.2 Well-Cemented Casing

Logging of a well-cemented casing was simulated to investigate the stiffness of a cemented casing, and to evaluate whether there is a sufficient stiffness contrast compared to a free pipe. This is also the same stiffness that should be experienced *after* closing a microannulus.

5.3 Simulation Results

5.3.1 Well-Cemented Casing Versus Free Pipe

The simulated AVT logging responses for a free pipe and a well-cemented casing are shown in Figure 5.2. The linear diametral displacement of the back surface of the pistons – which is similar to what would be measured by the tool's LVDT – is plotted versus the applied pad force. It is clear that there is a significant stiffness contrast between the free pipe and the well-cemented casing. The slope corresponding to the free pipe stiffness is 45.8 kN/mm, while the slope is 204.7 kN/mm for the well-cemented case. Further, it can be seen that the response is clearly linear for both cases, indicating that deformations are linearly elastic.

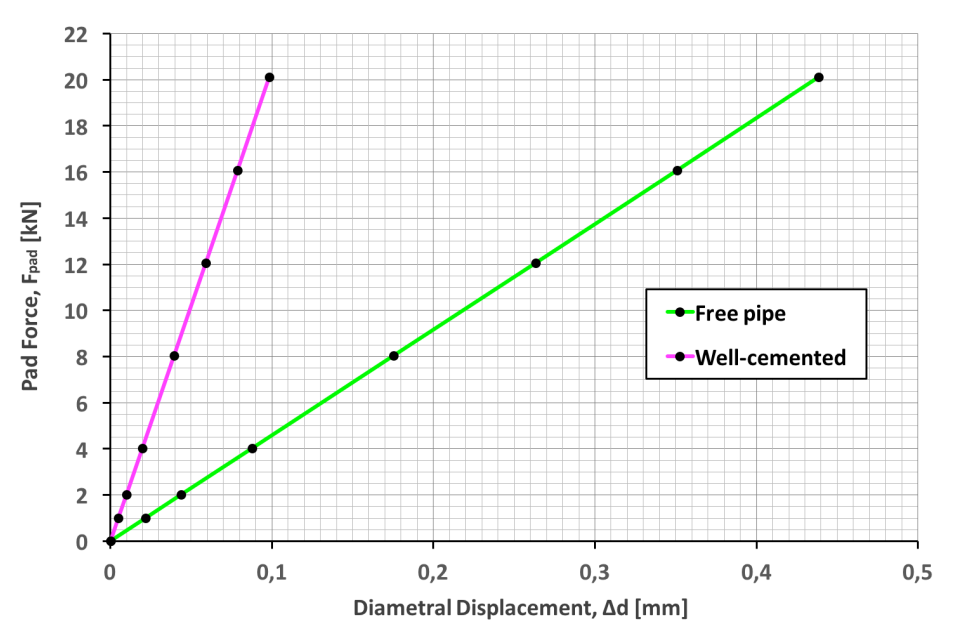

Figure 5.2: Simulated AVT logging responses in the cases of a free pipe and a well-cemented casing.

5.3.2 Further Results from the Free Pipe Case

The simulation results from the free pipe case were further investigated to increase the understanding of the AVT logging response. Particularly, this is helpful for the microannulus calculations, as these are performed using the free pipe region, which is the displacement contributing to closing a microannulus. Figure 5.3 shows a color map of the simulated radial displacement of an uncemented casing when applying a pressure of 250 bar at the pistons (corresponding to a pad force of 20.1 kN). It is clear that the casing is deformed mainly by ovalization. The casing is displaced by around 219 µm maximum in the direction of the pad force, while it contracts by close to the same amount (208 µm) in the perpendicular direction. This is further confirmed by the fact that there is little *compression* of the pads or the casing wall itself, as the same red color is seen on the entire tool pads, as well as through the entire casing wall in the direction of the pads.

To further evaluate this, the displacement at the piston surface (which is the same as the simulated free pipe logging response shown in Figure 5.2) was compared with the displacement occurring at the outer casing wall. This is shown in Figure 5.4. As expected, the displacement at the piston surfaces is slightly greater than the one occurring at the outer casing wall (for the same applied force), and the difference between the two increases with the applied force. However, for a typical microannulus of 100 µm (which would close at a diametral displacement of 0.2 mm), the difference between the two is only about 3 µm. This indicates that the LVDT, which is positioned at the backside of the pistons, is able to measure a displacement very close to the one contributing to the closing of a microannulus at the outer casing surface.

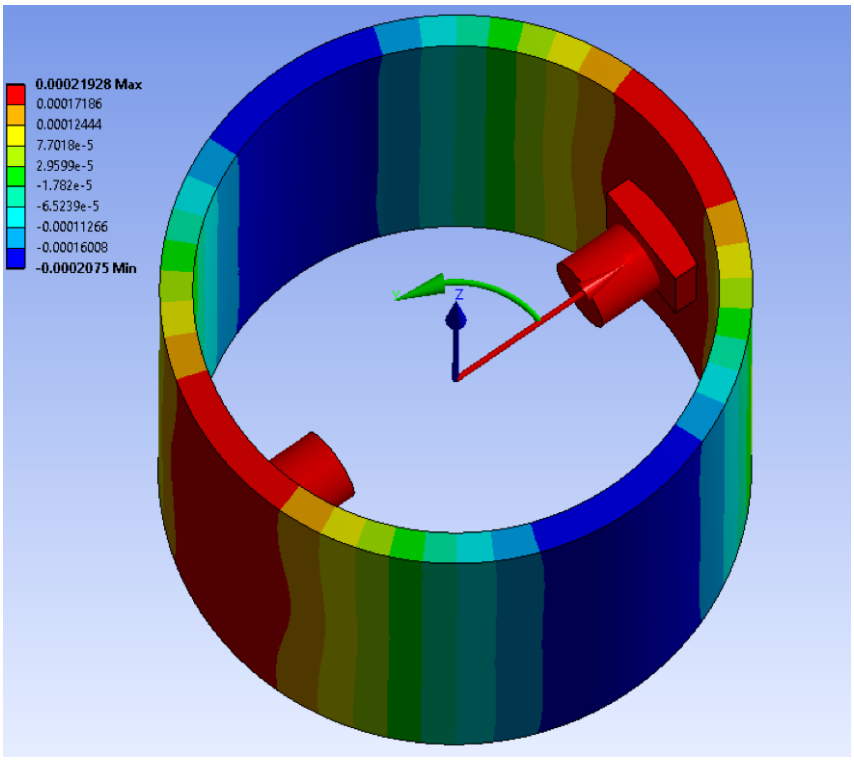

Figure 5.3: Simulated radial displacement of an uncemented casing, when applying a force of 20.1 kN. It is clear that the casing is predominantly deformed by ovalization.

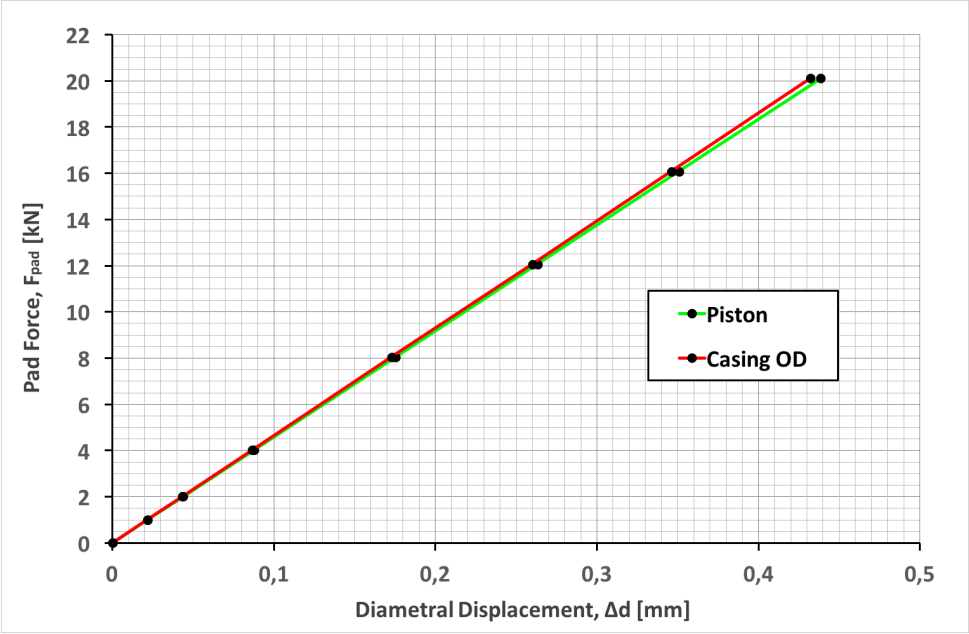

Figure 5.4: Simulated displacement at the piston surface (which is the one measured by the tool LVDT) and at the outer casing wall (which is the one contributing to the closing of a microannulus), plotted versus the applied pad force.

Chapter 6

Discussion

6.1 Implications of the Results and Findings

6.1.1 Experimental Testing

As this was the first experimental testing ever to be conducted with the AVT, it was chosen to construct samples representing relatively simplistic casing-cement-formation systems. This was done to be able to test the underlying principles of the tool, for a "proof of concept". However, to construct adequate samples representing the desired configurations of the casing-cement-formation system, proved quite challenging. A significant part of the experimental work performed was therefore related to evaluating and improving the procedures and set-up used for sample construction. After several modifications, it was possible to construct satisfactory full-scale diameter samples, with a geometry representative of a typical production casing cement job – both with and without a microannulus separating the casing from the cement sheath. When considering the challenges encountered, it becomes clearer why it is often challenging to properly cement a casing at a depth of several thousand meters, at conditions very different and far less predictable compared to the laboratory.

The experimental testing of the AVT has shown that an uncemented casing gives a characteristic and clearly linear response, represented by the mechanical properties of the casing itself. This makes a free pipe relatively easy to detect. A cemented casing, however, proved to give a more complex response: It is also linear, but seems to depend on other factors than solely the mechanical properties of the casing, cement, and formation. This is believed to include the conditions at the cement sheath's interfaces, as well as the stresses surrounding the sample. Especially, this became evident from the results described in Section 4.4.3, which indicated that the stress conditions of the sample (caused by temperature contraction) actually had a more significant effect on the logging response, than the cement quality itself. When also considering the fact that actual formations are sig-

nificantly less predictable and homogeneous in terms of mechanical properties, and that a typical wellbore will be geometrically more irregular, it seems that to infer the *quality* of the cement itself using the AVT, is challenging due to the response's dependency on several other factors.

However, a larger stiffness *is* evident in the cases where the casing is supported by an annular cement, compared to the case of a free pipe. As the free pipe response is so characteristic, it is also easy to detect whatever deviates from this response. This can be exploited to prove the *presence* of an annular cement sheath, identified as a stiffness in excess of the free pipe response. This also holds true in the case of a microannulus: As long as the microannulus is small enough, such that casing-cement contact can be obtained, the presence of a cement sheath behind the microannulus can be proven. This contrast in stiffness also makes the AVT able to prove the presence of a casing-cement microannulus through the change in slope on the logging response – from the free pipe stiffness to a greater stiffness once cement support of the casing is obtained.

To quantify the size of a microannulus, the characteristic free pipe response could once again be exploited. This could be done, as the microannulus-region on the AVT logging response (the interval between d_1 and d_2) corresponds to the free pipe stiffness. It was therefore assumed that, whenever the linear free pipe response is seen, the casing is displaced/ovalized to close the microannulus. The displacement which does not follow the straight line was assumed *not* to contribute to the closing of the microannulus. The results obtained from logging different microannulus sizes indicates that these assumptions were fair. The results show that the AVT is able to quantify the size of a uniform microannulus at the casing-cement interface, with an associated and rather small uncertainty. Keeping in mind that there also is an uncertainty related to the size of the microannulus which actually is generated when the casing is hoisted, these results are as one could expect. It is also clear that an incremental increase in the microannulus size of only 10 µm is picked up by the tool.

The diametral displacement of the casing is measured with an accuracy in the micrometer range, using the LVDT. However, it has to be combined with the pad force measurement as well as the drawn straight line representing the free pipe, in order to quantify the microannulus size. To ensure consistency in the microannulus size calculations, a semi-automatized procedure was formulated, using least squares linear regression to fit the straight line. A constant threshold was used to detect the diameters where the logging response departs from the straight line. However, the source data used for the linear regression had to be picked manually. For large microannuli, this is fairly straightforward, as the linear region is predominant. For small microannuli, the free pipe region is rather small, making it more challenging to select this data, hence also to fit the proper straight line. As the straight line is key for the selection of the two diameters (d_1 and d_2) used to calculate the microannulus size, this will give a reduced accuracy for small microannuli. To further increase the consistency and reduce the human impact on the measurement, it should be evaluated for further testing, to also automatize the identification of the

straight line region.

When evaluating these results, one should keep in mind that the microannulus created in the laboratory, is a very simplistic representation. It is a uniform and empty space, separating the casing from a perfect sheath of cement. In a real scenario, a microannulus might not be uniform around the wellbore and it might be partly filled with particles like solid fill or cement residue. On the other hand, when considering that the mechanisms causing a microannulus to form (like pressure and temperature variations within the casing) are typically uniform features, this representation is maybe not that atypical after all. However, for future testing, it should be evaluated to use the same mechanisms as in the field, to also generate a microannulus in the laboratory – for instance by cooling of the casing.

It was suspected that there might be some compression of the tool pads and the casing steel during displacement, and not only ovalization of the casing. This would cause the LVDT to measure a greater displacement than the one contributing to the closing of the microannulus. However, as the microannulus size estimated from the AVT measurement agrees well with the size calculated from the casing taper, this appears to not affect the measurement to a significant degree. In addition, if deformation of the pads/casing *was* affecting the measurement, it would be to an increasing extent as the size of the microannulus was increased. This is caused by the fact that a larger microannulus requires a greater force in order to obtain casing-cement contact, which then would cause a greater compression of the pads/casing. This is reflected in Figure 6.1, where the force needed to close the microannulus (at diameter d_2) is plotted versus the microannulus size. As the microannulus size results obtained from the AVT show no sign of an increasing error as the microannulus size increases, this further strengthens the indications that pad/casing compression is not very significant, and that the displacement of the casing is largely due to ovalization of the casing.

By experimental testing, it was confirmed that the AVT is prone to poor centralization within the casing, as it causes a mismatch in the alignment between the tool pads and the casing wall. This results in incomplete contact between the pads and the casing, and hence an apparent lower stiffness. It was suspected that a gradual increase in stiffness would be experienced, due to deformation of the tool pads and/or the casing giving an increasing contact area. However, this was not observed, further strengthening the indications that there is no significant deformation of the pads and the casing (for the pressure applied). Nevertheless, to be able to measure the true stiffness, it must be ensured that the tool is properly centralized.

Severe eccentricity is actually easy to detect, as a stiffness less than the free pipe stiffness. In addition, pad contact is obtained at a diameter significantly less than the casing ID. These features should be looked out for when interpreting the logging results. A slight mismatch in alignment, on the other hand, appears to be more difficult to detect. This becomes clear from the results from logging a well-cemented casing with a tilted tool (as presented in Section 4.4.4). Also here, contact is obtained at a diameter somewhat less

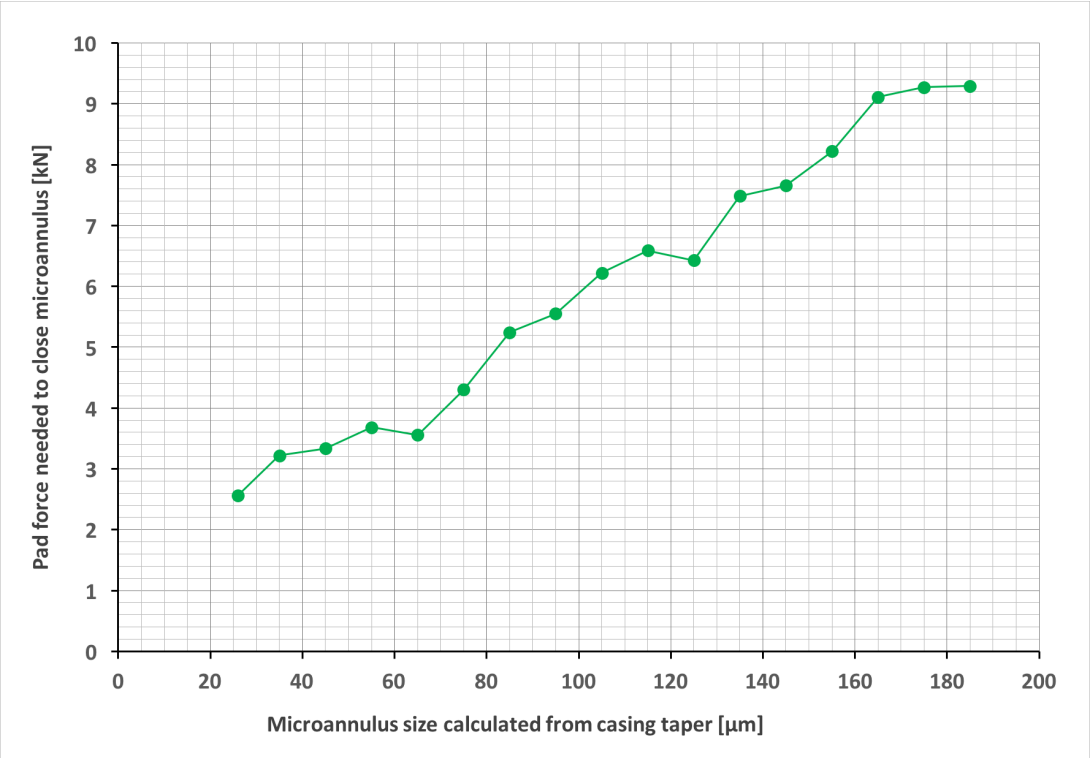

Figure 6.1: Force needed to obtain casing-cement contact plotted versus the microannulus size.

than the casing ID, however only by approximately 0.5 mm, which might not be enough to be detected. As the reduced stiffness due to the poor alignment is similar to that of free pipe, it could result in the well-cemented casing being interpreted as an uncemented casing. This further shows that proper centralization is important, and also that the response from the acoustic tools should be used in combination with the AVT for an increased understanding.

However, the tool has proven to be self-centralizing in the direction of pad movement. Only a small pad force was needed in order to push the tool into a centralized position, to then obtain a logging response almost identical to the centralized case. One should keep in mind that this force will be significantly larger for an actual logging string run into a wellbore, especially in highly deviated wells where the logging string may drop towards the low side. But still, this force is believed to be small compared to the pad force which is later applied to the casing wall. This self-centralizing characteristic could possibly be exploited by including an additional pair of pads, perpendicular to the original set. Self-centralization should then be achieved in both directions, and the system will also be statically determined. However, this will change the deformation "mechanism" since ovalization will no longer be possible, as the casing is deformed in four directions. If doing so, one should also ensure that the pads move synchronous towards the casing, for instance by using the same pressure chamber to pressurize all four pads. Another alternative would be to impose centralization by lifting/lowering the tool, or vibrating it, while the pads approach the casing. If premature pad-to-casing contact is obtained

due to eccentricity, the tool would then tend to "jump" towards a more centralized position. Actually, this behavior would be similar to what was experienced for the case of eccentricity perpendicular to the pad movement (as shown in Section 4.4.4). In this case, centralization improved after initial pad contact was obtained. However, complete centralization was never obtained in this case. These ideas should be evaluated further, to reduce the AVT's sensitivity to improper centralization.

The effect of eccentricity in the case of a microannulus has not been investigated. However, from what have been learned from the experimental testing conducted, this is expected to give a lower stiffness for the free pipe region due to insufficient pad contact. Further, since ovalization seems to be the main mechanism of deformation and it appears to be insignificant compression of the tool pads and the casing steel itself, the free pipe region is still believed to be fairly linear, but with a lower slope. This means that it should still be possible to fit the straight line representing the displacement closing the microannulus. Since the casing is ovalized as for the centralized case, the diametral displacement measurement should still be able to measure a rather accurate microannulus size. Once contact between the casing and the cement is obtained, the stiffness should start to deviate (upwards) from the straight line, towards a greater stiffness (which is less than the full well-cemented stiffness due to the eccentricity). This is something that should be investigated in future experimental testing.

For the samples constructed for microannulus generation, it was possible to inspect the cement sheath by pulling the tapered casing out of the sample after logging. This reveals the cement sheath that has been adjacent to the casing (as shown in Figure 4.14) and makes it possible to visually evaluate any damage imposed by logging. No cracks were visible to the naked eye. However, the logging before generating a microannulus was not performed to full pressure – just to avoid damaging the cement sheath. This also showed that it is not necessary to use the maximum force to be able to detect a well-cemented casing: In this case, around 9 kN was more than enough to confidently detect a good cement, proving that damage can be minimized. To further evaluate if the applied load could create smaller-scale damage like microcracks and debonding of cement, X-ray CT or pressure/leak testing should be evaluated. However, on a wellbore scale, the region affected by the measurement is rather small, meaning that any damage will be local.

6.1.2 Numerical Simulations

Numerical simulations were performed to compare with the experimental results, and aid for an increased understanding of the AVT logging response. Figure 6.2 shows the resulting AVT logging response from the numerical simulations together with the experimental results – both for a free pipe and for a well-cemented casing. Unsurprisingly, the simulated response is significantly more ideal, compared to the experimental results. Most of all, this is evident from the initial displacement region, where the experimental results show a non-linear trend due to the slight mismatch in the pad-casing contact (as described

earlier). This also makes it challenging to pick the diameter where contact occurs for the experimental results, as there is no precise point where contact is clearly obtained.

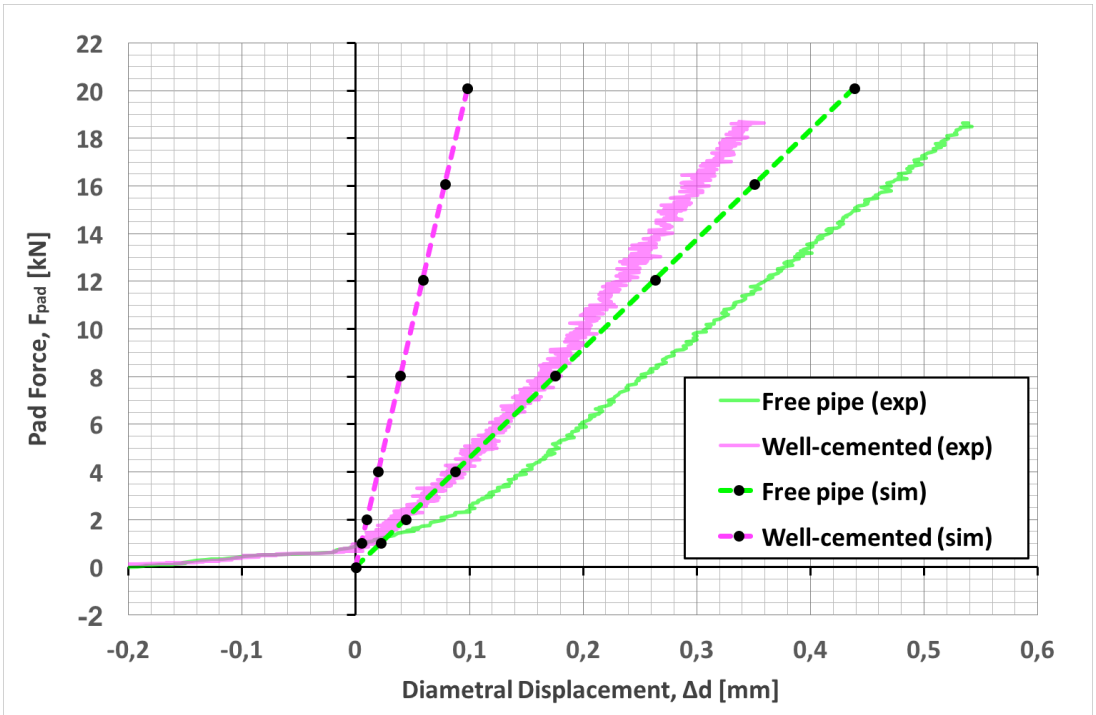

Figure 6.2: Results from numerical simulations (sim) and experimental testing (exp) of free pipe and well-cemented casing – for comparison.

The simulated free pipe stiffness was found to be slightly greater than the free pipe stiffness measured during experimental testing (45.8 kN/mm vs. 37.4 kN/mm), which can also be seen in Figure 6.2 from the difference in slope. This could be caused by a slight deviation in the actual casing dimensions and properties, compared to the values listed. It could also be caused by a slight mismatch in alignment between the pads and the casing during experimental testing, as testing has shown that this causes an apparent lower stiffness. This mismatch could be due to tool eccentricity or tilting, or simply due to a slight difference in curvature between the pads and the casing. Nevertheless, the simulated free pipe stiffness match quite decently with the experimental results.

For the well-cemented case, however, the simulated stiffness was found to be considerably greater than for the experimental results (204.7 kN/mm vs. 59.7 kN/mm). The two steel pipes (the casing and the "formation") should be relatively easy to characterize. The cement, however, is more difficult to model. Even though a relatively low cement Young's modulus (5.5 GPa) was used for the simulations, the simulated logging response showed a stiffness which is more than three times the stiffness found from experimental testing. This could be caused by the simulation model assuming a too perfect case, of a rock-solid cement sheath completely bonded at both surfaces. In reality, the conditions at the cement sheath's two interfaces may not be as perfect, which can affect the response. This is also in line with the experimental results from the attempt to infer the cement

quality from the measured stiffness, which indicated that the mechanical properties of the individual components are not the only factors affecting the logging response. However, this discrepancy does not affect the microannulus size calculation, as only the free pipe region is used for this.

Further analysis of the simulation results for the free pipe case, showed that a free pipe is predominantly deformed by ovalization of the casing and that the displacement of the tool pistons matches well with the displacement of the outer casing wall. This is an important finding, as it means that the LVDT (which has its fixation points at the pistons), can be used to measure the displacement which is closing the microannulus, with good accuracy. For a typical microannulus size of 100 µm, the simulated diametral displacement of the pistons was found to be only 3 µm greater than the displacement of the outer casing wall. Following this, the microannulus size calculated through Equation 3.4, would be overestimated by only 1.5 µm in this case. These findings also imply that the procedure used for calculating the microannulus size from the experimental results was reasonable.

The work on the numerical simulations should be continued, to further increase the understanding of the AVT logging response. It should be investigated why the simulated well-cemented logging response deviates considerably from the experimental results. This should be done by further evaluating how to model the conditions (bond, friction, etc.) at the cement sheath's interfaces, as the divergence is not believed to be caused (mainly) by the mechanical properties of the casing, cement, and formation.

Simulations should also be used further, to evaluate any potential damage imposed on the cement. This should be done by investigating simulated stresses in the cement sheath, as a function of the applied pad force. The possibility of cracking due to the applied pad force, as well as the possibility of debonding due to casing ovalization, should be considered. The findings should be evaluated against the force actually needed to confidently verify the presence of cement. From experimental testing, this force has proven to be less than the maximum force possible by the tool. The simulated stresses imposed on the casing should also be evaluated, for the possibility of casing yield. In this matter, the stresses already present in the casing in a real field scenario should also be taken into consideration.

6.2 AVT for Improved Cement Evaluation

Today, cement evaluation by logging is performed almost exclusively using the acoustic tools presented in Section 2.3. As presented, every tool has its strengths and weaknesses, and none of them are perfect as stand-alone tools. Especially, this is reflected by Table 2.1, where the importance of integrating several sources of data becomes evident. The AVT is therefore meant to complement the acoustic logging tools used today, to contribute to an improved evaluation of the annular cement. The effect of this, is summarized in Table 6.1 which serves as an extension to Table 2.1. A typical logging string used for cement evaluation today, consisting of the acoustic tools presented in Section 2.3, is shown in the leftmost column. The rightmost column shows the combination of these acoustic tools together with the AVT.

The most important advancement provided by the AVT is the ability to quantify the size of a casing-cement microannulus. Today, a microannulus could relatively easily be detected, but no tools are able to measure its size. Hence, the AVT enables an evaluation of the microannulus's effect on the integrity of the cement. As described in Section 2.2.2, the microannulus size (together with the fluid type) has an immense effect on the leak rate through the microannulus. To infer what fluid type is present in the microannulus, the ultrasonic pulse-echo measurement could possibly be used, as it shows a differing response in the case of a gas- versus a liquid-filled microannulus (as described in Section 2.3.3.3).

In addition, the AVT is able to detect the presence of an annular cement sheath, even when a microannulus is present. Especially, this is beneficial in the case of a gas-filled microannulus, where none of the acoustic tools are able to detect the cement sheath, but gives a response similar to that of a free pipe. However, it seems that evaluating the quality of the detected cement is a challenge also for the AVT.

The additional information supplied by the AVT gives an increased understanding of the downhole situation – especially about the condition at the casing-cement interface. As all the acoustic logging tools predominantly evaluate the condition at the casing-cement interface (through acoustic waves traveling in/along the casing), this information can increase the understanding of the acoustic logging response to possibly give a better interpretation of the acoustic logs.

The AVT is believed to be especially valuable for P&A operations where an existing annular cement sheath is evaluated for serving as a barrier in an eternal perspective. Such a cement sheath has been subjected to pressure and temperature variations during production/injection over the lifetime of the well and may, therefore, be particularly prone to microannulus formation. As a microannulus *is* a potential leak path and also difficult to remedy, the solution is therefore often to initiate heavy operations to restore the annular seal behind the casing if a microannulus is suspected. As described in Section 1.1, these are also time-consuming and costly operations, contributing to the high costs associated with P&A. Following this, the decision of using (or not using) an annular cement as a

permanent barrier, should be taken based upon the best possible foundation of data. By enabling an evaluation of a potential microannulus's effect on the integrity of the annular cement, the AVT is believed to improve this decision basis.

Table 6.1: Summary of the characteristics of the AVT. The characteristics of a typical acoustic logging string is shown in the leftmost column. The combination of the acoustic tools with the AVT is shown in the rightmost column.

	CBL/VDL + pulse-echo + flexural	AVT	CBL/VDL + pulse-echo + flexural + AVT
Cement evaluation if:			
Liquid-filled microannulus	Yes/good	Partial/fair	Yes/good
Gas-filled microannulus	No/poor	Partial/fair	Partial/fair
Channeling evaluation:			
Azimuthal channels	Yes/good	Partial/fair	Yes/good
Radial channels	Yes/good	Partial/fair	Yes/good
Information about:			
Cement-formation bond	Partial/fair	Partial/fair	Partial/fair
Casing ID	Yes/good	Yes/good	Yes/good
Casing condition	Yes/good	No/poor	Yes/good
Casing position in borehole	Yes/good	No/poor	Yes/good
Microannulus size	No/poor	Yes/good	Yes/good
Log cement types:			
Heavy cement	Yes/good	Yes/good	Yes/good
Lightweight cement	Yes/good	Yes/good	Yes/good
Contaminated cement	Yes/good	Yes/good	Yes/good
Operation in:			
Heavy mud	Yes/good	Partial/fair	Yes/good
Insensitive to:			
Tool eccentricity	Partial/fair	No/poor	Partial/fair
Fast formations	Yes/good	Yes/good	Yes/good
Concentric casings	Yes/good	Yes/good	Yes/good
Casing size & weight	Yes/good	No/poor	Yes/good
Pressure & temperature	Yes/good	Yes/good	Yes/good
Wellbore fluid	Yes/good	Yes/good	Yes/good
Resolution:			
Vertical resolution	Yes/good	*	Yes/good
Azimuthal resolution	Yes/good	*	Yes/good

*Dictated by number of measurements taken

Yes/good
Partial/fair
No/poor

6.3 Field Implementation

For cement evaluation, the AVT should be integrated into the same wireline tool string as the acoustic tools. However, while acoustic logging is performed while pulling the string upwards at a constant logging speed of several hundreds of meter per hour, the AVT necessitates stationary measurements. This means that, in order to perform logging with the AVT, the tool string has to be stopped until the measurement is completed. Hence, the number of AVT measurement points and where to take them should be thoroughly evaluated. This should be done based on real-time interpretation of the acoustic logs, and a casing collar locator (CCL) should be used to avoid logging casing collars. Following this, two-way real-time communication with the downhole tools is needed. This enables real-time interpretation of the acoustic logging data, as well as the possibility to communicate with the AVT when measurements are to be taken. It also allows for real-time interpretation of the logging results from the AVT. This should not be an issue, as the acoustic logs have long been presented in real time, using electrical wireline [53, 54].

To make the AVT fit for downhole application, several changes are necessary compared to the prototype constructed for this initial experimental testing. First of all, the tool design needs to be suitable for integration into a typical wireline logging string. This includes the tool itself, as well as a hydraulic fluid tank. The fluid tank should be in pressure equilibrium with the wellbore surrounding the tool. A downhole hydraulic power unit (HPU) is needed to pressurize the AVT with the fluid from the tank. The HPU needs to be able to generate the necessary overpressure to give the sufficient piston force, as well as to supply a satisfactory rate to ensure efficient logging. The HPU could be powered from surface through the electrical wireline or from a battery included in the tool string. Two pressure measurements are needed, in order to quantify the overpressure exerted on the pistons. This could be solved by including a pressure gauge connected to the tool body (not unlike the prototype), as well as an external gauge measuring the wellbore pressure (alternatively, the fluid tank pressure if in equilibrium with the wellbore). A fail-safe mechanism should be incorporated with the AVT, in the case of power outage. To allow for pulling the string out of the well, it must ensure the overpressure to be relieved, as well as make the pistons retract (e.g. with the present spring configuration). It should also be considered to include a pressure relief valve (PRV), to prevent overpressurization from damaging the casing, the cement or the tool itself.

AVT measurements should be taken in intervals where a microannulus is detected or suspected, based on the acoustic logs. By also interpreting the AVT results real time, the need for additional measurements in the same or another interval could be evaluated. At the end of the day, the value of the *additional* information provided by the AVT measurement has to be compared with the cost (i.e. the time) of performing the measurement. However, in the context of P&A, anything that could aid in the decision-making of using an existing annular cement sheath as a permanent barrier by increasing the understanding of its sealing capability, should be of primary interest.

Chapter 7

Conclusion

A novel cement evaluation tool – the Annulus Verification Tool (AVT) – has been introduced, with the aim to improve cement evaluation:

- By applying a radial force on the inner casing wall while recording the resulting displacement, the tool gives a measurement of the stiffness of the casing and any surrounding material.
- From the recorded stiffness, the AVT can evaluate the presence or absence of an annular cement sheath.
- A casing-cement microannulus can be detected as an increase in stiffness – from the free pipe stiffness to the cemented stiffness – as casing-cement contact is obtained.
- This also means that the AVT is able to prove the presence of an annular cement, even when a microannulus exists (regardless of the microannulus fluid).
- By recording the diametral displacement with a resolution in the micrometer range, the *size* of the microannulus can be quantified by pinpointing the location where casing-cement contact is obtained during displacement.
- By quantifying the size of a microannulus, the AVT enables an evaluation of the microannulus's effect on the *integrity* of the annular cement.
- The AVT is meant to complement the acoustic tools used for cement evaluation today, to give an improved understanding of the downhole situation, leading to better decisions regarding the cement sheath's sealing capability.
- Especially, this is believed to be useful in the context of P&A, where an existing annular cement sheath is evaluated for serving as a barrier in an eternal perspective.

A prototype of the AVT has been constructed and an experimental set-up for testing of the tool has been designed. This included construction of full-scale diameter samples representing a casing/cement/formation system with the possibility to generate a uniform microannulus at the casing-cement interface. From the experimental testing performed, it can be concluded that:

- The tool prototype is able to measure the casing displacement with high resolution (micrometer range) while applying a radial force on the casing.
- The AVT is able to differentiate a casing supported by an annular cement sheath from a free pipe due to a contrast in stiffness, hence enabling cement detection both for cases with and without a microannulus.
- A well-cemented casing can be confidently identified by only applying a relatively small force, to ensure minimum damage to the cement sheath.
- Results show that the AVT is able to quantify the size of a uniform microannulus at the casing-cement interface, with good accuracy.
- Inferring the quality of the cement sheath itself, proved to be challenging as the recorded stiffness seems to be affected by other factors than solely the individual mechanical properties of the casing, cement, and formation.
- Testing has shown that the AVT is prone to poor centralization within the casing, as this results in improper alignment between the pads and the casing, giving an apparent lower stiffness.
- Severe eccentricity is easy to detect as a low stiffness and pad contact obtained at a diameter less than the casing ID.
- Slight eccentricity/tilting of the tool, however, might not be detectable. If not detected, it may result in a well-cemented casing being interpreted as free pipe due to the apparent stiffness reduction.
- Visual inspection of the cement sheath after logging did not reveal any damage imposed by the logging. However, one can not exclude the possibility of smaller scale damage like microcracks or debonding.

Numerical simulations (FEA) have been performed to further evaluate the logging response of the AVT and to compare with the experimental results. From these results, it can be concluded that:

- There is a significant contrast in stiffness between a free pipe and a casing supported by an annular cement.
- The free pipe stiffness match quite decently with the experimental results.
- In the case of a free pipe, the casing is deformed predominantly by ovalization.
- The radial displacement at the LVDT measurement point is almost identical to the displacement of the outer casing wall, showing that the LVDT can be used to measure the size of the microannulus with good accuracy.
- For a well-cemented casing, the simulated stiffness is considerably higher than for the experimental results. This is believed to be caused mainly by the conditions used to model the cement sheath's interfaces.

Chapter 8

Recommendations for Further Work

For further experimental testing of the AVT, the following should be considered:

- Testing of the AVT on known microannulus sizes should be continued, and statistical analysis should be used to evaluate the accuracy/error associated with the measurement.
- It should be considered to fully automatize the procedure for calculation of the microannulus size from the log response, to increase both consistency and efficiency.
- The effect of improper tool centralization on the measured microannulus size should be investigated by logging casing-cement microannuli with an eccentric/tilted tool.
- The effect of wellbore solids on the measurement should be evaluated. This could simply be done by logging a casing filled with weighted mud.
- The effect of an irregular inner casing wall should be tested.
- The effect of a cement-formation microannulus should be evaluated.
- It should be evaluated to use more realistic mechanisms for generation of a microannulus, compared to the simplistic representation used here. Casing cooling or pressure changes could be used.
- In general, it should be considered to test the tool on more complex cement samples, like channeled cement, partial microannuli, irregular hole shapes, etc.
- Installation of the ultrasonic transducers (AE sensors) within the tool pads should be considered, to be able to detect potential damage created by logging.
- X-ray CT scanning or leak testing of the cement samples before and after logging should be considered. This would enable an evaluation of the initial condition of the constructed samples, as well as any damage induced by logging.

Numerical simulations should be used further, to increase the understanding of the AVT logging response and also to evaluate the tool's impact on the logged environment:

- It should be further investigated why the simulated response is so different from the experimental results for a well-cemented casing. Especially, the boundary conditions at the cement sheath's interfaces should be investigated.
- The stresses imposed on the cement should be evaluated to consider potential cracking and debonding due to logging.
- The stresses imposed on the casing should be investigated to evaluate the possibility of casing yield.
- Simulation cases should be run with a microannulus, to further establish the basis for the microannulus size calculations from the log response.
- It should be evaluated to simulate improper tool centralization, to investigate the effect on the measured stiffness and its effect on the microannulus size calculations.

In a longer perspective, the AVT should be made ready for downhole application. The following modifications (compared to the prototype) should then be considered:

- The tool design should be modified to allow for integration in a conventional wireline tool string.
- A suitable downhole hydraulic power unit (HPU) is needed to supply the necessary pressure and flow rate.
- Two pressure measurements are needed to determine the overpressure exerted on the pistons.
- Fail-safe mechanisms should be developed, in the case of power outage or overpressurization.
- Certain parts of the tool might have to be modified to endure the pressure and temperature conditions in a well.
- The effect of temperature on expansion of the steel in the tool should be considered.
- Evaluate what is necessary (in terms of centralizers, etc.) in order to ensure sufficient centralization of the AVT downhole.
- To reduce the AVT's sensitivity to eccentricity, tool vibration or movement during pressurization should be evaluated.
- Evaluate the time (and cost) related to stopping the logging string for performing AVT measurements in a real logging scenario.

References

[1] V. Myrseth, G. A. Perez-Valdes, S. J. Bakker, K. T. Midthun, and M. Torsæter, "Development of a Norwegian Open-Source Plug-and-Abandonment Database With Applications," *SPE Economics & Management*, vol. 9, no. 01, pp. 27–31, 2017.

[2] *NORSOK Standard D-010, Well integrity in drilling and well operations*, 2013. Rev. 4.

[3] T. E. Ferg, H.-J. Lund, D. Mueller, M. Myhre, A. Larsen, P. Andersen, G. Lende, C. Hudson, C. Prestegaard, and D. Field, "Novel Approach to More Effective Plug and Abandonment Cementing Techniques," in *SPE Arctic and Extreme Environments Conference & Exhibition, 18-20 October 2011*, (Moscow, Russia), Society of Petroleum Engineers, 2011.

[4] M. Khalifeh, A. Saasen, H. Hodne, and T. Vrålstad, "Techniques and Materials for North Sea Plug and Abandonment Operations," in *Offshore Technology Conference, 6-9 May 2013*, (Houston, Texas, USA), Offshore Technology Conference, 2013.

[5] S. Fagerås, "A Study of Available Technology for Cement Evaluation and a Novel Tool for Measuring the Size of a Microannulus," Specialization Project, Norwegian University of Science and Technology, Faculty of Engineering Science and Technology, Department of Petroleum Engineering and Applied Geophysics, 2016. Unpublished.

[6] E. B. Nelson and D. Guillot, eds., *Well Cementing*. Schlumberger, 2 ed., 2006.

[7] W. H. Fertl, P. E. Pilkington, and J. B. Scott, "A Look at Cement Bond Logs," *Journal of Petroleum Technology*, vol. 26, no. 06, pp. 607–617, 1974.

[8] R. M. Havira, "Ultrasonic Cement Bond Evaluation," in *SPWLA 23rd Annual Logging Symposium, 6-9 July 1982*, (Corpus Christi, Texas, USA), Society of Petrophysicists & Well Log Analysts, 1982.

[9] L. G. Carter and G. W. Evans, "A Study of Cement-Pipe Bonding," *Journal of Petroleum Technology*, vol. 16, no. 02, pp. 157–160, 1964.

[10] A. Bonett and D. Pafitis, "Getting to the Root of Gas Migration," *Oilfield Review*, vol. 8, no. 1, pp. 36–49, 1996.

[11] S. E. Gasda, S. Bachu, and M. A. Celia, "Spatial characterization of the location of potentially leaky wells penetrating a deep saline aquifer in a mature sedimentary basin," *Environmental Geology*, vol. 46, no. 6, pp. 707–720, 2004.

[12] C. Baumgarte, M. Thiercelin, and D. Klaus, "Case Studies of Expanding Cement To Prevent Microannular Formation," in *SPE Annual Technical Conference and Exhibition, 3–6 October 1999*, (Houston, Texas, USA), Society of Petroleum Engineers, 1999.

[13] A.-P. Bois, A. Garnier, F. Rodot, J. Saint-Marc, and N. Aimard, "How to Prevent Loss of Zonal Isolation Through a Comprehensive Analysis of Micro-Annulus Formation," in *SPE Annual Technical Conference and Exhibition, 4-7 October 2009*, (New Orleans, Louisiana, USA), Society of Petroleum Engineers, 2009.

[14] B. F. McGhee and H. L. Vacca, "Guidelines for Improved Monitoring of Cementing Operations," in *SPWLA 21st Annual Logging Symposium, 8-11 July 1980*, (Lafayette, Louisiana, USA), Society of Petrophysicists & Well Log Analysts, 1980.

[15] J. J. Jutten and A. J. Hayman, "Microannulus Effect on Cementation logs: Experiments and Case Histories," in *SPE Asia Pacific Oil & Gas Conference & Exhibition, 8-10 February 1993*, (Singapore), Society of Petroleum Engineers, 1993.

[16] P. E. Pilkington, "Pressure needed to reduce microannulus effect on CBL," *Oil & Gas Journal*, vol. 86, no. 22, pp. 68–74, 1988.

[17] *Cased Hole Log Interpretation Principles/Applications*. Schlumberger Educational Services, 1989.

[18] M. Grosmangin, F. P. Kokesh, and P. Majani, "A Sonic Method for Analyzing the Quality of Cementation of Borehole Casings," *Journal of Petroleum Technology*, vol. 13, no. 02, pp. 165–171, 1961.

[19] W. L. Anderson and T. Walker, "Research Predicts Improved Cement Bond Evaluations With Acoustic Logs," *Journal of Petroleum Technology*, vol. 13, no. 11, pp. 1093–1097, 1961.

[20] NDT Resource Center, "Modes of Sound Wave Propagation." `https://www.nde-ed.org/EducationResources/CommunityCollege/Ultrasonics/Physics/modepropagation.htm` [Online; accessed Feb 10, 2017].

[21] D. V. Ellis and J. M. Singer, *Well Logging for Earth Scientists*. Springer, 2 ed., 2007.

[22] G. H. Pardue, R. L. Morris, L. H. Gollwitzer, and J. H. Moran, "Cement Bond Log - A Study of Cement and Casing Variables," *Journal of Petroleum Technology*, vol. 15, no. 05, pp. 545–555, 1963.

[23] J. J. Jutten, D. Guillot, and P. A. Parcevaux, "Relationship Between Cement Slurry Composition, Mechanical Properties, and Cement-Bond-Log Output," *SPE Production Engineering*, vol. 4, no. 01, pp. 75–82, 1989.

[24] T. Walker, "A Full-Wave Display of Acoustic Signal in Cased Holes," *Journal of Petroleum Technology*, vol. 20, no. 08, pp. 811–824, 1968.

[25] P. E. Pilkington, "Cement Evaluation - Past, Present, and Future," *Journal of Petroleum Technology*, vol. 44, no. 02, pp. 132–140, 1992.

[26] R. A. Lester, "The Segmented Bond Tool: A Pad-Type Cement Bond Device," in *Transactions of the 12th Annual Canadian Well Logging Society Formation Evaluation Symposium, 26–29 September 1989*, (Calgary, Canada), Canadian Well Logging Society, 1989.

[27] R. M. Bateman, ed., *Cased-Hole Log Analysis and Reservoir Performance Monitoring*. Springer, 2 ed., 2015.

[28] L. H. Gollwitzer and J. P. Masson, "The Cement Bond Tool," in *SPWLA 23rd Annual Logging Symposium, 6-9 July 1982*, (Corpus Christi, Texas, USA), Society of Petrophysicists & Well Log Analysts, 1982.

[29] R. H. Winn, T. O. Anderson, and L. G. Carter, "A Preliminary Study of Factors Influencing Cement Bond Logs," *Journal of Petroleum Technology*, vol. 14, no. 04, pp. 369–372, 1962.

[30] J. J. Jutten and E. Corrigall, "Studies With Narrow Cement Thickness Lead to Improved CBL in Concentric Casings," *Journal of Petroleum Technology*, vol. 41, no. 11, pp. 1158–1192, 1989.

[31] H. D. Leslie, J. de Selliers, and D. J. Pittman, "Coupling and Attenuation: a New Measurement Pair in Cement Bond Logging.," in *SPE Production Operations Symposium, 8-10 March 1987*, (Oklahoma City, Oklahoma, USA), pp. 243–250, Society of Petroleum Engineers, 1987.

[32] D. D. Fitzgerald, B. F. McGhee, and J. A. McGuire, "Guidelines for 90% Accuracy in Zone-Isolation Decisions," *Journal of Petroleum Technology*, vol. 37, no. 11, pp. 2013–2022, 1985.

[33] B. Froelich, A. Dumont, D. Pittman, and B. Seeman, "Cement Evaluation Tool: A New Approach to Cement Evaluation," *Journal of Petroleum Technology*, vol. 34, no. 08, pp. 1835–1841, 1982.

[34] A. J. Hayman, R. Hutin, and P. V. Wright, "High-Resolution Cementation And Corrosion Imaging By Ultrasound," in *SPWLA 32nd Annual Logging Symposium, 16-19 June 1991*, (Midland, Texas, USA), Society of Petrophysicists & Well Log Analysts, 1991.

[35] R. van Kuijk, S. Zeroug, B. Froelich, M. Allouche, S. Bose, D. Miller, J.-L. Le Calvez, V. Schoepf, and A. Pagnin, "A Novel Ultrasonic Cased-Hole Imager for Enhanced Cement Evaluation," in *International Petroleum Technology Conference, 21-23 November 2005*, (Doha, Qatar), International Petroleum Technology Conference, 2005.

[36] A. Al-Suwaidi, J. L. Bustillos, D. Guillot, J. Rondeau, P. Vigneaux, H. Helou, J. A. M. Ramírez, and J. L. R. Robles, "Light as a Feather, Hard as a Rock," *Oilfield Review*, vol. 13, no. 2, pp. 2–15, 2001.

[37] Z. L. Al-Kindi, A. S. Al-Suwaidi, M. E. Ibrahim, K. Jammeli, F. M. Al Marri, E. Sultan, and A. Elkadi, "Increased Certainty in the Determination of Zonal Isolation Through the Integration of Annulus Geometry Imaging and Improved Solid-Fluid Discrimination," in *SPE Middle East Oil and Gas Show and Conference, 15-18 March 2009*, (Manama, Bahrain), Society of Petroleum Engineers, 2009.

[38] R. Hayden, C. Russell, A. Vereide, P. Babasick, P. Shaposhnikov, and D. May, "Case Studies in Evaluation of Cement with Wireline Logs in a Deep Water Environment," in *SPWLA 52nd Annual Logging Symposium, 14-18 May 2011*, (Colorado Springs, Colorado, USA), Society of Petrophysicists & Well Log Analysts, 2011.

[39] G. Catala, V. de Montmollin, A. Hayman, R. Hutin, R. Gilles, D. Guillot, J. Jutten, U. Qureshi, B. Kelly, B. Piot, T. Simien, and I. Toma, "Modernizing Well Cementing Design and Evaluation," *Oilfield Review*, vol. 3, no. 2, pp. 55–71, 1991.

[40] TE Connectivity, "LVDT Tutorial." `http://www.te.com/usa-en/industries/sensor-solutions/insights/lvdt-tutorial.html#chapter-3-dl` [Online; accessed Feb 17, 2017].

[41] NDT Resource Center, "Introduction to Acoustic Emission Testing." `https://www.nde-ed.org/EducationResources/CommunityCollege/Other%20Methods/AE/AE_Intro.php` [Online; accessed May 19, 2017].

[42] A. T. Bourgoyne Jr., K. K. Millheim, M. E. Chenevert, and F. S. Young Jr., *Applied Drilling Engineering*, vol. 2 of *SPE Textbook Series*. Society of Petroleum Engineers, 1986.

[43] Schlumberger, "Cement Bond Logging Tools." `http://www.slb.com/~/media/Files/production/product_sheets/well_integrity/cement_bond_logging_tools.pdf` [Online; accessed May 30, 2017].

[44] D. Patterson, S. Dighe, P. J. Matuszyk, A. Holley, X. Yao, and W. Han, "Extending the Understanding of In-Situ Cement Properties," in *SPWLA 57th Annual Logging Symposium, June 25-29, 2016*, (Reykjavik, Iceland), Society of Petrophysicists & Well Log Analysts, 2016.

[45] *ISO 10426-1, Petroleum and natural gas industries – Cements and materials for well cementing – Part 1: Specification*, 3 ed., 2009. (Equivalent to API Spec 10A, 24th edition).

[46] The Engineering Toolbox, "Coefficients of Linear Thermal Expansion." `http://www.engineeringtoolbox.com/linear-expansion-coefficients-d_95.html` [Online; accessed Mar 18, 2017].

[47] K. Xhanari and M. Finšgar, "Organic corrosion inhibitors for aluminum and its alloys in chloride and alkaline solutions: A review," *Arabian Journal of Chemistry*, 2016.

[48] H. Kinoshita, P. Swift, C. Utton, B. Carro-Mateo, G. Marchand, N. Collier, and N. Milestone, "Corrosion of aluminium metal in OPC- and CAC-based cement matrices," *Cement and Concrete Research*, vol. 50, no. August, pp. 11–18, 2013.

[49] S.-I. Pyun and S.-M. Moon, "Corrosion mechanism of pure aluminium in aqueous alkaline solution," *Journal of Solid State Electrochemistry*, vol. 4, no. 5, pp. 267–272, 2000.

[50] G. E. Monfore and B. Ost, "Corrosion of Aluminum Conduit in Concrete," *Journal of the PCA Research and Development Laboratories*, vol. 7, no. 1, pp. 10–22, 1965.

[51] H. Woods, "Corrosion of Embedded Material Other Than Reinforcing Steel," *Significance of Tests and Properties of Concrete and Concrete-Making Materials*, vol. 1, no. 169-A, pp. 230–238, 1966.

[52] "Corrosion of Nonferrous Metals in Contact with Concrete," tech. rep., Portland Cement Association, 1969.

[53] Y. Guo, J. Qi, Y. S. Zheng, S. Taoutaou, R. Wang, Y. An, and H. Guo, "Cementing Optimization through an Enhanced Ultrasonic Imaging Tool," in *SPE/IATMI Asia Pacific Oil & Gas Conference and Exhibition, 20–22 October 2015*, (Nusa Dua, Bali, Indonesia), Society of Petroleum Engineers, 2015.

[54] T. Sheives, L. Tello, M. V.E., T. Standley, and T. Blankinship, "A Comparison of New Ultrasonic Cement and Casing Evaluation Logs With Standard Cement Bond Logs," in *SPE Annual Technical Conference and Exhibition, 5-8 October*, (New Orleans, LA, USA), Society of Petroleum Engineers, 1986.

[55] S. Rivas-Gómez, J. Cruz-Hernández, J. A. González-Guevara, and A. Pineda-Muñoz, "Block Size and Fracture Permeability in Naturally Fractured Reservoirs," in *Abu Dhabi International Petroleum Exhibition and Conference, 13-16 Oct, 2002*, (Abu Dhabi, United Arab Emirates), Society of Petroleum Engineers, 2002.

[56] J. Kleppe, "Derivation of Fluid Flow Equations," 2016. `http://www.ipt.ntnu.no/~kleppe/TPG4150/equations.pdf` [Online; accessed Feb 7, 2017].

[57] J. C. Stormont, R. Ahmad, J. Ellison, M. R. Taha, and E. N. Matteo, "Laboratory measurements of flow through wellbore cement-casing microannuli," in *49th US Rock Mechanics / Geomechanics Symposium, 28 June - 1 July*, (San Francisco, CA, USA), American Rock Mechanics Association, 2015.

Appendices

Appendix A

Leak Rate Through a Microannulus

Permeability and Flow Area

A microannulus will increase the apparent permeability of the cement sheath, as fluids are allowed to move along the cement sheath's interface. By using the theory for an open planar fracture, the equivalent permeability of an otherwise impermeable cement sheath can be approximated as a function of the microannulus size as [15, 55]:

$$k_{ma} = \frac{w_{ma}^2}{12} \tag{A.1}$$

where

$$\begin{aligned} k_{ma} &= \text{Equivalent permeability of a microannulus} && [m^2] \\ w_{ma} &= \text{Microannulus size} && [m] \end{aligned}$$

As the microannulus size is small compared to the casing diameter, the cross-sectional flow area of a microannulus can be approximated as the outer casing circumference times the width of the microannulus:

$$A = \pi d_{o,csg} w_{ma} \tag{A.2}$$

where

$$\begin{aligned} A &= \text{Cross-sectional flow area of the microannulus} && [m^2] \\ d_{o,csg} &= \text{Outer diameter of the casing} && [m] \end{aligned}$$

Liquid Leak Rate

For a liquid-filled microannulus, laminar flow and incompressible fluid is assumed. Hence, Darcy's law can be used to express the flow rate as [56]:

$$Q = -\frac{kA}{\mu}\left(\frac{dp}{dL} + \rho g \cos\theta\right) \tag{A.3}$$

where

Q = Flow rate through the microannulus $[m^3/s]$
k = Permeability $[m^2]$
μ = Viscosity of the flowing fluid $[Pa \cdot s]$
$\frac{dp}{dL}$ = Pressure change per unit length along the flow $[Pa/m]$
ρ = Density of flowing fluid $[kg/m^3]$
g = Gravitational acceleration $[m/s^2]$
θ = Wellbore inclination $[^o]$

Note that the pressure change along the path of the flow is typically negative. By combining Equations A.1, A.2 and A.3 the liquid leak rate through a microannulus can be expressed as:

$$Q = vA = -\frac{\pi d_{o,csg} w_{ma}^3}{12\mu}\left(\frac{dp}{dL} + \rho g \cos\theta\right) \tag{A.4}$$

Gas Leak Rate

For short intervals, gas can also be approximated as an incompressible fluid [15]. However, in order to order to obtain accurate estimates of the flow rate through a gas-filled microannulus, the additional pressure loss caused by non-Darcy effects (second-order pressure loss) should be included. This can be done by using the Forchheimer equation, given as [57]:

$$-\left(\frac{dp}{dL} + \rho g \cos\theta\right) = \frac{\mu}{kA}Q + \frac{\beta\rho}{A^2}Q^2 \tag{A.5}$$

where

β = Forchheimer coefficient $[m^{-1}]$

By combining Equations A.1, A.2 and A.5 the following (implicit) equation for the gas leak rate through a microannulus is obtained:

$$-\left(\frac{dp}{dL} + \rho g \cos\theta\right) = \frac{12\mu}{\pi d_{o,csg} w_{ma}^3}Q + \frac{\beta\rho}{(\pi d_{o,csg} w_{ma})^2}Q^2 \tag{A.6}$$

Note that the Forchheimer coefficient itself also will depend on the size of the microannulus, as a larger microannulus gives less second-order pressure loss.

Appendix B

Constructed Samples

A summary of the parameters for all samples constructed in the laboratory is given in Table B.1.

Table B.1: Summary of the casing-cement-formation samples constructed in the laboratory.

#	Casing OD at top	Casing OD at bottom	Length of taper	Radial casing taper	Cemented	Release agent on casing	Outer pipe	Curing temperature	Sample covered	Water added	Comment
[-]	[mm]	[mm]	[mm]	[µm/mm]				[°C]			
1	original	original	N/A	0	No	N/A	N/A	N/A	N/A	N/A	Free pipe
2	original	original	N/A	0	Yes	No	Alu*	66	No	Yes	
3	original	original	N/A	0	Yes	No	Alu*	66	No	Yes	
4	245.60	243.20	232	5.17	Yes	No	Alu*	66	No	Yes	Not able to extrude casing
5	245.60	240.90	232	10.13	Yes	Yes	Alu*	40	Yes	Yes	
6	244.96	240.20	238	10.00	Yes	Yes	Coated alu	40	Yes	No	Bond broke at cmt-alu interface
7	original	original	N/A	0	Yes	No	Steel	40	Yes	No	Well-cemented sample
8	244.96	240.20	238	10.00	Yes	Yes	Steel	40	Yes	No	Microannulus sample
9	original	original	N/A	0	Yes	No	Coated alu	40	Yes	No	Well-cemented (compare with #3)

*Cement-aluminum interaction degrading the cement quality

Appendix C

Further Experimental Results

C.1 Casing-Cement Microannulus

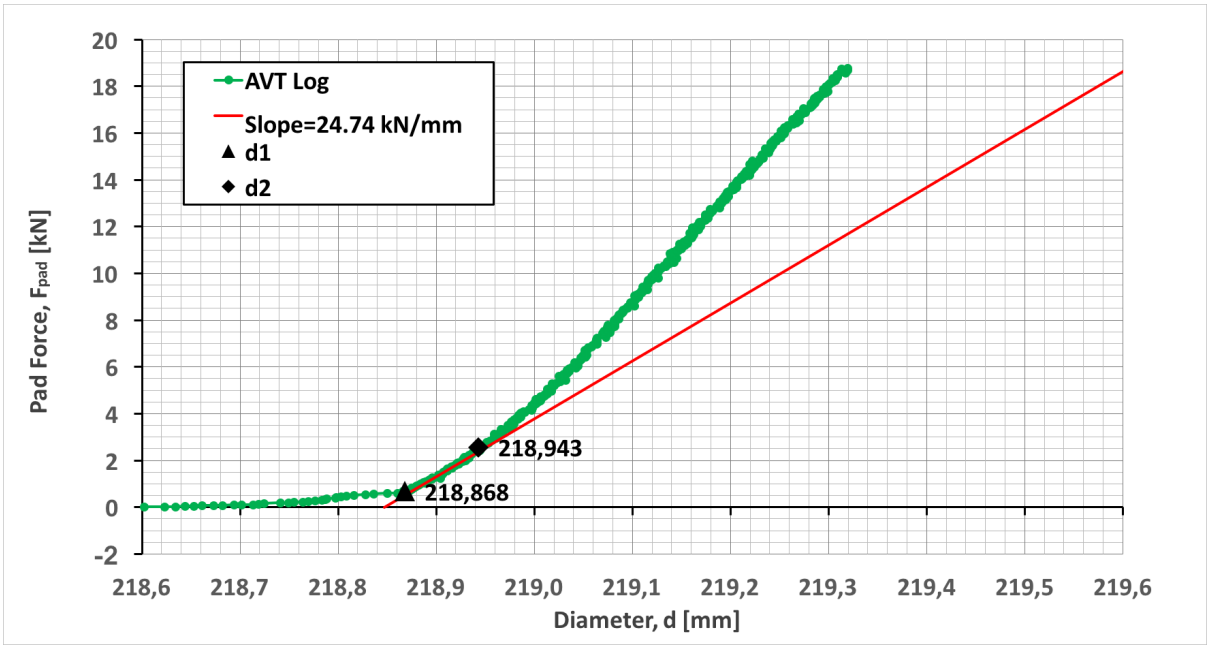

Figure C.1: Results from logging a 26 µm microannulus.

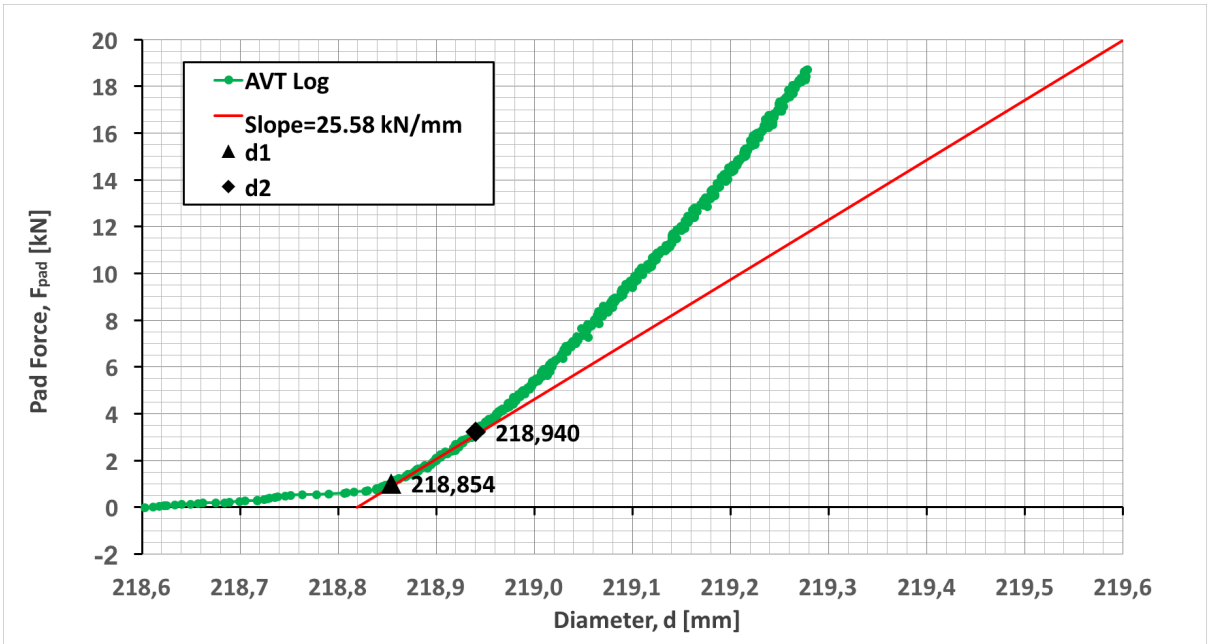

Figure C.2: Results from logging a 35 µm microannulus.

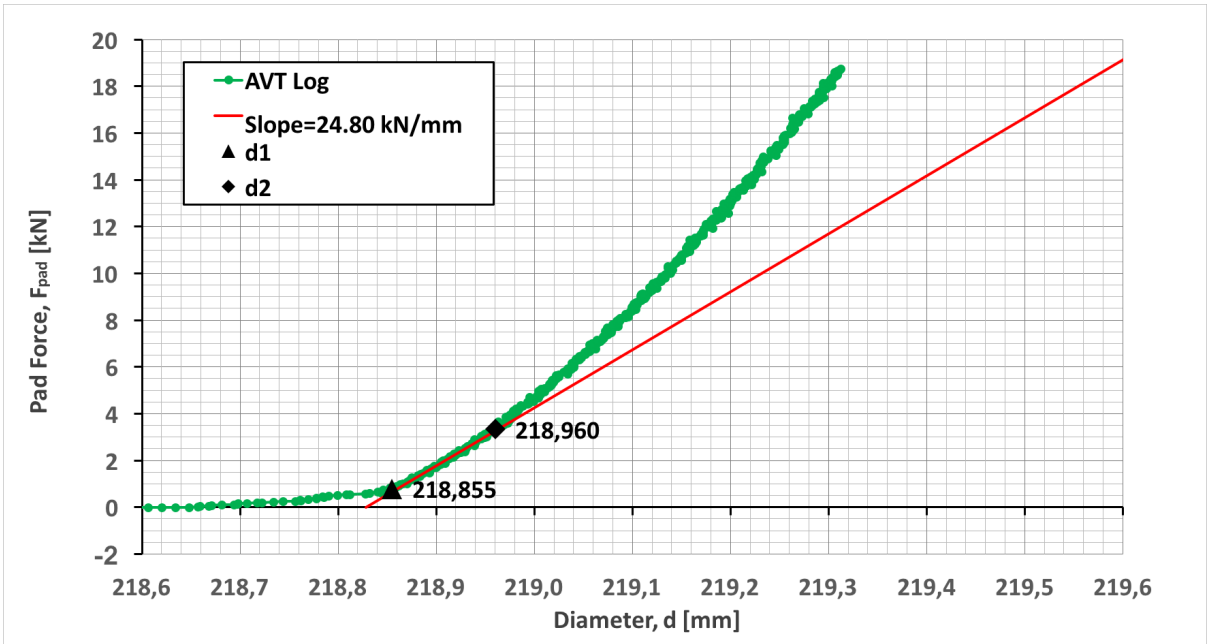

Figure C.3: Results from logging a 45 µm microannulus.

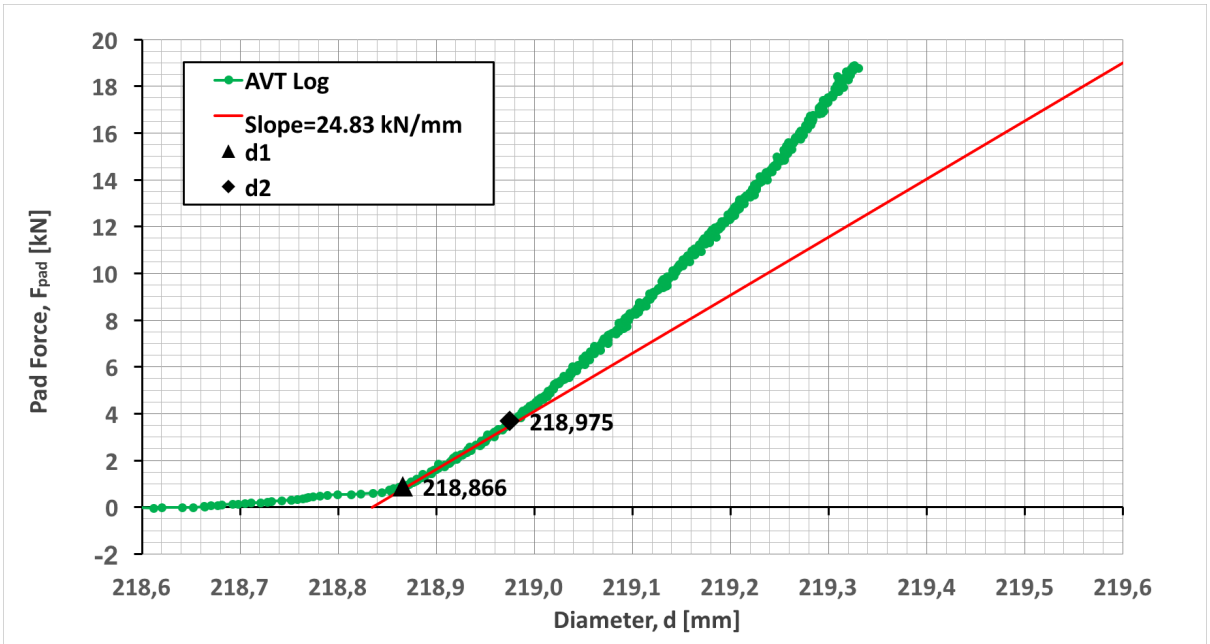

Figure C.4: Results from logging a 55 µm microannulus.

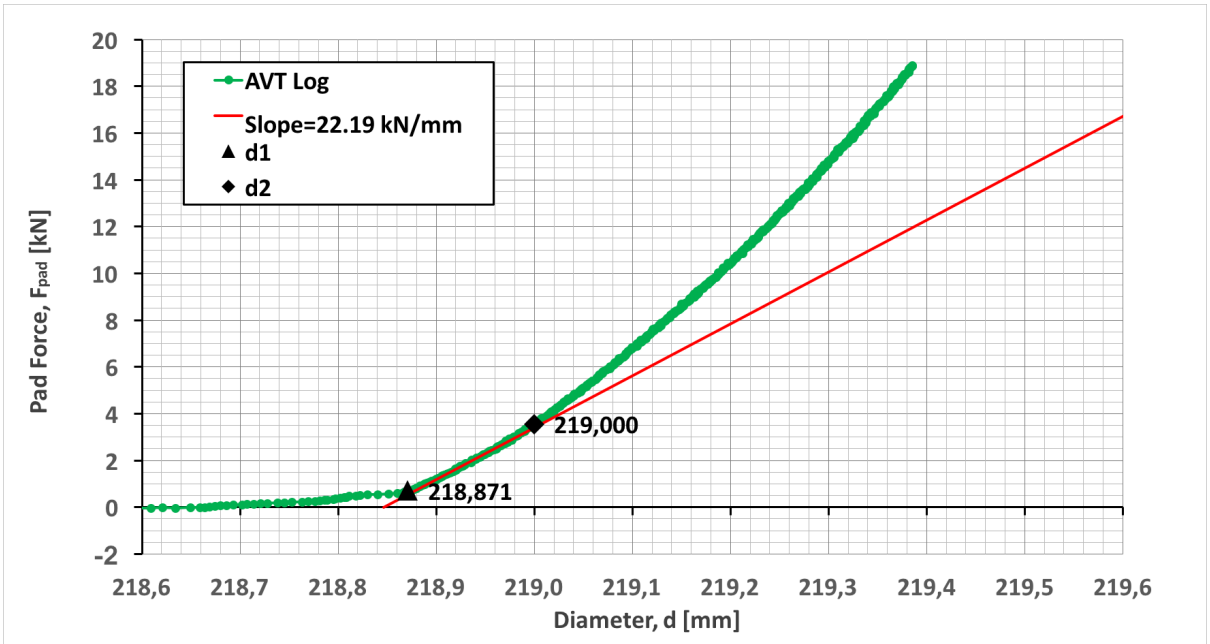

Figure C.5: Results from logging a 65 µm microannulus.

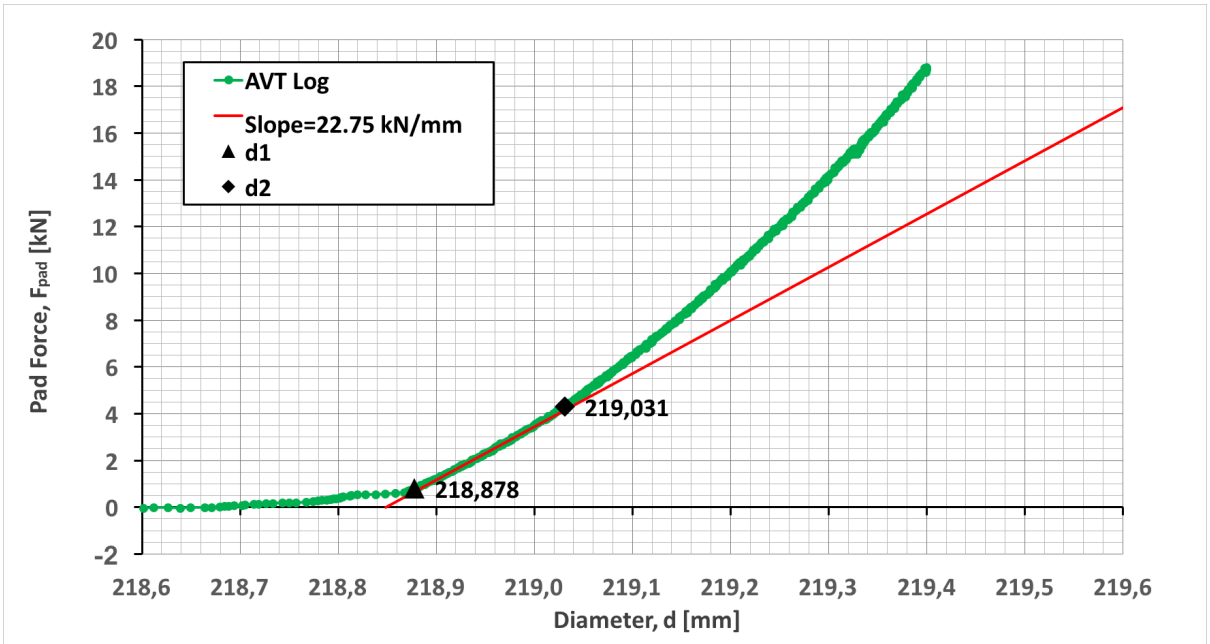

Figure C.6: Results from logging a 75 µm microannulus.

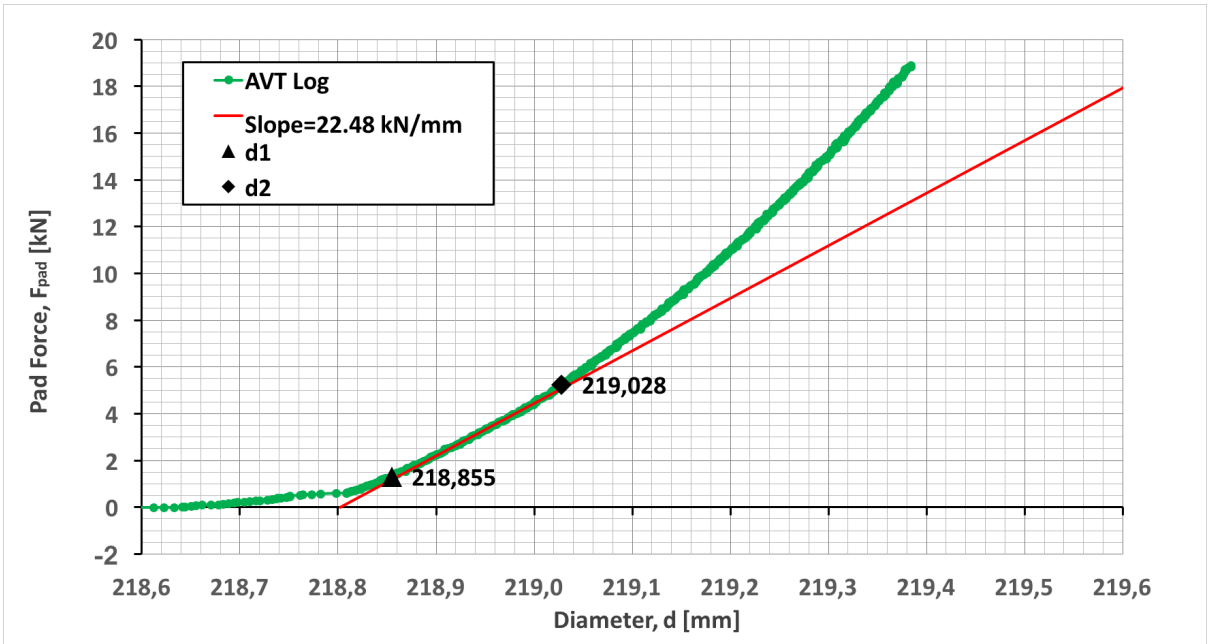

Figure C.7: Results from logging a 85 µm microannulus.

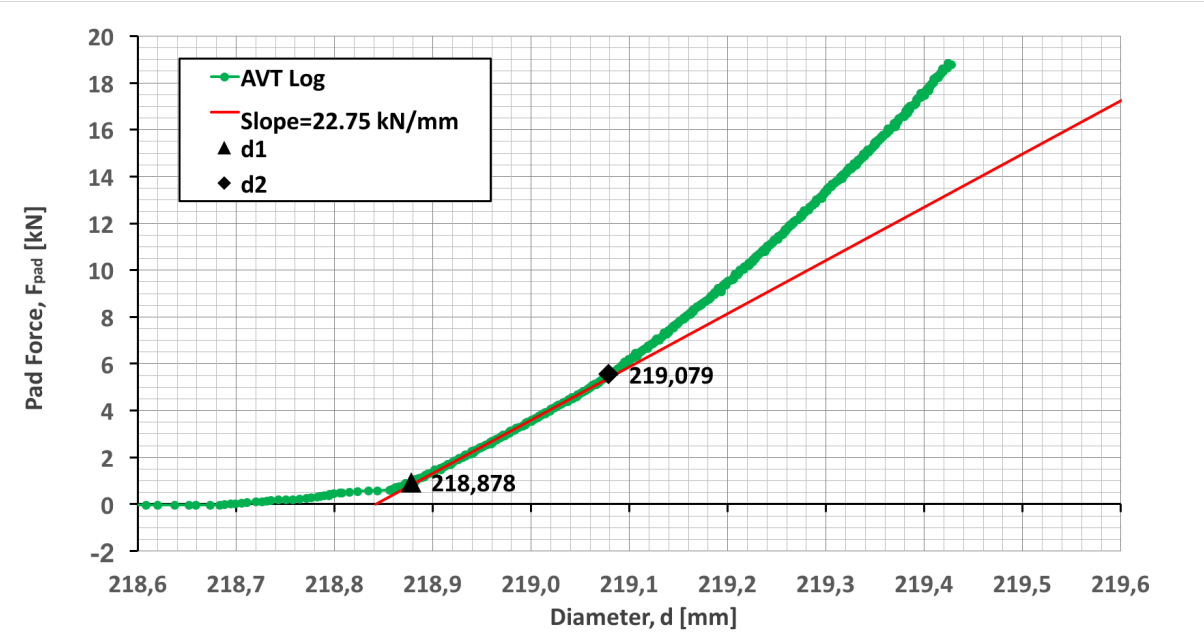

Figure C.8: Results from logging a 95 µm microannulus.

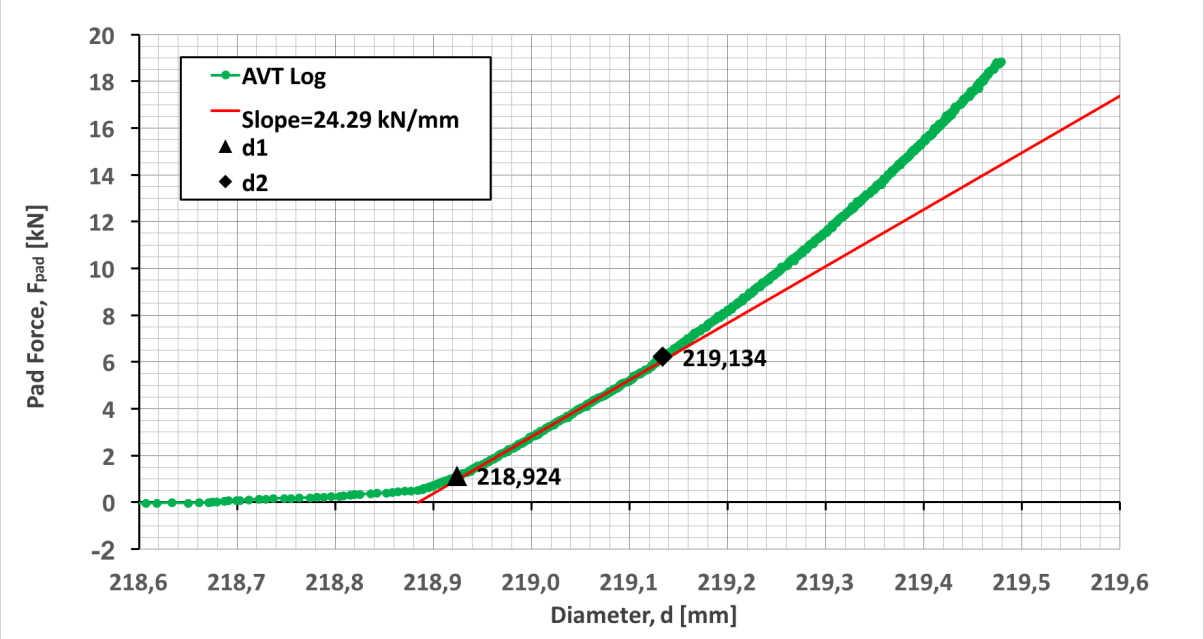

Figure C.9: Results from logging a 105 µm microannulus.

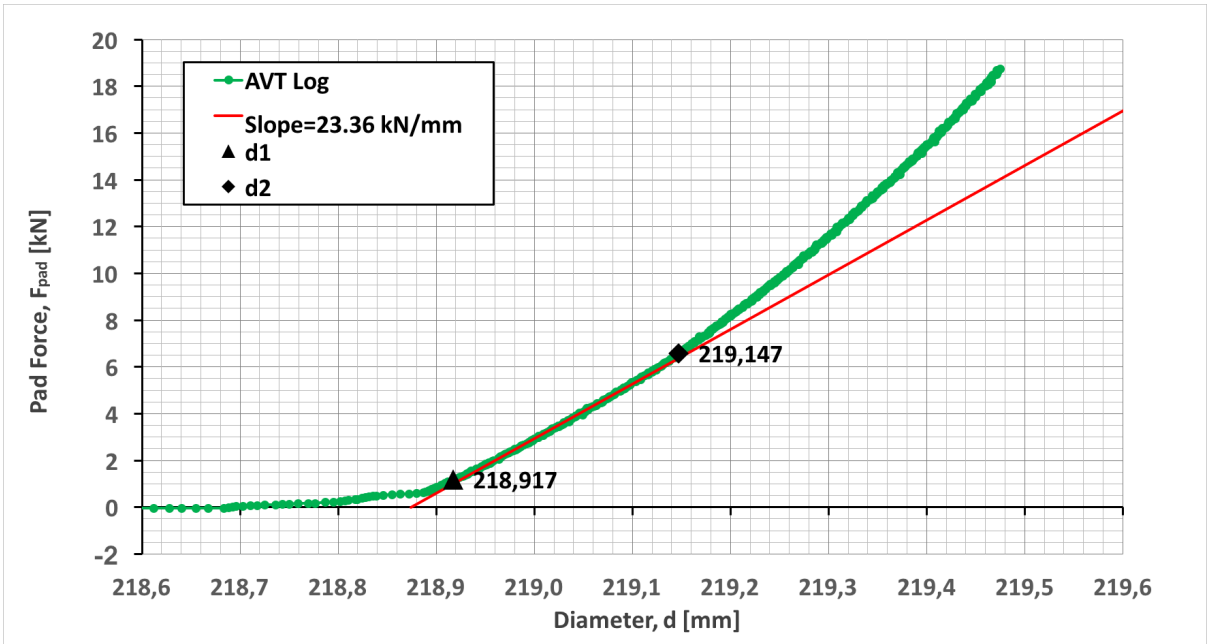

Figure C.10: Results from logging a 115 µm microannulus.

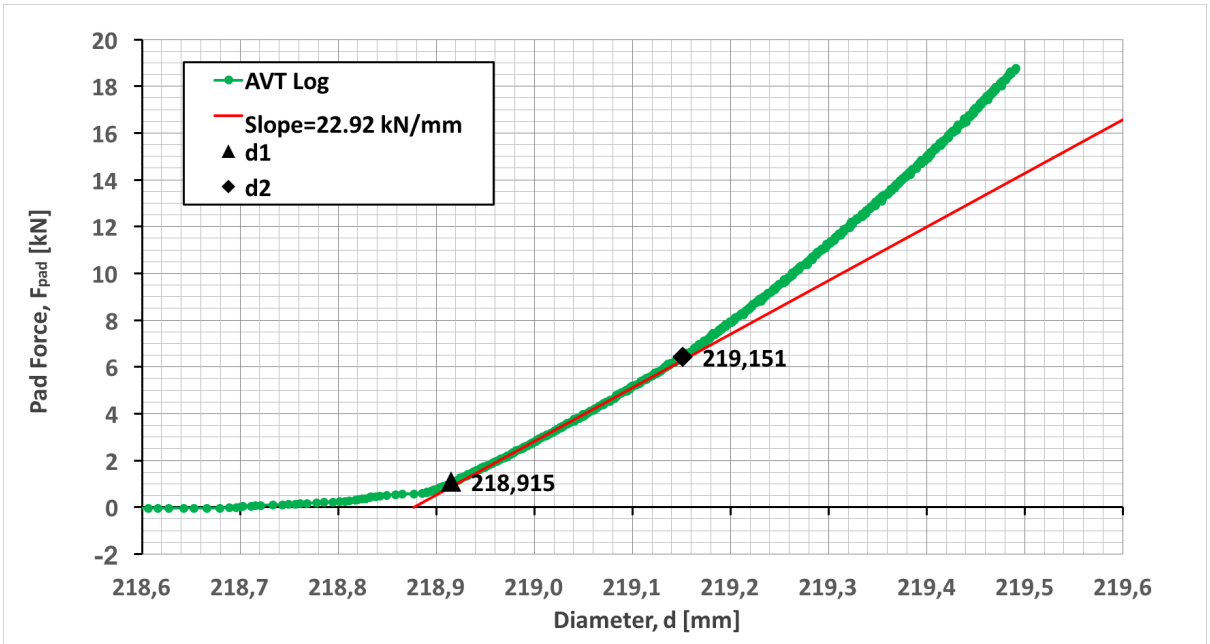

Figure C.11: Results from logging a 125 µm microannulus.

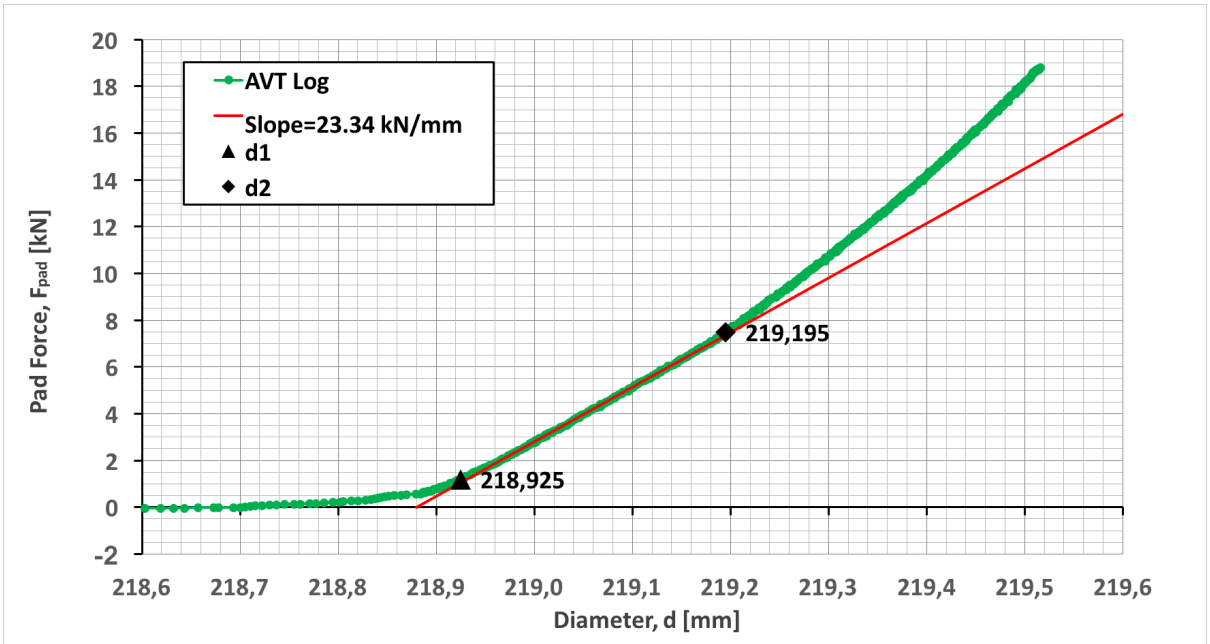

Figure C.12: Results from logging a 135 µm microannulus.

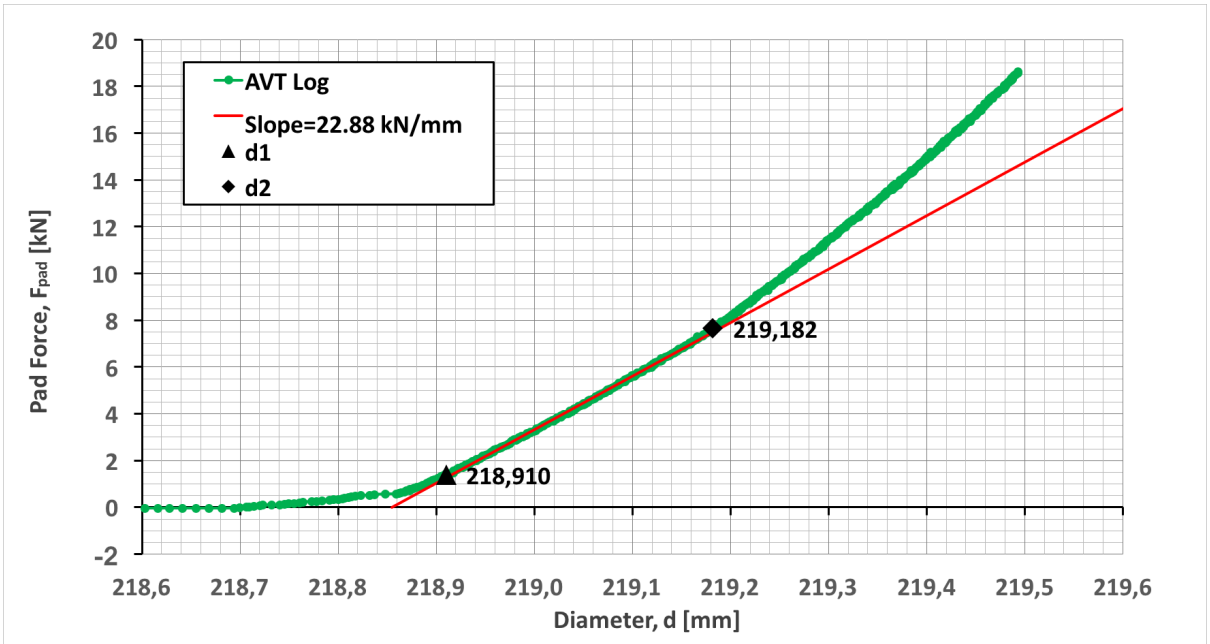

Figure C.13: Results from logging a 145 µm microannulus.

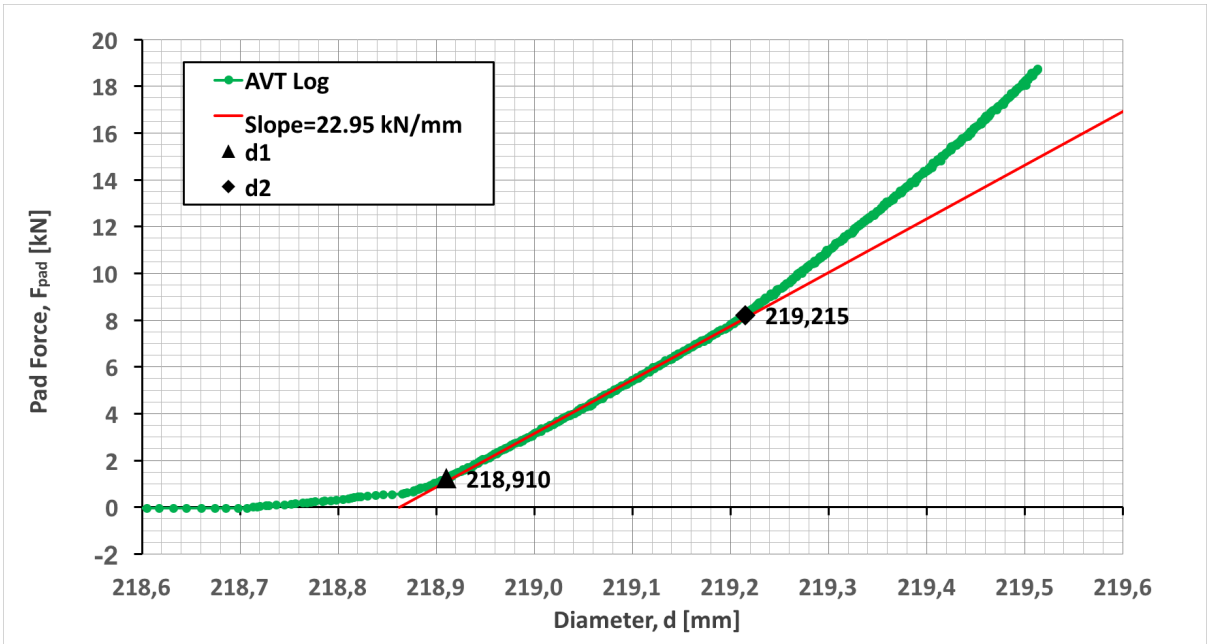

Figure C.14: Results from logging a 155 µm microannulus.

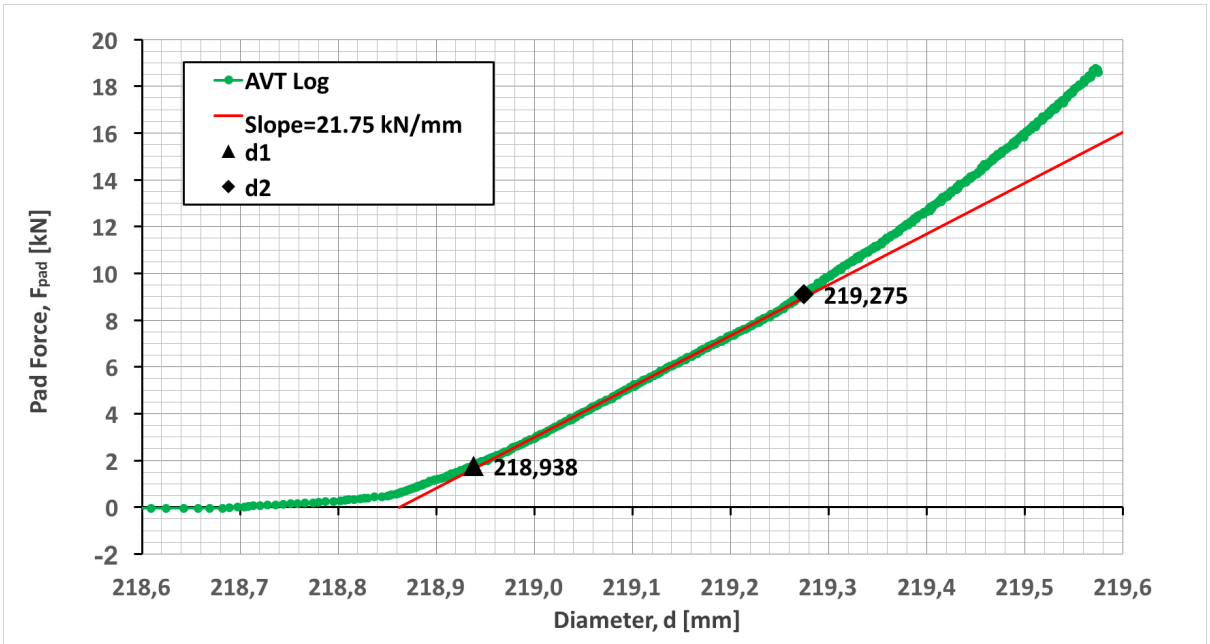

Figure C.15: Results from logging a 165 µm microannulus.

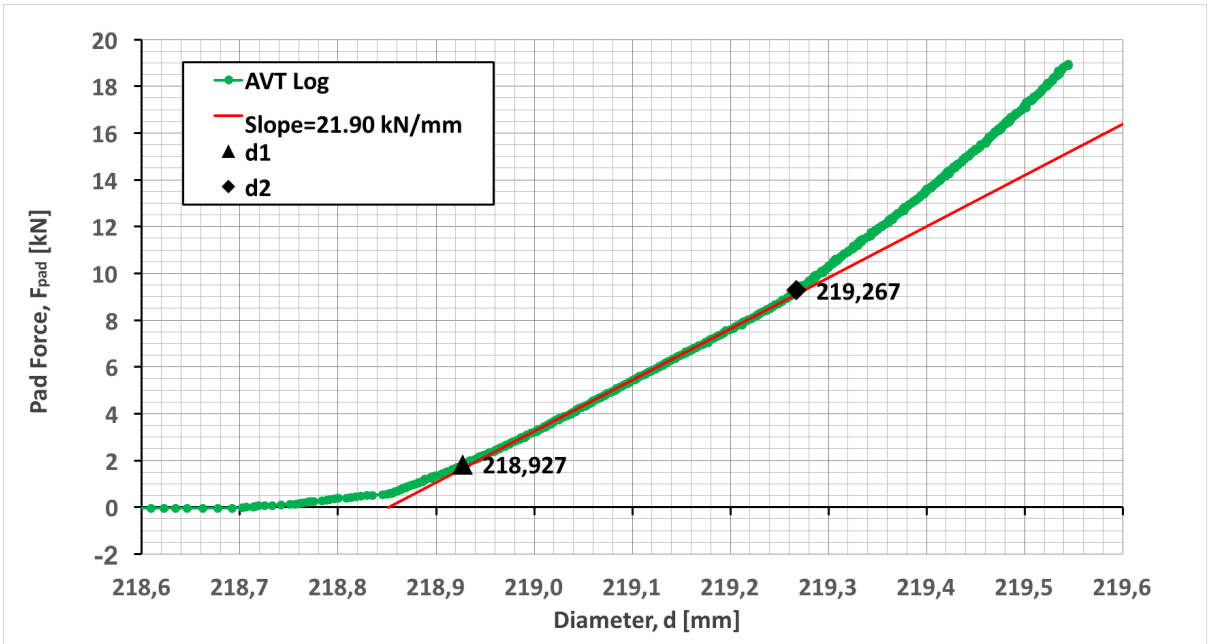

Figure C.16: Results from logging a 175 µm microannulus.

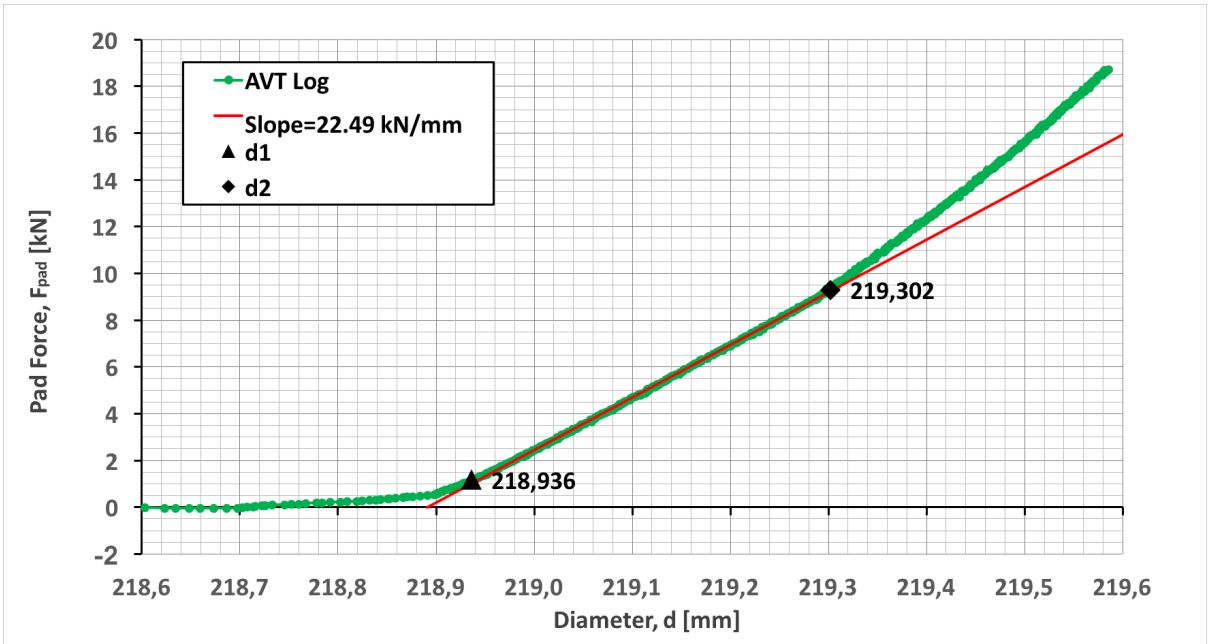

Figure C.17: Results from logging a 185 µm microannulus.

C.2 Tool Eccentricity and Tilting

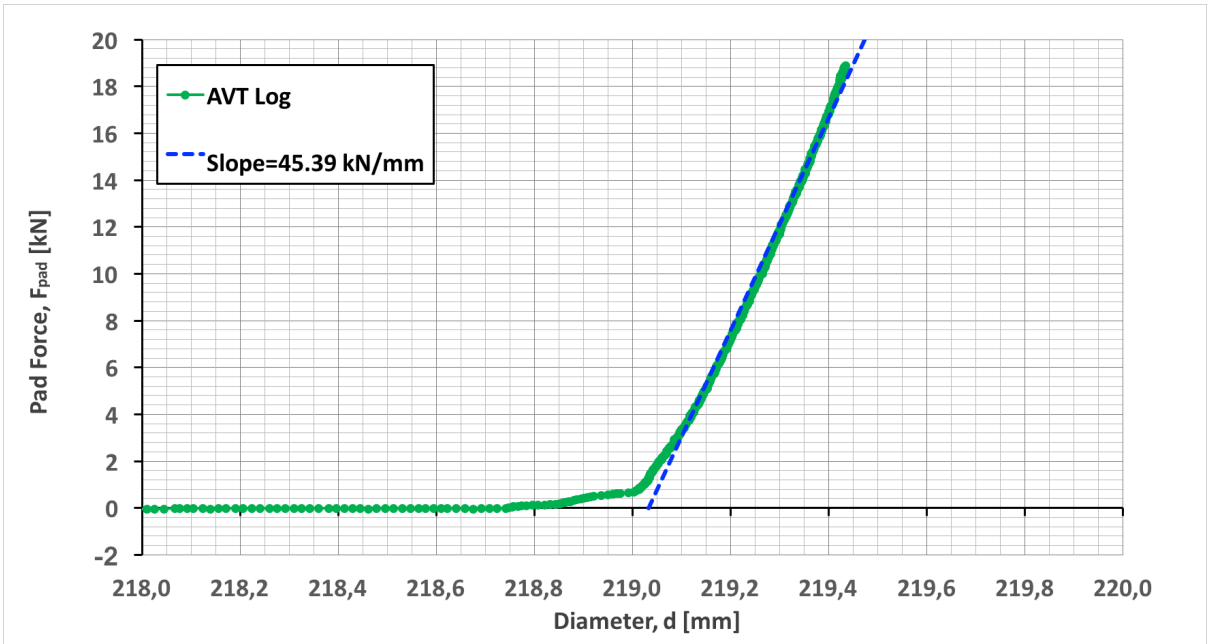

Figure C.18: Results from logging a well-cemented sample with a properly centralized tool.

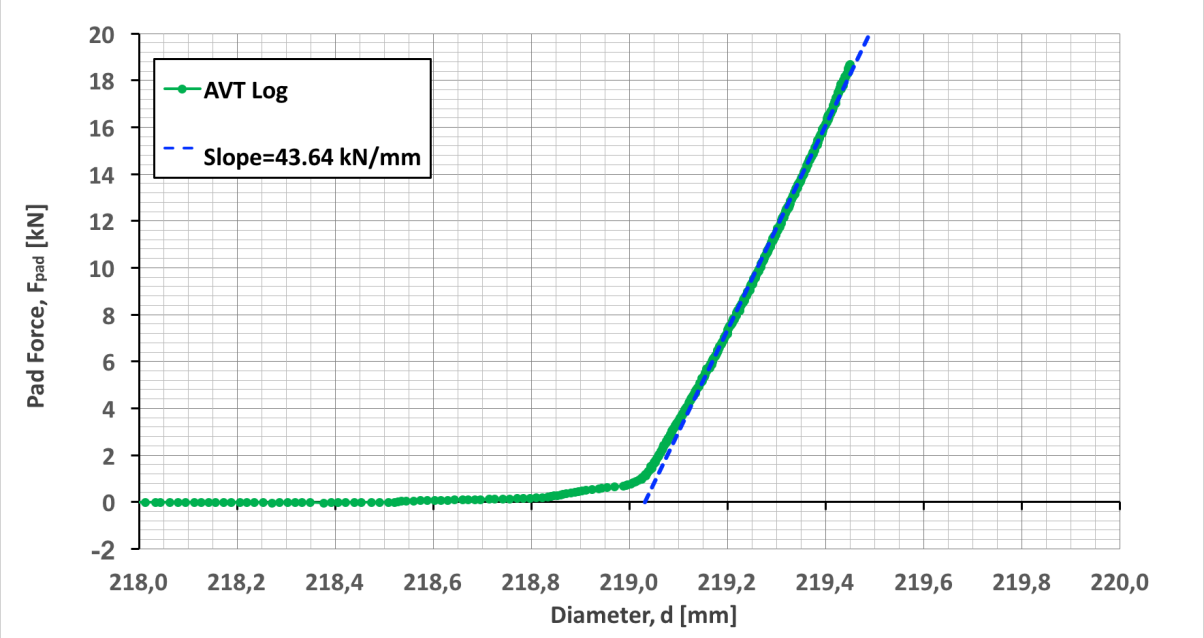

Figure C.19: Results from logging a well-cemented sample with tool eccentricity in the direction of the pad movement.

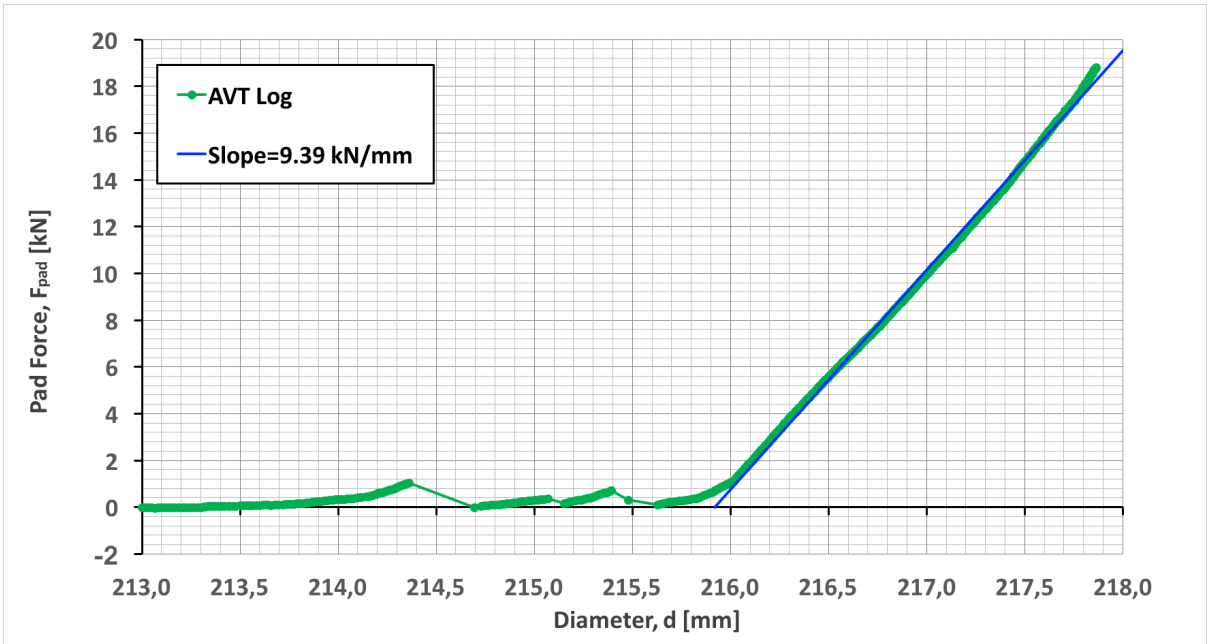

Figure C.20: Results from logging a well-cemented sample with tool eccentricity in the direction perpendicular to the pad movement.

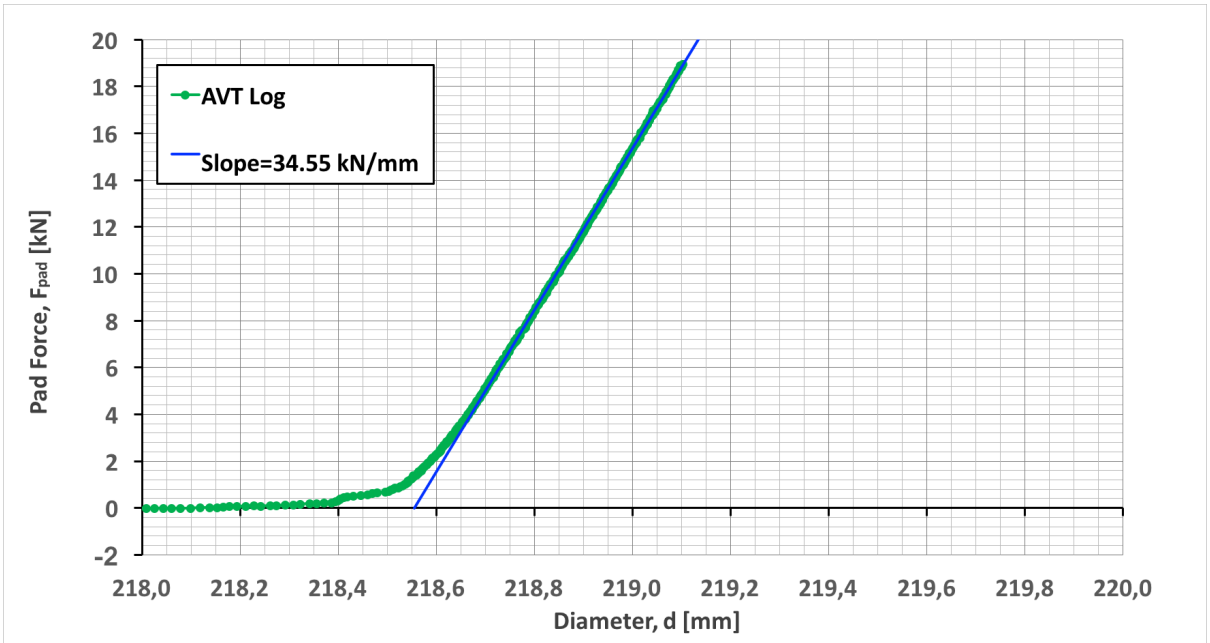

Figure C.21: Results from logging a well-cemented sample with a tilted tool.

Appendix D

Risk Assessment

This appendix includes the risk assessment conducted for the experimental work.

Detailed Risk Report

ID	16914	**Status**	**Date**
Risk Area	Risikovurdering: Helse, miljø og sikkerhet (HMS)	Created	31.01.2017
Created by	Sondre Jakobsen Fagerås	Assessment started	31.01.2017
Responsible	Sigbjørn Sangesland	Actions decided	
		Closed	

Laboratory Work for Master's Thesis

Valid from-to date:

1/9/2017 - 7/1/2017

Location:

4 - Sydområdet / 444 - Petroleumsteknisk senter / 1030 - 3. etasje / 313C

Goal / purpose

Experiments for testing of a new cement logging tool.

Background

Lab experiments will be conducted as part of the Master's thesis, for testing of a new logging tool for cement evaluation. Cement samples will also be constructed.

Description and limitations

Prerequisites, assumptions and simplifications

[Ingen registreringer]

Attachments

TestRig.png
AVTSetup.png
LabSketch.png

References

[Ingen registreringer]

Summary, result and final evaluation

The summary presents an overview of hazards and incidents, in addtition to risk result for each consequence area.

Hazard:	**Fluid leakage**

Incident:

Not to be analyzes.

Hazard:	**Loosening parts under pressure**

Incident:

Not to be analyzes.

Hazard:	**Dropped object**

Incident:

Not to be analyzes.

Final evaluation

Detailed Risk Report

Units this risk assessment spans

- Institutt for petroleumsteknologi og anvendt geofysikk

Participants

Sondre Jakobsen Fagerås
Jesus Alberto De Andrade Correia

Readers

[Ingen registreringer]

Others involved/stakeholders

[Ingen registreringer]

The following accept criteria have been decided for the risk area Risikovurdering: Helse, miljø og sikkerhet (HMS):

Helse	Materielle verdier	Omdømme	Ytre miljø
			

Overview of existing relevant measures which have been taken into account for this risk assessment

The table below presents existing measures which have been take into account when assessing the likelihood and consequence of relevant incidents.

Hazard	Incident	Mesaures taken into account

Existing relevant measures with descriptions:

Personal protective equipment

Safety glasses are used when working with fluids and high pressure equipment.
Protective shoes are used when working with heavy equipment.
Lab coat is always used.
Chemically resistant gloves are used when handling fluids.

Covering of high pressure equipment

High pressure equipment is always covered the first time it is pressurised to a previously not tried pressure.
This is to reduce the consequence of a fluid leakage or loosened parts.
Also for other tests with high pressure, the equipment will be covered as well as possible.

Waste handling

Waste like hydraulic fluids and cement residue is placed in adequate containers.

Risk analysis with evaluation of likelyhood and consequence

This part of the report presents detailed documentation of hazards, incidents and causes which have been evaluated. A summary of hazards and associated incidents is listed at the beginning.

The following hazards and incidents has been evaluated in this risk assessment:

Overview of risk mitigating actions which have been decided, with description:

Appendix E

Data Sheets

This appendix includes data sheets and specifications for the tool components and other equipment used for the experimental work described in this report:

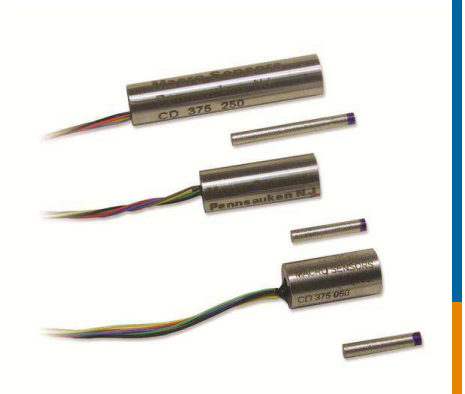

MINIATURE

LVDT Position Sensors
MACRO CD 375

Overview

Macro Sensors' LVDT CD 375 Series of 3/8 inch (9.5 mm) diameter AC-operated LVDTs are small size contactless linear position sensors for both OEM and end user applications. They are available in full scale measuring ranges from ±0.025 inch (±0.63 mm) to ±1.0 inches (±25 mm). The low mass of their cores makes these miniature LVDTs well suited for high response dynamic measurements. CD 375 Series sensors feature the high resolution, excellent repeatability, and low hysteresis associated with LVDT technology, as well as high sensitivity consistent with good linearity. The maximum linearity error for a CD 375 sensor is ±0.25% of full range output, using a statistically best-fit straight line derived by the least squares method.

The proven reliability of CD 375 Series LVDTs is a direct result of manufacturing processes and assembly techniques developed and optimized by Macro Sensors personnel over many years of making LVDTs. Their environmental robustness stems from the materials of their construction, such as glass-filled polymer coil forms for thermal stability and stainless steel housings that act as magnetic shields to reduce the effects of any external AC magnetic fields. Their external sealing meets IEC standard IP-61.

Macro Sensors offers several standard options that permit a user to customize CD 375 LVDTs, including Teflon® bore liners and metric threaded cores. In addition to these standard options, Macro Sensors can design and produce special CD 375 LVDTs, including units with different lead wire exit points and connectors; vented units for operation in pressurized fluids; units for higher ambient temperatures; and units constructed of materials resistant to mild nuclear radiation. Contact the highly experienced Applications Engineers at Macro Sensors for help with any special requirements.

All CD 375 Series LVDTs will operate properly with any conventional differential input LVDT signal conditioners, but operation with ratiometric LVDT signal conditioning circuits is not recommended. Macro Sensors offers a full line of LVDT signal conditioners that will deliver optimum performance from any CD 375 Series LVDTs.

GENERAL PURPOSE
CD 375 | Miniature LVDT Position Sensors

Benefits

- Miniature 3/8 inch size, low core mass
- Ranges of ±0.025" to ±1.0" [±0.63 mm to ±25 mm]
- Non-linearity less than ±0.25% of FRO
- 220°F (105°C) operating temperature
- Coil assembly sealed to IEC IP-61
- Magnetically shielded SS housing

Applications

- Machine tools
- Robotic grippers
- Medical equipment
- Valve position sensing
- ATMs and copy machines
- Pneumatic cylinder position

General Specifications

***Also Available in High Pressure & Temperature Configurations**

Input Voltage	3.0 Vrms (nominal)
Input Frequency	2.5 to 3.0 kHz
Linearity Error	< ±0.25% of FRO
Repeatability Error	< 0.01% of FSO
Hysteresis Error	< 0.01% of FSO
Operating Pressure *	20 kpsi
Operating Temperature *	-65 °F to +220 °F -55 °C to +105 °C -65 °F to +400 °F -55 °C to +200 °C
Thermal Coefficient of Scale Factor:	-0.01%/°F (nominal) -0.02%/°C (nominal)
Vibration Tolerance	20 g to 2 kHz
Shock Survival	1000 g, 11 ms

Ordering Information

- For standard CD 375 or CDM 375, order by model number with range.
- For metric threaded core option, add -006 after model number with range.
- For Teflon® bore liner option, add -010 after model number with range.
- Not available for CDM 375-500 or CDM 375-1000
- For both options, add -016 after model number with range.

GENERAL PURPOSE

CD 375 | Miniature LVDT Position Sensors

Specifications

Model ▶ / Parameter ▼	CD 375 025	CD 375 -050	CD 375 -100	CD 375 -250	CDM 375 -500	CDM 375 -1000
Nominal Range (inches)	±0.025	±0.050	±0.100	±0.250	±0.500	±1.00
Nominal Range (mm)	±0.63	±1.25	±2.50	±6.25	±12.5	±25
Sensitivity (mV/V/.001 in)	3.3	1.6	1.6	2.2	1.6	0.7
Sensitivity (mV/V/mm)	130	63	63	87	63	28
Impedance, Primary (Ω)	90	340	340	500	125	235
Dimension "A" (inches)	0.50	0.75	1.00	1.75	3.30	5.60
Dimension "A" (mm)	12.7	19.1	25.4	44.5	83.8	142.2
Dimension "B" (inches)	0.40	0.63	0.64	1.13	2.00	3.00
Dimension "B" (mm)	10.2	16.0	16.3	28.6	50.8	76.2
Dimension "N" (inches)	0.25	0.38	0.50	0.88	1.65	2.8
Dimension "N" (mm)	6.35	9.5	12.7	22.1	41.9	71.1
Weight, Body (ounces)	0.10	0.20	0.21	0.40	0.63	0.95
Weight, Body (grams)	2.8	5.7	6.0	11.3	18.0	27.0
Weight, Core (ounces)	0.008	0.014	0.015	0.033	0.056	0.088
Weight, Core (grams)	0.23	0.40	0.42	0.94	1.60	2.50

Dimensions

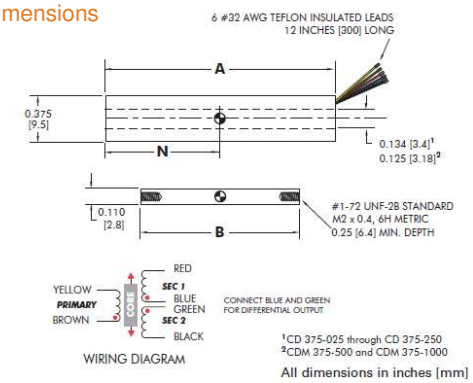

¹CD 375-025 through CD 375-250
²CDM 375-500 and CDM 375-1000

All dimensions in inches [mm]

NORTH AMERICA

AST Macro Sensors,
a TE Connectivity company
7300 US Route 130 North
Pennsauken, NJ 08110-1541 USA
Tel +1 856 662 8000
Fax +1 856 317 1005
sales@macrosensors.com

TE.com/sensorsolutions

CD 375 11/01/15

SIGNAL CONDITIONER

LVDT/RVDT
MACRO EAZY-CAL™ LVC-4000

Overview

The EAZY-CAL™ LVC-4000 is a standalone signal conditioner, supporting a wide range of AC LVDTs, RVDTs, and VR half-bridges, while providing several choices of voltage, current, and digital RS-485 outputs. Push-button calibration offers intuitive operation as compared to signal conditioners with span and offset trim pots. Fault conditions, such as a wire break on LVDT/RVDT connections, are indicated by blinking LEDs, fault condition error output, and Error Flag Open Collector signal (see manual for details). The LVC-4000 operates from a 9-30V DC power supply and is housed in a polyamide DIN rail-mounted enclosure. Calibration instructions, terminal functions, LVDT connection diagram and DIP switch functions are printed on the side panels for convenience.

Synchronization to other signal conditioners is accomplished by a daisy chain connection to a synchronization bus. One unit will assume the Master function based on DIP switch priority setting. If a fault should occur, the next highest priority unit will take over as Master.

With the use of the RS-485 port, a host computer is able to retrieve measurement data, receive operational status, perform remote calibration, and perform hot swap reconfiguration.

SIGNAL CONDITIONER
EAZY-CAL™ LVC-4000

Features

- Push-button or RS-485 command auto-calibration
- Analog voltage or current loop output
- Digital RS-485 interface
- Supports standard AC LVDTs, RVDTs, and VR half-bridge sensors
- Master/slave excitation synchronization
- DIN-rail mountable
- Color-coded terminal blocks

User Selectable Features

- 0-5V DC, 0-10V DC, 0.5-4.5V DC, ±5V DC, ±10V DC or 4-20 mA output
- 1.5V_{rms} or 3.0V_{rms} sensor excitation
- 2.5, 5, 7.5, or 10 kHz excitation frequency

Environmental Data

Operating Temperature	-20 to 75°C (0 to 165°F)
Temperature Sensitivity	<0.02% of FSO/°C (<0.01% of FSO/°F)
EMC Compliance	Emissions: EN55011:2007 Immunity: EN61000-4-2:2009 EN61000-4-4:2004 EN61000-4-6:2009 EN61000-4-3:2010+A2:2010

Electrical Data

Power Input	9-30V DC (90 mA max. @ 24V DC)	**Output Non-Linearity**	≤±0.1% full scale output
Sensor Excitation	3.0V_{rms} (1.5V_{rms} selectable)	**Output Voltage Ripple**	1 mV_{rms} max. (2.5 kHz excitation, no filter) 2 mV_{rms} max. (10 kHz excitation, no filter)
Sensor Excitation Frequency	2.5 kHz, 5 kHz, 7.5 kHz, or 10 kHz		
Input Sensitivity Range	55 mV_{rms} to 5.5 V_{rms} full scale input produces full scale DC output	**Output Current Ripple**	10 µA_{rms} max. (2.5 kHz excitation, no filter) 20 µA_{rms} max. (10 kHz excitation, no filter)
Full Scale Outputs	0-5V DC, 0-10V DC, 0.5-4.5V DC, ±5V DC, ±10V DC or 4-20 mA output	**Frequency Response (-3dB)**	500 Hz max.

SIGNAL CONDITIONER
EAZY-CAL™ LVC-4000

Connection Diagrams

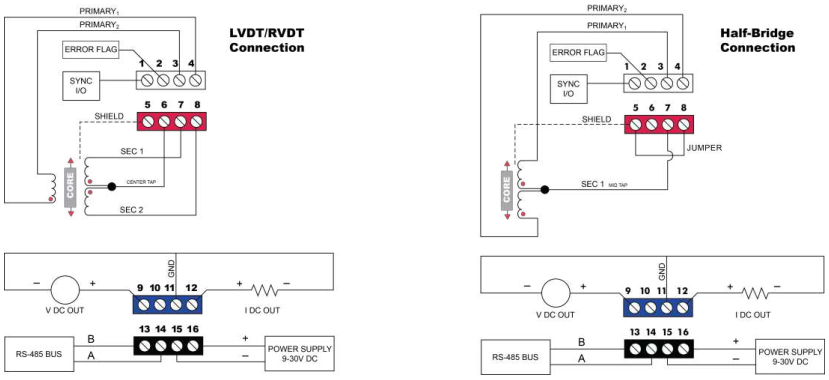

Dimensions

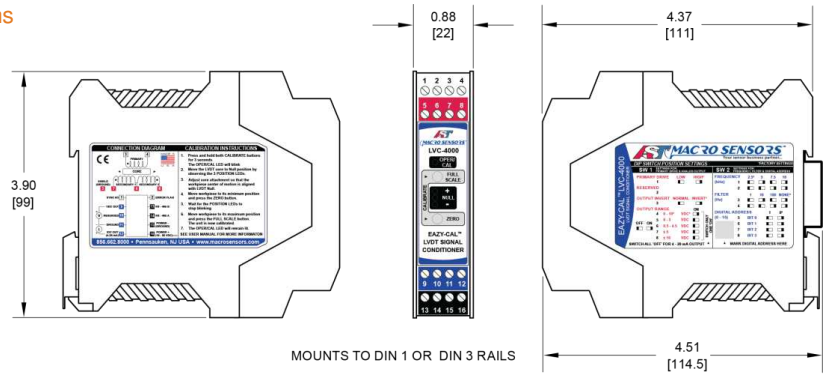

All dimensions in inches [mm].

NORTH AMERICA

AST Macro Sensors,
a TE Connectivity company
7300 US Route 130 North
Pennsauken, NJ 08110-1541 USA
Tel +1 856 662 8000
Fax +1 856 317 1005
sales@macrosensors.com

TE.com/sensorsolutions

LVC-4000 11/01/15

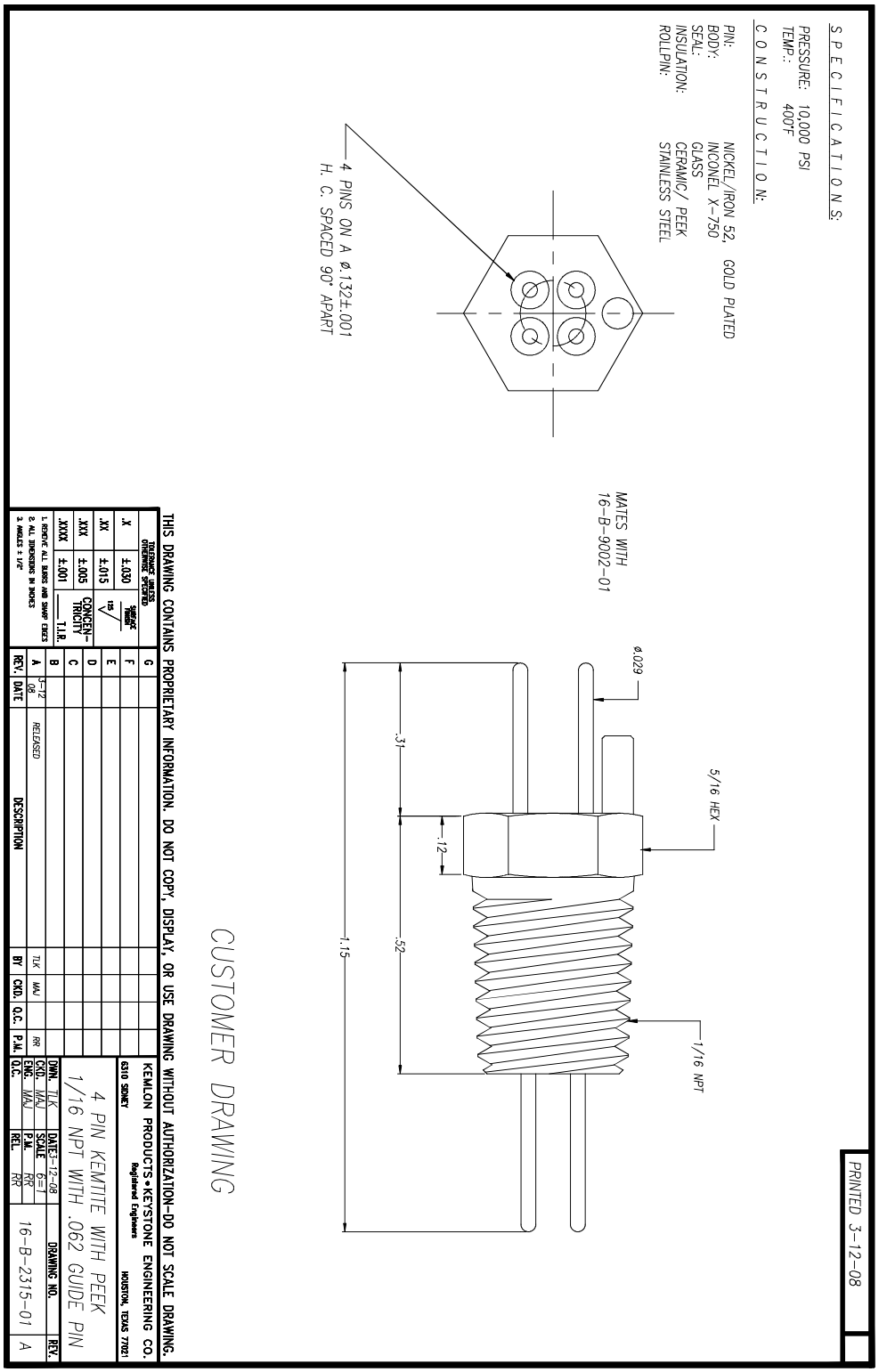
SPECIFICATIONS:
PRESSURE: 10,000 PSI
TEMP.: 400°F
CONSTRUCTION:
PIN: NICKEL/IRON 52, GOLD PLATED
BODY: INCONEL X-750
SEAL: GLASS
INSULATION: CERAMIC/ PEEK
ROLLPIN: STAINLESS STEEL
4 PINS ON A Ø.132±.001
H. C. SPACED 90° APART
MATES WITH
16-B-9002-01
Ø.029
5/16 HEX
1/16 NPT
.31
.12
.52
1.15
CUSTOMER DRAWING
PRINTED 3-12-08
THIS DRAWING CONTAINS PROPRIETARY INFORMATION. DO NOT COPY, DISPLAY, OR USE DRAWING WITHOUT AUTHORIZATION-DO NOT SCALE DRAWING.
KEMLON PRODUCTS•KEYSTONE ENGINEERING CO.
Registered Engineers
6310 SIDNEY HOUSTON, TEXAS 77021
4 PIN KEMTITE WITH PEEK
1/16 NPT WITH .062 GUIDE PIN
DRAWING NO. 16-B-2315-01
REV. A
DWN. TLK DATE 3-12-08
CKD. MAJ SCALE 6=1
ENG. MAJ P.M. RR
Q.C. REL. RR
REV. DATE DESCRIPTION BY CKD. Q.C. P.M.
A 3-12-08 RELEASED TLK MAJ RR
TOLERANCES UNLESS OTHERWISE SPECIFIED
.X ±.030
.XX ±.015
.XXX ±.005
.XXXX ±.001
CONCENTRICITY T.I.R.
1. REMOVE ALL BURRS AND SHARP EDGES
2. ALL DIMENSIONS IN INCHES
3. ANGLES ± 1/2°

PRINTED: 10-7-03

S P E C I F I C A T I O N S:

PRESSURE: 20,000 PSI
TEMP.: 350°F

C O N S T R U C T I O N:

BODY: PEEK
SPRING INSERT: BeCu (GOLD PLATED)

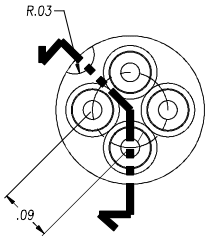

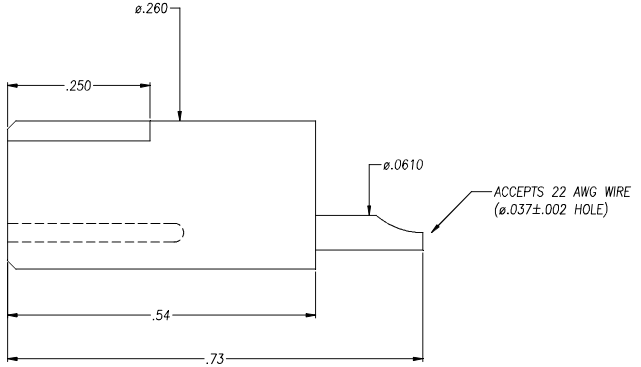

CUSTOMER DRAWING

MATES WITH 16-B-2315-01

TOLERANCE UNLESS OTHERWISE SPECIFIED		SURFACE FINISH
.X	±.030	125
.XX	±.015	
.XXX	±.005	CONCEN-TRICITY
.XXXX	±.001	____ T.I.R.

1. REMOVE ALL BURRS AND SHARP EDGES
2. ALL DIMENSIONS IN INCHES
3. ANGLES ± 1/2°

REV.	DATE	DESCRIPTION	BY	CKD.	Q.C.	P.M.
G						
F						
E						
D						
C						
B						
A						

KEMLON PRODUCTS • KEYSTONE ENGINEERING CO.
1424 N. MAIN ST. Registered Engineers PHONE: 281-997-3300
PEARLAND, TEXAS 77581 FAX: 281-997-1300

4-PIN PEEK BLOCK
WITH ø.030 SPRING INSERT

DWN. TLD	DATE 10-7-03	DRAWING NO.	REV.
CKD.	SCALE 6:1	16-B-9002-00	
ENG.	P.M.		
Q.C.	REL.		

Genspec®GS4000

GENERAL PURPOSE TRANSDUCER

- THICK FILM STRAIN GAUGE TECHNOLOGY
- PRESSURE RANGES 0-500mbar TO 0-700bar
- OUTPUT OPTIONS 2mV/V, 0-5Vdc, 0-10Vdc AND 4-20mA
- ACCURACY ±0.40% NLHR
- ALL STAINLESS STEEL CONSTRUCTION
- LOW COST

DESCRIPTION

The Genspec GS4000 series of general-purpose pressure transducers is designed for applications where economical price and reliable pressure measurement is required. Incorporating bonded strain gauge technology and utilising unique manufacturing techniques results in a low cost, high quality transducer ideal for O.E.M applications.

Constructed from stainless steel with 17/4PH stainless steel diaphragm for ranges above 20bar, and a ceramic diaphragm for lower ranges, the GENSPEC series of transducers are of a robust yet compact design. Applications include the continuous pressure monitoring of oil, gas, water and other liquids in a wide range of industries.

GENSPEC transducers are compatible with the PM8000 range of panel meters and controllers which together offer a simple low cost and accurate pressure measuring and control system.

Available in pressure ranges from 0-0.5bar to 0-700bar, gauge or absolute and electrical outputs 2mV/V, 0-5Vdc, 0-10Vdc and 4-20mA.

PRESSURE RANGES

0 - 1 bar vac through to 700bar, see table below for list of all standard pressure ranges.

Range (bar)	Order Code	Range (bar)	Order Code	Abs Range (bar)	Order Code
0-1 Vac	V001	0-25	0025	0-0.5	0.5A
0-0.5	00.5	0-40	0040	0-1	001A
0-1	0001	0-60	0060	0-1.6	1.6A
0-1.6	01.6	0-100	0100	0-2.5	2.5A
0-2.5	02.5	0-160	0160	0-4	004A
0-4	0004	0-250	0250	0-6	006A
0-6	0006	0-400	0400	0-10	010A
0-10	0010	0-600	0600	0-16	016A
0-16	0016	0-700	0700	0-25	025A

DIMENSIONS (in mm)

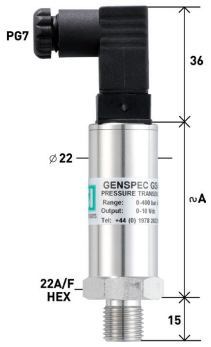

Model	Dimension 'A'
GS4000/GS4100	36
GS4101,2,3	55
GS4001,2,3	64

ELECTRICAL CONNECTION (mA)

Pin No.	2 wire
1	+supply
2	4-20mA signal
3	not fitted
⏚	to case

ELECTRICAL CONNECTION (Vdc)

Pin No.	4 wire	3 wire
1	-supply	common
2	+supply	+supply
3	+output	+output
⏚	-output	to case

ORDERING INFORMATION

GS4000 - xxxx xx

- Model
- Electrical Connector/Option
- Pressure Range - Bar
- Process Connection

Output	Model No.	Ranges
2mV/V	GS4000	above 20 bar
0-5Vdc	GS4001	above 20 bar
0-10Vdc	GS4002	above 20 bar
4-20mA	GS4003	above 20 bar
2mV/V	GS4100	20 bar and below
0-5Vdc	GS4101	20 bar and below
0-10Vdc	GS4102	20 bar and below
4-20mA	GS4103	20 bar and below
Electrical Connection / Option		**Order Code**
Micro DIN plug and socket		-
Cable outlet 1 metre screened		A
M12 connector		B
Cable outlet 1metre IP67 gland		L
Process Connection		**Order Code**
1/4" BSP male thread		AB
1/4" NPT male thread		AM
EXAMPLE		**Order Code**
Output signal 4-20mA (20 bar and below)		GS4103
Micro DIN plug and socket		-
Pressure range 0-6 barg		0006
Pressure connection 1/4" BSP male		AB
Correct Part Number		GS4103-0006AB

For options not listed contact sales team

SPECIFICATION

PRESSURE REFERENCE

Gauge (to 700bar) or absolute (to 25bar)

OVERPRESSURE

Pressure can exceed rated range by the multiple shown below with no damage or change in calibration above ±0.5%FS.
1.6x for ranges -1bar to 20bar
2x for ranges 25bar to 250bar
1.5 for 400bar to 700bar

OUTPUT SIGNAL (OPTIONS)

4-20mA (2 wire),
0-5Vdc (3 or 4 wire),
0-10Vdc (3 or 4 wire),
2mV/V (4 wire)

ZERO OFFSET AND SPAN TOLERANCE

± 1.0 % FS

SUPPLY VOLTAGE (U_b)

Measured across supply terminals on connector plug
13-36Vdc for 4-20mA versions
13-30Vdc for 0-5Vdc and 0-10Vdc versions
5-15Vdc for 2mV/V versions

PROTECTION OF SUPPLY VOLTAGE

Protected against supply voltage reversal up to 50Vdc

LOAD DRIVING CAPABILITY(4-20mA VERSION ONLY)

Calculate maximum load Rs=(Ub-13V)/20mA
e.g. with supply voltage load of 36vdc, maximum load is 1150ohms.

ACCURACY (NON LINEARITY, HYSTERESIS & REPEATABILITY)

±0.40% FS. Typical max. Best fit straight line.

PRESSURE MEDIA

All fluids compatible SAE 303 stainless steel, Alumina and Nitrile seal for ranges up to 20bar, and 17/4PH and SAE 303 stainless steel for ranges above.

OPERATING TEMPERATURE RANGE

Ambient/Media: -20°C to +85°C
Storage: +5°C to +40°C

TEMPERATURE EFFECTS

±2%FS total error band for -20°C to +70°C Typical thermal zero and span coefficients ±0.03%FS/°C

ELECTROMAGNETIC-COMPATIBILTY

Emissions; EN61000-6-4
Immunity; EN61000-6-2
Certification; CE marked

PRESSURE CONNECTION

1/4"BSP or 1/4"NPT male (others on request)

ELECTRICAL CONNECTION

Mating micro DIN socket with screw terminal connections, rated IP65. Options include flying lead with optional cable length and IP67 cable gland or M12.